DESTRESS

Demonstration of soft stimulation treatments of geothermal reservoirs

Detailed report on reservoir performance in terms of sustainability

Application to the geothermal well GPK-4, Soultz-sous-Forêts

Deliverable D4.3

WP 4: Demonstration of combined hydraulic-thermal-chemical treatments in sandstones, carbonatic rocks and granites

Abstract

This report is done in the framework of EU project Destress related to sustainability of geothermal exploitation. It is divided in three distinct parts.

Part A done by UoS provides an overview of the experimental pre-stimulation tests done on an analog two micas granite to assess the permeability evolution of the Soultz GPK4 well during long term acid treatments with or without thermal treatments. A complementary modelling of acid stimulation has been performed using the KIRMAT code that uses single and double porosity models and account for a wide range of mineralogy. The model evaluates changes in porosity and permeability in the vicinity of the geothermal wells (up to 6m) based on changes in the amount of primary and secondary minerals and as a function of time.

Part B done by ESG provides an update of the monitoring and investigations made onsite and especially on the injection well GPK-4 from the Soultz-sous-Forêts power plant (France), confirming MS28. The well hydraulic monitoring is presented. The injectivity index varies between 0.54 kg/s/bar and 0.65 kg/s/bar during the reporting period, from early 2017 to February 2020. In parallel to the hydraulic performance during exploitation, a chemical monitoring of the geothermal brine has been carried out since January 2018 by collecting geochemical data from the production well GPK-2 and the second reinjection well GPK-3. Several geochemical analyses have been done and confirm the high TDS and the gas content of the native brine.

Part C done by GFZ and ESG, describes the soft chemical stimulation of the Soultz-sous-Forêts injection well GPK-4 from the concept to the operation (executed in December 2019), with observed environmental and hydraulic consequences and results.

This project has received funding from the European Union's Horizon 2020 research and innovation programme under grant agreement No 691728

Authors

Part A from UoS: Patrick Baud, Jamie Farquharson, Alexandra Kushnir, Yann Lucas, Viet V. Ngo, Alain Clément, Bertrand Fritz, Gerhard Schäfer, Jean Schmittbuhl

Part B & C from ESG: Régis Hehn, Nicolas Cuenot, Justine Mouchot, Vincent Maurer, Albert Genter, Olivier Seibel, Abigaelle Peterschmitt, Benoit Imbs

Part C from GFZ: Thomas Reinsch, Ernst Huenges

Lead Beneficiary	UoS
Type	☑ R - report, document etc. ☐ OTHER - software, technical diagram etc. ☐ DEM - demonstrator, pilot etc. ☐ E - ethics ☐ DEC - website, patent filing etc.
Status	☐ Draft ☑ WP manager accepted ☑ Project coordinator accepted
Dissemination level	☑ PU - Public ☐ CO - Confidential: only for members of the consortium
Contributors	☑ 1-GFZ ☐ 5-GES ☐ 9-GTL ☐ 13-SNU ☐ 2-ENB ☐ 6-TNO ☑ 10-UoS ☐ 14-KIC ☑ 3-ESG ☐ 7-ETH ☐ 11-TUD ☐ 15-ECW ☐ 4-UoG ☐ 8-GTN ☐ 12-NEX ☐ 16-WES
Creation date	1.10.2019
Last change	25.02.2020
Version	final
Due date	29.02.2020
Submission date	28.02.2020

Context and objectives

DESTRESS is aimed at creating EGS (Enhanced Geothermal Systems) reservoirs with sufficient permeability, fracture orientation and spacing for economic use of underground heat. The concepts are based on experience in previous projects, on scientific progress and developments in other fields, mainly the oil & gas sector. Recently developed stimulation methods are adapted to geothermal needs, applied to new geothermal sites and prepared for the market uptake. The DESTRESS concept takes into account the common and specific issues of different sites, representative for large parts of Europe, and will provide a generally applicable workflow for productivity enhancement measures. The project mainly focuses on stimulation treatments with minimized environmental hazard ("soft stimulation"), to enhance the reservoir in several geological settings covering granites, sandstones, and other rock types.

This deliverable was written in the framework of Task 4.3 ("Realization of chemical injection tests during long-term circulation (GPK-2/GPK-4 Soultz-sous-Forêts) & verification of injectivity index and permeability enhancement with low seismic nuisance (GRT-1 Rittershoffen)) of WP4 ("Demonstration of combined hydraulic-thermal-chemical treatments in sandstones, carbonate rocks and granites"). It compiles all the work done for the Soultz-sous-Forêts site with a focus on the chemical stimulation executed in December 2019.

A. Soultz-sous-Forêts: pre-stimulation laboratory tests and modeling

1 Laboratory-scale acid stimulation of Soultz-sous-Forêts granite

1.1 Background and sample selection

The GPK-4 well was completed in 2004 and has been used variously for both production and injection. It reaches a vertical depth of 4982 m, but strong deviation means that the overall length of the well is ~5260 m. The open-hole section of the well is estimated to be around 200 °C, and intersects a fine-grained two mica granite. The material recovered from the drilling operation is insufficient for the purposes of our experiments; instead, blocks of granite were collected from a site near Forbach in Germany, where the surface expression of the granite basement is accessible. The variably-altered granites contain muscovite and biotite—determined by X-ray powder diffraction (XRD) and energy-dispersive X-ray microanalysis (EDX), and appear to be an ideal analogue for the deep reservoir material at Soultz-sous-Forêts. Many of the granites were found to host macroscopic fractures. Although previous studies have identified fractures in the Soultz basement to host illite and calcite, we were unable to confirm the presence of either mineral through XRD or EDX analyses.

Samples were divided into three suites for experimentation (shown in Figure 1): a fine-grained leucocratic 2-mica granite (G2M-A): a slightly hydrothermally altered granite containing additional secondary minerals such as apatite (G2M-B): and an unaltered granite identical to G2M-A, but containing abundant macroscopic fractures (G2M-F).

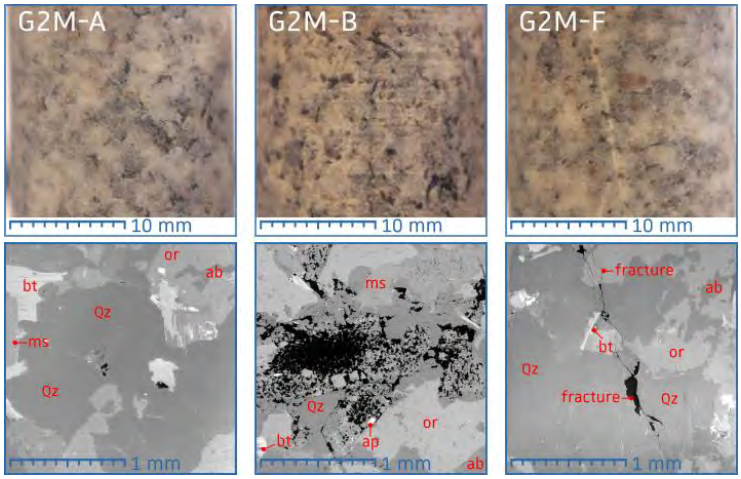

Figure 1: Examples of three classes of granite collected at Schwarzenbach. [above] sample photographs. [below] Scanning Electron Microscope images. Mineral phases identified using XRD and EDX: Qz = quartz; or = orthoclase; ab = albite; bt = biotite; ms = muscovite; ap = apatite.

1.2 Equipment and experiment design

1.2.1 Acid permeameter

In order to explore the influence of aggressive permeants treatments on the two mica granite, over a range of relevant pressures and temperatures, a new permeameter has been custom-designed and constructed at Université de Strasbourg. The apparatus is comprised of a pressure vessel connected to a two-cylinder fluid pump. Confining pressure is applied by silicone thermofluid using a two-stage manual hand pump, up to a maximum of 70 MPa. The pressure vessel is wrapped in high temperature AMOXTM fabric tapes, and the whole ensemble is enclosed in a bespoke clamshell jacket. This jacket is composed of layers of Tempmat (mechanically bonded glass fiber matting), fiberglass cloth, and silicone-impregnated fiberglass cloth, which insulates the pressure vessel effectively due to the low thermal conductivity of the constituent materials. The AMOXTM tapes are connected to a programmable PID temperature controller. The controller reads temperature from a thermocouple embedded beneath the insulating jacket, and the power output to the heat tapes is adjusted accordingly in order to heat the pressure vessel to the desired (user-set) temperature. Within the pressure vessel, thermofluid surrounds a flanged seal, custom-moulded from temperature- and acid-resistant rubber. The sample and two spacers are inserted into the seal. Another k-type thermocouple is in contact with the sample, in this case a mineral insulated k-type probe coated in Halar®, an acid-resistant copolymer of ethylene and chlorotrifluoroethylene. Temperatures of the sample and vessel exterior are recorded using a National Instruments voltage input module integrated into a custom-built data acquisition hub. The acquisition hub communicates with a programme written in LabVIEW, which is also used to send commands and receive flowrate, pore pressure, and fluid volume data from the Quizix pump. Figure 2 presents the details of our new permeameter designed and built for this project.

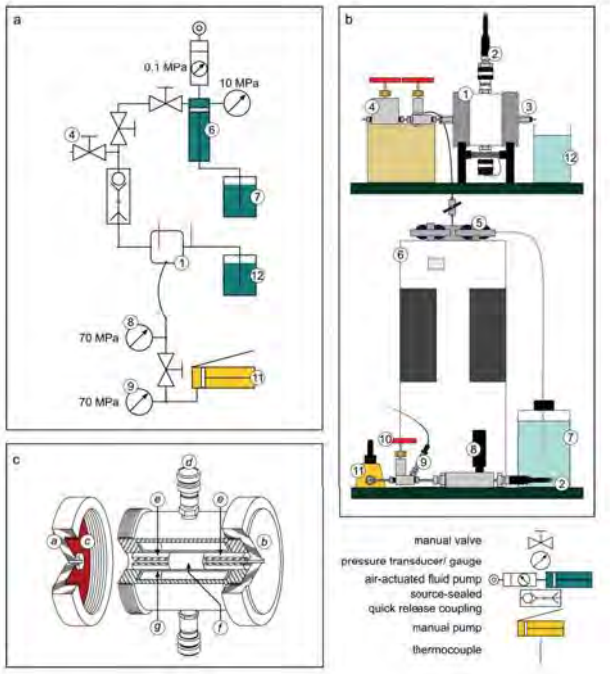

Figure 2: Schematic of acid permeameter. [a] Technical diagram of permeameter circuit. [b] Sketch of primary components. [c] Diagram of pressure vessel interior. (1): pressure vessel; (2): confining pressure inlet/outlet; (3) pore fluid outlet; (4): vent valve; (5): pore fluid inlet/outlet ports; (6) Quizix pore fluid pump; (7): permanent reservoir; (8) pressure gauge; (9): analogue pressure transducer; (10): confining pressure outlet valve; (11): confining pressure pump/oil reservoir; (12): effluent reservoir. (a): upstream endcap; (b): downstream endcap; (c): silicone gasket; (d): confining pressure inlet/outlet; (e) silicone gasket; (d) confining pressure inlet/outlet; (e) steel spacers; (f): sample; (g): annular sleeve.

1.2.2 Batch reaction tests

Alongside the development of the acid permeameter, sample suites were immersed in acid solutions for varying periods of time. For the purposes of this study, two different concentrations of hydrochloric acid were prepared (0.2 N and 2.0 N HCl), by combining concentrated HCl with distilled and deionised water. Mass, porosity, and permeability of all samples were measured prior to immersion. Periodically, samples were removed and re-characterised in order to monitor the evolution of these physical properties. Additionally, some samples underwent thermal stressing in a furnace, whereby they were heated at 1 °C min-1 until a target temperature, left to dwell at that temperature for 2 hours, then cooled again at the same rate. A control suite of granites was set aside for mechanical testing (uniaxial compressive strength), against which to compare acid-treated samples.

1.3 Results

1.3.1 Batch reaction and thermal stressing tests

Naturally fractured samples (G2M-F) are markedly more permeable (10^{-16} m^2) than their non-fractured counterparts, highlighting that fractures provide the most important fluid pathways within the granitic basement: this is in agreement with previous estimations of the reservoir structure at depth. Further,

the altered granite (G2M-B) is more permeable than the unaltered (G2M-A), with permeabilities on the order of 10^{-18} and $<10^{-21}$ m^2, respectively. The initial permeability of G2M-A is extremely low. However, by heating samples to incrementally higher temperatures, we observe an onset of measurable permeability between 200 and 300 °C, coinciding with an uptick in porosity formation (from <0.3 vol.% to 1.6 vol.%), presumably due to thermal microcracking (a product of thermal expansion mismatch between constituent grains). By thermally stressing samples to 600 °C and higher, permeability was increased by over 5 orders of magnitude (up to 10^{-16} m2). Immersion in 0.2 N HCl for 1008 hours (42 days) yielded an increase in permeability of intact G2M-A samples from $<10^{-21}$ m^2 to $>10^{-18}$ m^2. Under the same conditions, G2M-B samples increased in permeability by a factor of approximately 1.5 over the same timeframe. Permeability of G2M-B samples was only increased by a factor of 2 by increasing the acid concentration by an order of magnitude (2.0 N HCl). Example data are shown in Figure 3, which gives the mass loss and permeability increase (relative to the initial values) as a function of immersion. (However, 2.0 N proved too strong a concentration for some wetted stainless steel components of the apparatus, which underwent extreme acid pitting and became brittle: an important caution to consider when introducing logging tools or other equipment into the wellbore post-stimulation.)

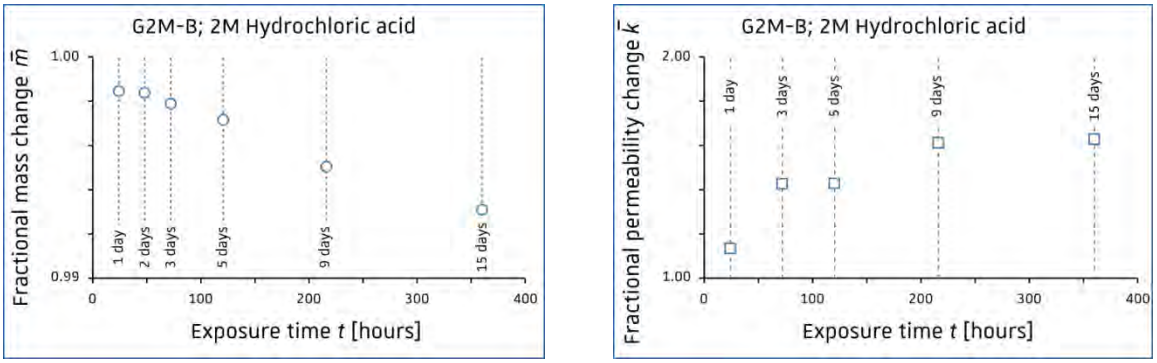

Figure 3: Experimental data from acid batch reaction tests. (L) Decrease in relative sample mass over time. (R) Relative increase in sample permeability over time.

When pre-fractured samples (both naturally and experimentally fractured) were immersed in 0.2 N HCl for 1008 hours, a slight decrease in permeability was observed (from ~1×10^{-15} m^2 to 7×10^{-16} m^2: approximately half). As such, acid stimulation was clearly not an effective permeability enhancement method following high-temperature thermal stressing (600 or 700 °C). In such cases, permeability had already been increased significantly (from $<10^{-21}$ m^2 to $>10^{-16}$ m^2) due to the introduction of new microcracks. Mineral dissolution by HCl was not sufficient to increase permeability beyond this value. Similarly, the naturally fractured granites (suite G2M-F) exhibited a decrease in permeability following acid treatment, presumably due to their high pre-stimulation permeabilities and the remobilisation rather than removal of any dissolvable minerals. Figure 4 summarized the evolution of the physical properties of the samples subjected to immersion in HCl.

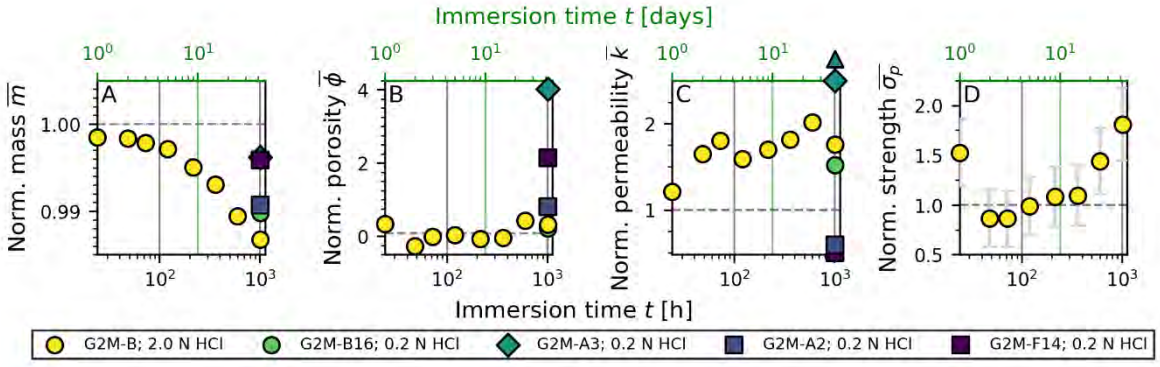

Figure 4: Normalised physical property data for samples subject to acid immersion. Symbols and colours distinguish different starting materials and acid molarities. Dashed horizontal lines indicates no change. [a] Change in mass over time. [b] Change in porosity. [c] Change in permeability. [d] Change in strength relative to untreated samples.

1.3.2 Acid permeameter tests

Measurements of permeability have been carried out on the Schwartzenbach granite under incrementally higher confining pressures using water as the pore fluid. As observed in other experimental studies, permeability declines with the increase of confining pressure (analogous to depth). This phenomenon is expected, as the confining pressure serves to close pre-existing fractures, especially those aligned parallel or sub-parallel to the sample axis.

Whereas the batch reaction tests comprise a relatively large acid volume compared to centimetric-scale samples, our acid flow-through apparatus precludes acid solution external to the samples, and so the relative volume of acid in the system is much lower. Using 0.2 N HCl acid as a permeant fluid, flow-through tests were performed on granite samples previously heated to 200 °C. By using samples that had experienced temperatures corresponding to the in-situ reservoir conditions, we preclude the potential for significant generation of thermally-induced microcracks over the course of our experiment. Figure 5 shows representative results for experiments performed at 25 °C and at 100 °C (under 1 MPa confining pressure). Only slight and non systematic variations in sample permeability were observed throughout the stimulation phase (6 hours). Given that initial permeabilities are on the order of 10^{-21} m^2, maximum relative permeability changes of ±0.1 only correspond to permeability variations on the order of 10^{-22} m^2.

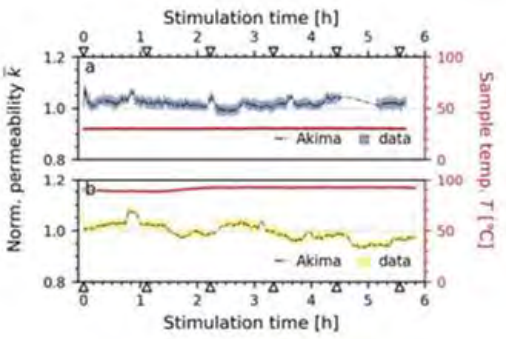

Figure 5: Evolution of sample permeability during acid flow-through experiments. [a] Sample A5, subject to approximately 6 hours of stimulation with 0.2 N HCl solution, at a sample temperature of 30 °C. Triangles indicate times whereat aliquots of effluent acid solution were sampled for further analysis. Normalised data are shown in colour, and dash-dot line is an Akima spline function used to interpolate missing data. [b] Sample A6, subject to approximately 6 hours of stimulation with 0.2 N HCl solution, at a sample temperature of 100 °C. Triangles indicate times whereat aliquots of effluent acid solution were sampled for further analysis. Normalised data are shown in colour, and dash-dot line is an Akima spline function used to interpolate missing data. Note that only the acid flow-through portion of the experiments are shown: the pre and post-stimulation stages using deionised H2O are omitted for clarity.

The effluent fluid was collected at time-resolved intervals throughout the experiments and Induced coupled plasma atomic emission spectroscopy (ICP-AES) was performed (Figure 6).

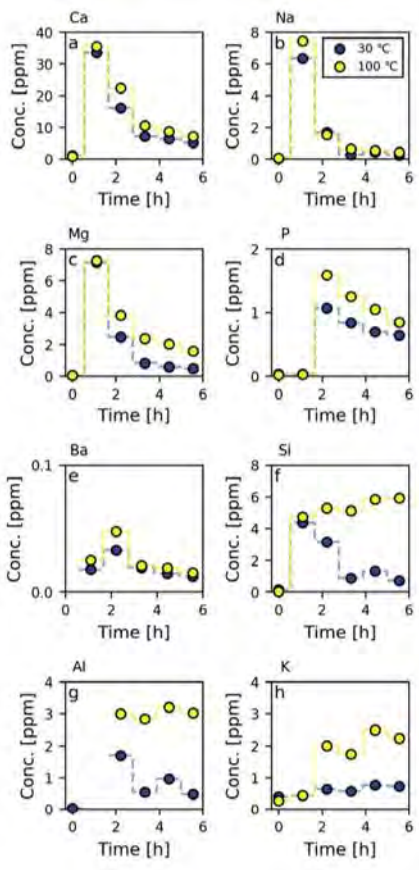

Figure 6: Evolution of sample permeability during acid flow-through experiments. [a] Sample A5, subject to approximately 6 hours of stimulation with 0.2 N HCl solution, at a sample temperature of 30 °C. Triangles indicate times whereat aliquots of effluent acid solution were sampled for further analysis. Normalised data are shown in colour, and dash-dot line is an Akima spline function used to interpolate missing data. [b] Sample A6, subject to approximately 6 hours of stimulation with 0.2 N HCl solution, at a sample temperature of 100 °C. Triangles indicate times whereat aliquots of effluent acid solution were sampled for further analysis. Normalised data are shown in colour, and dash-dot line is an Akima spline function used to interpolate missing data. Note that only the acid flow-through portion of the experiments are shown: the pre and post-stimulation stages using deionised H2O are omitted for clarity.

Generally, ICP-AES data indicates relatively rapid (about 4 hour) spikes in Ca, Na, Mg, and P, both during the room-temperature and high-temperature experiments. These highly mobile cations are presumably derived from the apatite, albite and biotite identified in our samples, although it is possible that minerals such as calcite, previously identified in Soultz-sous-Forêts basement rock are also present in low abundance and contribute to the recorded pattern of element evolution in the acid solution.

Similarly, Ba appears in the effluent fluid in trace amounts suggesting that additional minerals were present in the initial material but were below the detection limit of the initial XRD and EDX analyses. Baryte is known to be a precipitation product within the Soultz-sous-Forêts reservoir, along with calcite, quartz, and galena. However, baryte is not highly soluble in HCl, so the source of the trace amounts of Ba in the effluent fluid remains unclear. Over the course of the experiments, these elements (Ca, Na, Mg, P, Ba) are flushed out quickly, and continue to be removed from the granite at a rate asymptotically decreasing towards zero. The decreasing rate of cation removal suggests that the process is limited by the availability of these reactive minerals, which is in agreement with their generally low abundance in the unaltered granite. Although there appears to be some dependence on temperature, the difference between cation removal rate at low and high temperature is negligible.

The pattern of cation concentration evolution for Si, Al, and K tell a different story. We interpret the coincident evolution of K to reflect the dissolution of silicate minerals; in particular K-feldspar (orthoclase and microcline), but also perhaps muscovite and illite, which appear in lesser abundance in the initial material. The dissolution of feldspar exhibits a much more pronounced dependence on temperature, as demonstrate by previous experimental studies.

1.4 Conclusions

Using a combination of batch reaction tests and a new, custom-built high-temperature acid permeameter, we explore the potential for porosity and permeability increase in a two-mica granite, analogous to that at depth in the Soultz-sous-Forêts basement. Altered granites proved to be relatively susceptible to dissolution during batch reaction tests, reflected in a loss of sample mass and a general increase in porosity and permeability over time. We note only a slight increase in total mass loss (i.e. dissolution), absolute porosity change, and permeability increase when we compare similar samples subjected to HCl at a higher molarity (2.0 as opposed to 0.2 N). Thermal treatment of Soultz-sous-Forêts granite above 200–300 °C is clearly a highly effective method by which to induce new fractures and increase permeability. While it is not the focus of our experiments, we suggest that the operational feasibility of a thermal stimulation campaign (taking into account commercial sustainability and the potential for induced seismicity) warrants further study. Both thermally and naturally-fractured granites, initially the most permeable sample, exhibited a decrease in permeability as a result of acid immersion, either due to mineral precipitation or clogging of pre-existing fluid pathways in the granites. While we do demonstrate that permeability can be initiated in formerly impermeable unaltered granite, the ratio of acid to rock required likely renders this approach impossible to deploy in a real-world scenario. When we stimulate granite from the same sample suite using an acid flow-through system, time resolved ICP-AES data from the effluent fluid highlights the fact that dissolution is indeed occurring. In particular, relatively mobile elements such as Ca, Na, Mg, and P (presumably derived from apatite, albite, and biotite) are rapidly leached from the granite. Framework elements

(from quartz and feldspars) are dissolved at a temperature-dependent rate for the duration of the experiments, characterised by the presence of Si, Al, and K in the effluent fluid (in greater abundance at elevated temperature). Despite clear evidence for mineral dissolution, however, the recorded permeability change over a period of six hours is not significant. Ultimately, the potential for permeability enhancement at Soultz-sous-Forêts using HCl alone is low. We find that the permeability increase in the least permeable granites is almost negligible when acid is flushed through these samples, despite promising results in initial batch reaction experiments. On the other hand, it appears that HCl can act to decrease the permeability of the more permeable reservoir constituents: altered and fractured granites. The Soultz-sous-Forêts granite exhibits a general lack of Ca-rich feldspars, which are much more easily broken down by HCl than Na–K members, such as the microcline and albite which are present, even under similar experimental. It has been shown that, contrary to the calcium end-member, the dissolution mechanism (and rate thereof) of albite is relatively insensitive to acid pH. It is questionable, therefore, whether a higher molarity HCl stimulation would prove more effective in the long-term. Nevertheless, effective chemical stimulation of the reservoir using alternative acidic agents cannot be discounted: chemical data collected during our experiments illuminate a number of dissolution mechanisms operative throughout. If these reactions could be targeted and promoted, then acid enhancement of the Soultz-sous-Forêts reservoir may yet bear fruit. Critically, we recommend that a thorough experimental campaign should be used to inform any future stimulation campaigns. Our results will be presented in a manuscript submitted to Geothermal Energy.

2 Modelling acid stimulation in the enhanced geothermal system of Soultz-sous-Forêts (Alsace, France)

In geothermal systems, acidizing stimulation is expected to affect the target zone around the injection well as much as possible, and therefore should penetrate more deeply into the formation via fracture zones with pre-existing secondary mineralogy. At the Soultz geothermal site, the natural fractures are very heterogeneous and irregularly localized. This causes the different hydraulic characteristics of the fractures, and hence makes an acidizing operation challenging in regard to the effective distribution of chemicals. Before performing chemical stimulation in the Soultz geothermal system, a modelling approach is considered in order to discuss different scenarios in terms of the choice of acid, and the amount and duration of acid injection.

The approach used in this work is based on the geochemical numerical code KIRMAT, which enables us to represent the geothermal reservoir using single and double porosity models and account for a wide range of mineralogy. The model evaluates changes in porosity and permeability in the geothermal reservoir based on changes in the amount of primary and secondary minerals as a function of time in the geothermal system.

2.1 Materials and methods

2.1.1 The numerical reactive transport model

Governing equations of reactive mass transport

The hydrochemical model developed in this study is based on the numerical code KIRMAT (Kinetic Reaction and Mass Transport) (Gerard, 1996), which combines geochemical reactions and 1D mass transport equations. The mass balance equation of reactive transport in a one-dimensional porous medium is written as (Lichtner, 1988; Gérard et al., 1998):

$$\frac{\partial}{\partial t}\left(\phi\Psi_j\right) = \phi D\left(\frac{\partial^2\Psi_j}{\partial x^2}\right) - U\frac{\partial\Psi_j}{\partial x} - \sum_{r=1}^{M}\alpha_{jr}\frac{\partial}{\partial t}\left(\phi_r\widetilde{V_r^{-1}}\right) \quad (j = 1, \ldots, N) \qquad (1)$$

and

$$\frac{\partial}{\partial t}\left(\phi_r\widetilde{V_r^{-1}}\right) = v_r \quad (r = 1, \ldots, M) \qquad (2)$$

where Equation (1) refers to N aqueous primary species and Equation (2) refers to M primary species of reacting minerals. In these equations, Ψj denotes the generalized (or total) concentrations (in moles per water mass or volume) of primary species, ϕ denotes the porosity of the porous medium, ϕ_r and α_{jr} denote the volume fraction and the stoichiometric reaction coefficients, respectively, of the rth mineral with molar volume $\widetilde{V_r}$, v_r represents the reaction rates of the irreversible reaction of minerals and fluids equivalent to the rate of precipitation or dissolution of reacting minerals r per unit of the rock and fluid system (by convention, v_r is positive for precipitation and negative for dissolution reactions), D denotes the hydrodynamic dispersion coefficient, and U denotes the Darcy velocity. x is the space variable and t is the time. The generalized concentration Ψ_j is defined according to the expression:

$$\Psi_j = C_j + \sum_i \alpha_{ji} C_i \quad , \text{ with } C_i = K_i\gamma_i^{-1}\prod_{j=1}^{N}\left(\gamma_j C_j\right)^{\alpha_{ji}}, \qquad (3)$$

where C_j refers to the concentration of the jth primary species, and the sum runs over all aqueous secondary species with concentration C_i related to the concentrations of the primary species through the mass action equation. The quantity α_{ji} denotes the molar stoichiometric coefficient of species j in secondary species i, γ is the activity coefficient of the aqueous species, and K_i denotes the equilibrium constant. Using Equations (1) and (2), one obtains a system of (N +M) coupled nonlinear partial differential equations.

In the case of a double-porosity medium, divided between the matrix and a fractured medium, the mass balance equations of reactive transport are written as:

in a fractured medium:

$$\frac{\partial}{\partial t}\left(\phi^f\Psi_j^f\right) = \phi^f D\left(\frac{\partial^2\Psi_j^f}{\partial x^2}\right) - U\frac{\partial\Psi_j^f}{\partial x} + \varphi_j^f + \frac{\alpha}{e}\phi^f D_{diff}\left(\Psi_j^m - \Psi_j^f\right) \quad (j = 1, \ldots, N) \quad (4)$$

in the matrix, where it is assumed that no flow and no mass transport take place,

$$\frac{\partial}{\partial t}\left(\phi^m\Psi_j^m\right) = \varphi_j^m - \frac{\alpha}{e}\phi^m D_{diff}\left(\Psi_j^m - \Psi_j^f\right) \quad (j = 1, \ldots, N) \qquad (5)$$

where Ψ_j^f and Ψ_j^m are the dissolved global concentrations of primary species j in fractured medium and matrix, respectively (mol.L-3); ϕ^f and ϕ^m are the porosity of fractured medium and matrix, respectively (L3.L-3); D is the effective hydrodynamic dispersion coefficient (L2.T-1) in fractures; Ddiff is the diffusion coefficient (L2.T-1) in matrix; U is the Darcy velocity (L.T-1); φ_j^f and φ_j^m are the sink terms corresponding to the geochemical fluxes in fractured medium and matrix, respectively (mole.L-3.T-1); α is the surface contact between fractured medium and matrix (L2); e is the volume contact between fractured medium and matrix (L3).

KIRMAT aims to contribute to the understanding of water-rock interactions in different frameworks as groundwater salinization (Lucas et al., 2010), weathering processes (Lucas et al., 2017; Ackerer et al., 2018) or hydrothermal alteration (Ngo et al., 2016). It can also be used to simulate clay minerals evolution under specific environmental conditions, such as the storage of nuclear waste (Montes et al., 2005a; 2005b; Marty et al., 2009, 2010; 2006; Ngo et al., 2014).

Water-rock interactions

In KIRMAT, interactions between water and rock involve dissolution and precipitation. In our study, only mineral dissolution is modelled by irreversible kinetics, while precipitation is modelled at equilibrium. Kinetic rock dissolution rate rd (in mole per water mass) is quantified by (Gérard, 1996):

$$r_d \equiv \mathrm{v_r} = k_{d,r} \mathrm{S_r^{eff}} \alpha_{\mathrm{H^+}}^{\mathrm{n}} \left(1 - \left(\frac{\mathrm{Q_r}}{\mathrm{K_r}}\right)^{\mathrm{n1}}\right)^{\mathrm{n2}}, \quad (6)$$

where kd,r denotes the dissolution rate constant (mol.m-2.year-1) of the reactive mineral r, Sreff stands for the reactive surface area of mineral r (m2.kgH2O-1), $\alpha_{H^+}^n$ denotes the proton activity where n depends on the pH of the solution, n1 and n2 are exponents depending on the pH of the solution, Qr is the ion activity product of reactive mineral r and Kr denotes the thermodynamic equilibrium constant of the hydrolysis reaction of mineral r at a given temperature and pressure.

The KIRMAT code can describe the feedback effect of the chemical and mineralogical evolution of porosity and permeability at any node of the mesh due to dissolution and precipitation reactions. The intrinsic permeability k (m2) is updated after each time step as follows (Gerard, 1996):

$$\mathrm{k} = \mathrm{C_0}[\,\phi^{\mathrm{c-1}} \left(\frac{\phi^3}{(1-\phi)^2 S^2}\right)]^2 \quad (7)$$

where C0, ϕ and S denote an experimental constant, the porosity of the porous medium and the grid cell surface in contact with the adjacent cell (m2), respectively.

The relationship of the effective diffusion coefficient (Ddiff) to the porosity is expressed as:

$$\mathrm{D_{diff}} = \mathrm{D_0}\phi^{\mathrm{C-1}} \quad (8)$$

where D0 is the diffusion coefficient of the solute in free water and ϕ is the porosity.

The porosity at the time increment n is determined as follows:

$$\phi^{\mathrm{n}} = 1 - \left[\frac{\mathrm{S\Delta x}\left(1-\phi^{\mathrm{n-1}}\right)+\mathrm{Bv^n}}{\mathrm{S\Delta x}}\right] \quad (9)$$

where ϕ^n and ϕ^{n-1} are the porosities at the time increments n and n-1, respectively; Δx is the cell length (m) and Bv^{n} is the absolute volume balance of all minerals at time increment n (m^3).

2.2 Acid stimulation of the geothermal reservoir

2.2.1 Conceptual system

The acid stimulation method is applied to the geothermal reservoir for a few decades. This approach is generally expensive and complicated, and its success depends on many factors. Gathering knowledge about the well that is chosen for acid stimulation is the first task that should be thoroughly performed. The next step is to select a suitable chemical and/or a mixture of chemicals. When applying the acid stimulation, the acid solution can be injected stepwise into the geothermal reservoir using different steps, known as pre-, main- and post-flush. Each step needs to be designed and balanced carefully against the rest to achieve its own objective (GEIE EMC, 2017).

The GPK-4 well actually has a very poor connection with other wells in the Soultz system. According to the feasibility study completed recently by the GEIE Exploitation Minière de la Chaleur (GEIE EMC, 2017), the GPK-4 injection well is considered to be the most appropriate well for acid stimulation based on the evaluation of the technical and economic feasibility. Therefore, in the current modelling work, we assumed that well GKP-4 would be chosen for acid stimulation. Acid stimulation of well GPK-4 is expected to improve its connection with other wells, as well as improving the overall hydraulic regime of the Soultz system.

Knowledge about the reservoir petrology and fracture filling mineralogy is crucial for selecting a chemical. Additionally, other factors include which minerals need to be dissolved and if a composition of native brine and injection setup should be used also need to be considered to coordinate the best efficiency of the injected products and avoid unwelcome secondary reactions (GEIE EMC, 2017). The results obtained for previous acid stimulations in the Soultz system have shown that with a HCl solution, the carbonate minerals present in the deep reservoirs of wells GPK-2, GPK-3 and GPK-4 could be successfully removed by injecting an acid solution with a concentration up to 0.45% (Nami et al., 2008; Portier et al., 2009). Therefore, for this modelling work, the simple and inexpensive acid HCl will be tested. This simple acid was chosen, since it has a fast and strong dissolution effect and reacts with minerals quickly when it comes into contact with the system. Otherwise, it is also expected that a simple stimulation fluid can keep the environmental footprint of the stimulation operation as low as possible.

Figure 7 represents a conceptual system of the Soultz geothermal reservoir. The system consists of a 6 m thick layer initially saturated by water at 65°C. The temperature value of 65°C in the geothermal reservoir near the injection well was considered to be a constant value during the stimulation process. The injected acid solution is assumed to be heated up to 65°C and allowed to penetrate in the near field around the stimulation well. This simple approach of the transition between the stimulated acid solution and the Soultz geothermal reservoir used as the boundary condition will simplify the calculated chemical speciation. The conduction of heat in the system is not considered herein.

For the current work, the computation time was quite long, meaning that depending on the modelling case, it may take several months to accomplish one numerical simulation. We further acknowledge that the cell size may also have an impact on the modelling output when using the geochemical modelling code as reported in several modelling studies (Marty et al., 2009; Ngo et al., 2014). In the current work, we therefore attempted to evaluate the effects of cell size on the modelling results with different sizes as 0.1 m, 0.2 m, 0.5 m and 1 m, together with different lengths of the system, including 6 m, 10 m and 20 m. The different outputs were more or less different but not significantly, so they are not presented, and a cell size of 1 m and a length of 6 m were chosen as the default values because of the reasonably clear results and the computation time.

In the present work, special attention was paid to evaluate the impact of the injection conditions and the reservoir conditions on the evolution of the reservoir after the acid stimulation. There are two reasons that inspire us to focus on these issues. First, as discussed previously, the appropriateness of the injection conditions generally plays a critical role in the stimulation results. Second, depending on the geothermal reservoir properties, the capacity of the acid solution to penetrate into the geothermal reservoir and the interaction between the acid solution and different minerals in the reservoir must be different.

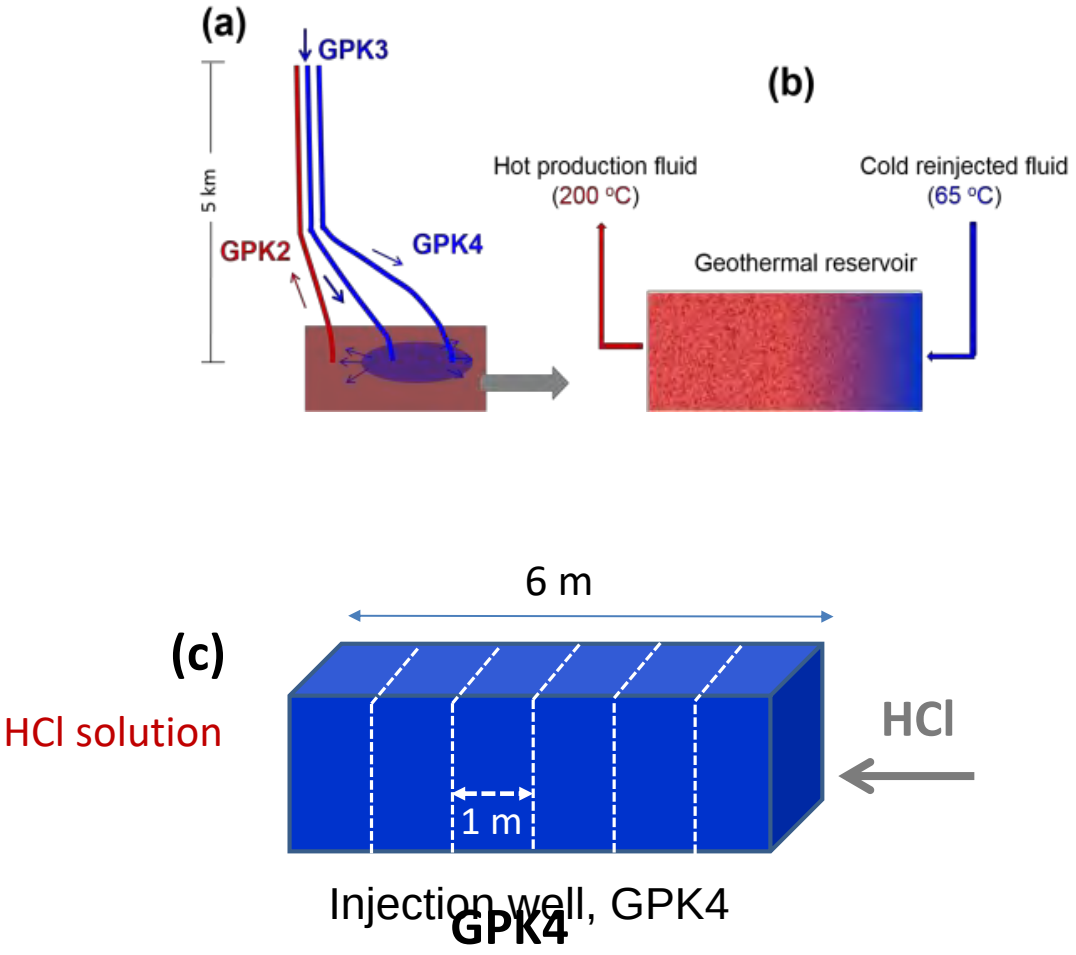

Figure 7: Conceptual schema of the stimulated Soultz geothermal system: (a) Cross-section of the Soultz EGS system (Alsace, France), GPK2 is the production well, while GPK3 and GPK4 are the re-injection wells; (b) conceptual model with the re-injection well (≈ 65°C) and the production well (≈ 200°C); (c) model domain used in KIRMAT simulations.

2.2.2 Modelling approach

In the framework of the single porosity model, a reference case was used for the input data presented in Tables 1, 3, 4 and 5. These data were collected from a literature review. Additionally, HCl concentration was 0.2% (pH =0.74), and injection duration was 2 days with a Darcy velocity of 1 $m.h^{-1}$. Three sensitivity cases were tested. It is important to highlight that the input data are the same for all three cases except for the tested sensitivity parameters. The numerical calculations performed in this way are able to distinguish the effects of the tested parameters on the evolution tendency of the system.

For the modelling tests using the double porosity model, the matrix and fracture fractions are presented separately by their own mineralogical compositions and physical properties such as porosity and permeability. Two modelling cases are conducted and the only difference between them is the parameter representing the ratio of surface contact to volume contact between the matrix and fracture zones (parameter $\frac{\alpha}{e}$ in equations 4 and 5). The comments and discussion of the modelling results are mainly based on two criteria, porosity and permeability.

2.2.3 Initial conditions

Mineralogical composition of the Soultz geothermal reservoir

As a potential host rock for an enhanced geothermal system, the Soultz system is the subject of many experimental and theoretical investigations (e.g., Ledésert et al., 1993a,b, 1999, 2009, 2010; Dubois et al., 1996, 2000; Sausse, 2002; Baldeyrou et al., 2003; Baldeyrou-Bailly et al., 2004; Sausse et al., 2006; Bartier et al., 2008; Hébert et al., 2010, 2011; Hébert and Ledésert, 2012), as well as modelling studies (e.g., Komninou and Yardley, 1997; Rabemanana et al., 2003; Bächler and Kohl, 2005; André et al., 2006; Fritz et al., 2010; Ngo et al., 2016). Various studies have reported that the mineralogy of the Soultz geothermal reservoir is very heterogeneous (e.g., Genter, 1989; Hébert et al., 2010). The heterogeneity, which depends on the location, comes from the fact that the fractions of fresh and altered granites are variable. Furthermore, there is a clear difference between the so-called fresh granites in the Soultz reservoir. For example, fresh granite mainly contains minerals such as K-feldspar, plagioclase, quartz, and biotite, while altered granite is generally comprised of quartz, K-feldspar, illite, smectite, mica, calcite, dolomite, pyrite, galena, and chlorite (e.g., Ledésert et al., 1999; Bartier et al., 2008; Hébert et al., 2010). A literature review reveals that the main secondary minerals in the Soultz reservoir are carbonates and illite/smectite. Depending on the degree of the fluid-rock interaction, the volume fraction of these newly formed minerals in the altered granite and vein alteration can reach approximately 50%.

As noted previously, the GPK-4 injection well was selected to apply the acid stimulation. The literature review shows that the fracture mineralogy of this well may have similar characteristics to the fracture zones of the upper and intermediate reservoir in terms of secondary fracture mineralization of quartz, calcite, illite, chlorite, sulfides, barite and haematite (Genter and Traineau, 1992; Dezayes et al., 2005). The dataset presented in the thesis of Jacquot (Jacquot, 2000) was chosen to describe the minerals that were initially present in the Soultz geothermal reservoir. Additionally, to estimate the volume fraction of each mineral, we assumed that the fractions of fresh and altered granites are 90% and 10%, respectively. Tables 1 and 2 present the composition and corresponding volume fraction of primary minerals for the single-porosity and double porosity models, respectively. To fit with the Thermoddem database (Blanc et al., 2012), several groups of minerals are represented by the most typical minerals in their group: plagioclase was replaced by albite and anorthite end-members; K-muscovite, annite, and phlogopite were used for mica; chlorite was represented by clinochlore and chamosite end-members; and illites are represented using three different compounds, known as Fe-illite, Mg-illite, and Al-illite.

In terms of physical properties, for the single-porosity model, the system has a porosity of 5% and a permeability of 10^{-16} m^2. For the double-porosity model, the system has the following parameters for matrix and fractured medium, respectively: porosities of 10% and 1%, and permeabilities of 10^{-16} m^2 and 10^{-14} m^2.

Table 1: Main mineralogical compositions, corresponding volume fractions and the estimated reactive surface areas of the Soultz granite considered in the current modelling work. The volume fraction values were taken from those in Jacquot. 2000 and based on the assumption that the fresh granite contains 90% of the volume fraction and the rest is vein alteration.

Minerals*	**Structural formula**	**Volume fraction** (%)	**Reactive surface area** (m^2 $kg^{-1}H_2O$)
Quartz	SiO_2	25.87	308.30
K-Feldspar	$KAlSi_3O_8$	22.63	7457.55
Albite	$NaAlSi_3O_8$	36.25	8262.75
Anorthite	$Ca(Al_2Si_2)O_8$	2.00	124.21
K-Muscovite	$KAl_2(AlSi_3)O_{10}(OH)_2$	2.82	631.77
Annite	$KFe_3(AlSi_3)O_{10}(OH)_2$	2.82	740.82
Phlogopite	$KMg_3(AlSi_3)O_{10}(OH)_2$	2.82	622.69
Calcite	$CaCO_3$	0.46	112.19
Mg-Illite	$K_{0.85}Mg_{0.25}Al_{2.35}Si_{3.4}O_{10}(OH)_2$	0.87	6375.75
Fe-Illite	$K_{0.85}Fe_{0.25}Al_{2.35}Si_{3.4}O_{10}(OH)_2$	0.87	6687.79
Al-Illite	$K_{0.85}Al_{2.85}Si_{3.15}O_{10}(OH)_2$	0.87	6611.52
Smectite	$[Ca_{0.009}Na_{0.409}K_{0.024}][(Si_{3.738}Al_{0.262}][Al_{1.598}Fe_{0.208}Mg_{0.214}]O_{10}(OH)_2$	0.97	5484.20
Dolomite	$CaMg(CO_3)_2$	0.08	20.71
Chamosite	$Fe_5Al(AlSi_3)O_{10}(OH)_8$	0.33	13.72
Clinochlore	$Mg_5Al(AlSi_3)O_{10}(OH)_8$	0.33	10.79

Physical properties	
Porosity	5 %
Permeability	10^{-16} m^2

*Plagioclase was replaced by Albite and Anorthite; Micas by Muscovite. Annite and Phlogopite. and Chlorite by Chamosite and Clinochlore.

Table 2: Main mineralogical composition, volume fraction and estimated reactive surface area of the matrix and facture Soultz granite considered in the current modelling work. The volume fraction values were taken from those in Jacquot (2000).

	Matrix			**Fracture**	
Minerals	**Volume fraction** (%)	**Reactive surface area** ($m^2\ kg^{-1}H_2O$)	**Minerals**	**Volume fraction** (%)	**Reactive surface area** ($m^2\ kg^{-1}H_2O$)
Quartz	24.2	288.40	Quartz	40.9	487.42
K-Feldspar	23.6	7777.20	K-Feldspar	13.9	4580.64
Albite	40.5	9231.49	Calcite	3.9	951.17
Anorthite	2	124.21	Mg-Illite	8.7	63757.49
Muscovite	3.13	701.22	Fe-Illite	8.7	66877.88
Annite	3.13	822.26	Al-Illite	8.7	66115.20
Phlogopite	3.13	691.15	Smectite	9.7	54841.96
Calcite	0.3	73.17	Dolomite	0.8	207.06
			Chamosite	2.4	137.19
			Clinochlore	2.4	107.86
Physical properties			**Physical properties**		
Porosity		10%	Porosity		1%
Permeability		$10^{-16}\ m^2$	Permeability		$10^{-14}\ m^2$

Pore-water composition

Reference pore-water composition and its evolution over time have to be estimated for the assessment of general performance. Generally, pH is considered as a key parameter of pore-water composition because it has important effects on the reactions in geothermal reservoirs. The pH of the geological fluid depends on the interaction of a variety of factors, such as the ion exchange of clay and the dissolution-precipitation reactions of trace carbonate minerals and major clay mineral components. In this work, the THERMA code (Ngo et al., 2016) was applied to determine the pore-water composition of the Soultz geothermal reservoir at 65°C. The chemical composition of geological fluid in equilibrium with the geothermal reservoir at 65°C is presented in Table 3. The input data for the THERMA code are taken from laboratory analyses of fluid collected from the production well head (Sanjuan et al., 2006; Scheiber et al., 2013) and from thermodynamic modelling (Sanjuan et al., 2006; Fritz et al., 2010; Ngo et al., 2016). The details regarding the modelling work completed using the THERMA code can be found in Ngo et al., (2016). The pH value of 5.39 is higher than the value of 4.8 of the saline fluid measured in situ at the well-heads (Scheiber et al., 2013). The CO2 partial pressure is estimated by the equilibrium calculations reported by Sanjuan et al. (2006).

Table 3: pH, Eh and chemical composition of the equilibrated solution of the Soultz geothermal reservoir at 65°C.

pH	5.39
Eh (mV)	-171
p_{CO2} (atm)	$4.7x10^{-2}$
Elements	Concentration (mol $kg^{-1}H_2O$)
K	$8.31x10^{-2}$
Na	$1.21x10^{0}$
Ca	$1.35x10^{-1}$
Mg	$5.14x10^{-3}$
Si	$2.20x10^{-4}$
Al	$3.92x10^{-8}$
Fe	$1.00x10^{-5}$
Pb	$1.48x10^{-6}$
S	$1.23x10^{-10}$
Cl	$1.56x10^{0}$
C	$3.74x10^{-2}$
Alkalinity (eq $kg^{-1}H_2O$)	$1.0x10^{-2}$

2.2.4 Input data

Thermodynamic data for hydrolysis reactions at 65°C of 15 primary minerals and 7 potential secondary minerals are presented in Table 4. These data are obtained from the Thermoddem database (Blanc et al., 2012). The choice of potential secondary minerals may have significant impacts on the dissolution of primary minerals (Gaucher and Blanc, 2006). The secondary minerals were chosen based on the literature review studies focused on fluid-rock interactions in the context of enhanced geothermal systems. The accuracy of thermodynamic data has an important impact on the output predictions (Savage et al., 2007; Zhu and Lu, 2009; Ngo et al., 2016).

It is well known that kinetic data for minerals are much less available than thermodynamic data, especially for precipitation of mineral phases. Because of this common issue in geochemical modelling works, in the current study, the kinetic approach is used for 15 primary minerals only, and all secondary-formed minerals are precipitated at thermodynamic equilibrium. Table 5 presents the kinetic data of the dissolution reactions for the primary minerals at 25°C and 65°C. The practical application of mineral dissolution requires us to know various parameters for each primary mineral, such as the reaction rate constant and reaction orders with respect to the pH of the solution. The collection of kinetic data of the dissolution processes at 65°C for all 15 primary minerals is a big issue due to the limited data at high temperatures. Therefore, the data at 65°C presented in this section were extrapolated from the data proposed by Palandri and Kharaka (2004) using the kinetic data at 25°C and activation energy terms.

In the kinetic approach of mineral dissolution, the reactive surface area of a mineral is used, as seen in Equation 6, given that it is a sensitive parameter for the modelling of a geochemical system. Unfortunately, the accuracy of the estimation for this key parameter is often questionable because some important factors are not considered, such as surface roughness and the presence of open pores.

Moreover, surface area can change following the progression of the reaction, e.g., temporarily increase if dissolution causes significant surface roughness or decrease when grains are dissolved or become covered by secondary minerals. Thus, the surface area becomes one of the most important uncertainties in dissolution studies (Savage et al., 2002). In the literature, modellers may estimate the reactive surface area with the BET, the edge site or the geometric surface area. In this work, the reactive surface of 15 primary minerals were estimated from their BET surface areas, assuming that they are proportional to the reactive surface areas. The reactive surface areas corresponding to the single and double porosity models are presented in Tables 1 and 2, respectively.

Table 4: Thermodynamic database of the primary minerals in the Soultz granite and secondary minerals tested in the current study. The thermodynamic constants at different temperatures were taken from the Thermoddem database (Blanc et al., 2012).

Minerals	**Structural formula**	**Molar volume (cm3 mol-1)**	**LogK65oC (-)**
Primary minerals			
Quartz	SiO2	22.69	-3.30
K-Feldspar	K(AlSi3)O8	108.74	-1.13
Albite	NaAlSi3O8	100.07	1.01
Anorthite	Ca(Al2Si2)O8	100.79	18.83
K-Muscovite	KAl2(AlSi3)O10(OH)2	140.81	8.26
Annite	KFe3(AlSi3)O10(OH)2	154.32	26.28
Phlogopite	KMg3(AlSi3)O10(OH)2	149.66	33.66
Calcite	CaCO3	36.93	1.26
Mg-Illite	K0.85Mg0.25Al2.35Si3.4O10(OH)2	140.25	5.67
Fe-Illite	K0.85Fe0.25Al2.35Si3.4O10(OH)2	140.53	4.34
Al-Illite	K0.85Al2.85Si3.15O10(OH)2	139.49	6.18
Smectite	[Ca0.009Na0.409K0.024][(Si3.738Al0.262]Al1.598Fe0.208Mg0.214]O10(OH)2	134.92	1.45
Dolomite	CaMg(CO3)2	64.12	2.06
Chamosite	Fe5Al(AlSi3)O10(OH)8	215.88	37.17
Clinochlore	Mg5Al(AlSi3)O10(OH)8	211.47	49.33
Secondary minerals			
FeIII-Illite	K0.85Fe0.25IIIAl2.6Si3.15O10(OH)2	140.56	5.98
K-Beidellite	K0.34Al2.34Si3.66O10(OH)2	134.15	0.48
Ca-Saponite	Ca0.17Mg3Al0.34Si3.66O10(OH)2	138.84	23.26
FeCa-Saponite	Ca0.17Mg2FeAl0.34Si3.66O10(OH)2	139.96	21.86
Siderite	FeCO3	29.38	-0.83
Ankerite	CAFe(CO3)2	70.79	1.04
Anhydrite	CaSO4	45.94	-4.88

Minerals	ka	kn	kb	pHa	pHb	na	nb	Ea	En	Eb
	(mol m-2 year-1)							(KJ mol-1)		
	25oC									
Quartz	1.44E-4[a]	1.44E-6[b]	1.62E-9[b]	4.0[a]	5.9[b]	0.50[a]	-0.50[b]	99.2[a.b]	90.1[b]	108.4[b]
K-Feldspar	2.75E-3[b]	1.23E-5[b]	1.99E-14[b]	4.7	10.7	0.5	-0.82	51.7	38.0	94.1
Albite	2.18E-3[b]	8.66E-6[b]	7.91E-9[b]	6[a]	8[a]	0.46	-0.57	65.0	69.8	71.0
Anorthite	9.95E+3[b]	2.39E-2[b]	7.91E-9[b]	6[a]	8[a]	1.41	-0.57	16.6	17.8	22.0
Muscovite	4.44E-5[b]	8.88E-6[b]	8.88E-8[b]	6[a]	8[a]	0.37	-0.22	22.0	22.0	22.0
Annite	4.60E-3[b]	8.88E-6[b]	8.88E-8[b]	6[a]	8[a]	0.53	-0.22	22.0	22.0	22.0
Phlogopite	4.44E-5[b]	1.25E5[b]	8.88E-8[b]	6[a]	8[a]	0.37	-0.22	22.0	29.0	23.5
Calcite	1.58E+7[b]	4.88E+1[b]	4.88E+1[a]	5.5[b]	8.0[a]	1.00[b]	0[a]	14.5[b]	23.5[b]	23.5[a.b]
Mg-Illite	6.29E-5[d]	6.29E-8[d]	3.15E-13[d]	5.0[d]	8.8[d]	0.60[d]	-0.60[d]	46[a.d.e]	14[a.d.e]	67[a.d.e]
Fe-Illite	6.29E-5[d]	6.29E-8[d]	3.15E-13[d]	5.0[d]	8.8[d]	0.60[d]	-0.60[d]	46[a.d.e]	14[a.d.e]	67[a.d.e]
Al-Illite	6.29E-5[d]	6.29E-8[d]	3.15E-13[d]	5.0[d]	8.8[d]	0.60[d]	-0.60[d]	46[a.d.e]	14[a.d.e]	67[a.d.e]
Smectite	3.30E-4[b]	5.23E-6[b]	9.52E-10[b]	5.3[b]	9.4[b]	0.34[b]	-0.40[b]	23.6[b]	35[b]	58.9[b]
Dolomite	2.03E+4[b]	9.31E-1[b]	9.31E-10[a]	8.7[b]	11.0[a]	0.50[b]	0[a]	36.1[b]	52.2[b]	52.2[a]
Chamosite	1.58E-2[c]	9.97E-6[c]	6.29E-10[c]	6.0[c]	9.5[c]	0.53[c]	-0.44[c]	66.5[f]	45[a]	66.5[b]
Clinochlore	2.44E-4[b]	2.18E-6[b]	4.35E-8[b]	6[a]	8[a]	0.26[b]	-0.2[b]	88.0[b]	93.41[b]	93.4[b]
	65ºC									
Quartz	1.64E-2	1.06E-4	2.86E-7							
K-Feldspar	3.24E-2	7.54E-5	1.77E-12							
Albite	4.85E-2	2.42E-4	2.34E-7							
Anorthite	2.20E+4	5.59E-2	2.34E-7							
Muscovite	1.27E-4	2.54E-6	2.54E-7							
Annite	1.31E-2	2.54E-5	2.54E-7							
Phlogopite	1.27E-4	4.99E-5	2.54E-7							
Calcite	3.16E+7	1.50E+2	1.50E+2							
Mg-Illite	5.65E-4	1.23E-7	7.71E-12							
Fe-Illite	5.65E-4	1.23E-7	7.71E-12							
Al-Illite	5.65E-4	1.23E-7	7.71E-12							
Smectite	1.02E-3	2.78E-5	1.58E-8							
Dolomite	1.14E+5	1.12E+1	1.12E+1							

Chamosite	3.77E-1	8.54E-5	1.50E-8
Clinochlore	1.63E-2	1.88E-4	3.75E-6

Table 5: Kinetic constants of dissolution reactions of the primary minerals in the Soultz geothermal reservoir at 25°C. The kinetic constant values at 65°C are extrapolated using the activated energy.

[a]These values are assessed by the authors [b]Palandri and Kharaka 2004; [c] Lowson et al. 2005; [d]Köhler et al. 2003; [e]Tang and Martin 2011; [f]Brandt et al. 2003

2.3 Results

2.3.1 Single porosity model

Reference case

The final porosity and permeability profiles are shown in Figure 8. In terms of porosity, the initial porosity of the system is assumed to be 0.05, but the porosity scale shown in Figure 8a varied from 0.045 to 0.075. This is because the stimulation resulted in temporally precipitating carbonates, which caused a temporal closing of the system. However, the increase of porosity from its initial value of 0.05 to the final value of approximately 0.075, occurred mainly within the zone in direct contact with the injection well, and the porosity is open mainly in the zone of 3 metres around the injection well. There are only small changes in porosity in the rest of the system. The change in porosity is related to the dissolution of primary minerals and the precipitation of secondary minerals occurring in the system. Similarly, permeability also increases in the system from the initial value of 10^{-16} m^2 to 1.53 10^{-16} m^2, mainly in the zone of 3 metres around the injection well, similar to the porosity increase. It increases less significantly in the rest of the system. The changes in porosity and permeability strongly depend on each other, because the evolution of permeability is also closely related to the mineralogical transformations.

Unfortunately, the modelling indicates that acid stimulation results in both the dissolution and precipitation of several minerals in the system. The evolution of significantly transformed minerals is presented in Figure 9. The acid stimulation results are seen for dissolving minerals such as calcite and anorthite, whereas minerals such as beidellite and siderite are locally and temporally precipitated. The dissolution of other minerals such as clay minerals, silicates and oxides remains low.

Calcite (Figure 9a) is strongly influenced by the acid stimulation. The dissolved amount of calcite varied from -3 to 4 moles kgH2O-1. The modelling results indicate that calcite is quickly dissolved when the acid solution fluids enter into the geothermal reservoir, especially in the zone near the acid-injected well. The dark grey zone in Figure 3a corresponds to negative values of the dissolution, which means that calcite is precipitated as well. However, this newly formed fraction is mostly re-dissolved at the end of the simulation. With respect to anorthite (Figure 3b), this mineral is also significantly dissolved under the attack of the acid solution (Figure 3b), especially in the zone of approximately 3.5 metres around the injection well. Its dissolution amount reached 2.5 moles kgH2O-1. Two minerals (beidellite and siderite) are also precipitated in this system. Beidellite (Figure 3c) is significantly

precipitated in the zone approximately 2-3 metres around the injection well. Its precipitation amounts reach 4 moles kgH2O-1. This fact can provide unexpected results in acid stimulation because this mineral is not re-dissolved at the end of the simulation, as calcite is. The model further indicates that siderite is locally and temporally precipitated (Figure 3d), however this mineral is quickly re-dissolved.

It is worth noting that in the current study, the precipitation process of minerals is treated using the thermodynamic approach. This approach may have numerous limitations, especially when applying quantitative geochemical modelling to a system that is very complex and scenario-dependent, and a limitedly understood chemical environment, such as the Soultz geothermal system. The precipitation of secondary phases may completely change the system geometry, and hence, the transport characteristics of the Soultz geothermal reservoir. Positive achievements of chemical stimulation can be nullified or even worsened by the precipitation of sparingly soluble minerals (GEIE EMC, 2017).

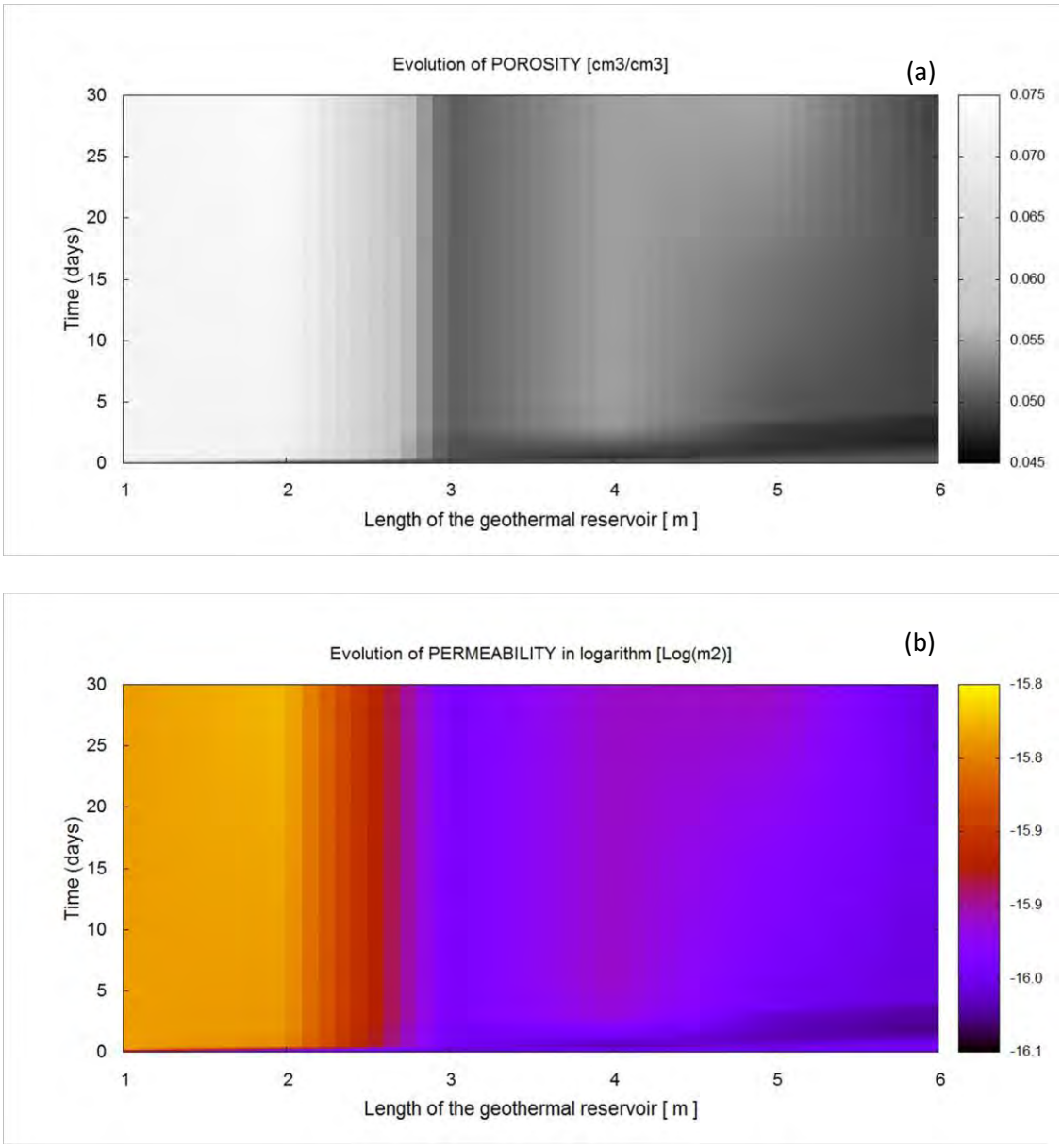

Figure 8: Calculated spatio-temporal evolution of (a) porosity and (b) permeability in the Soultz geothermal reservoir in the reference case. Permeability is presented with units in logarithm.

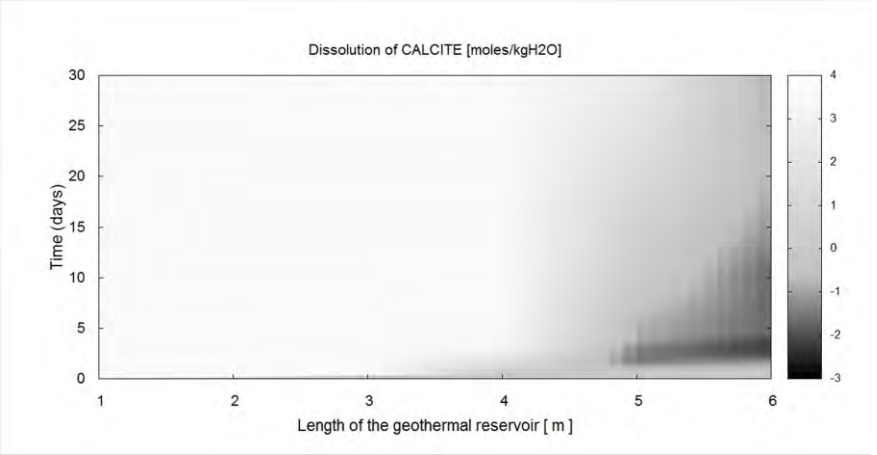
Dissolution of CALCITE [moles/kgH2O]
Time (days)
Length of the geothermal reservoir [m]

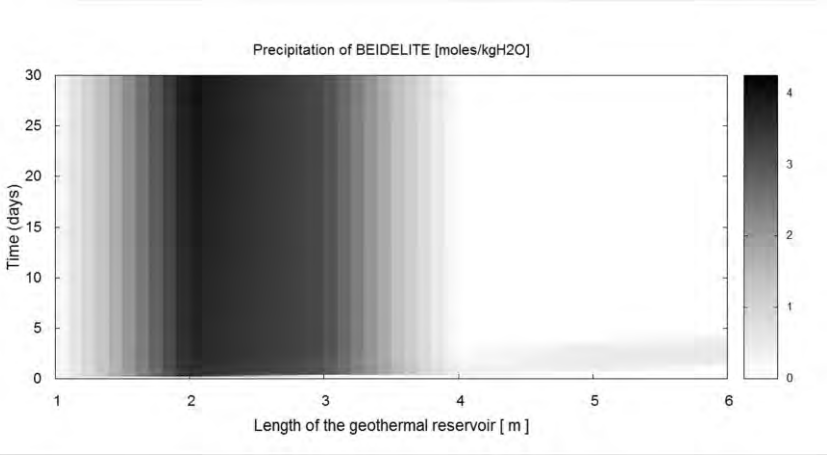
Precipitation of BEIDELITE [moles/kgH2O]
Time (days)
Length of the geothermal reservoir [m]

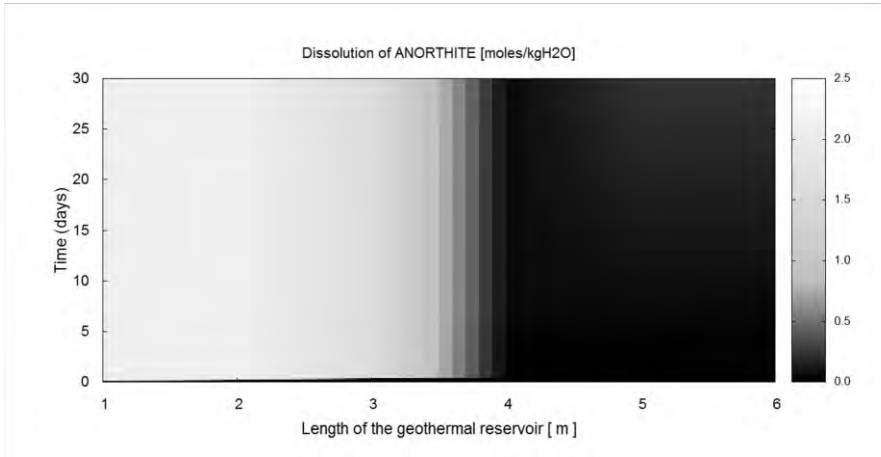
Dissolution of ANORTHITE [moles/kgH2O]
Time (days)
Length of the geothermal reservoir [m]

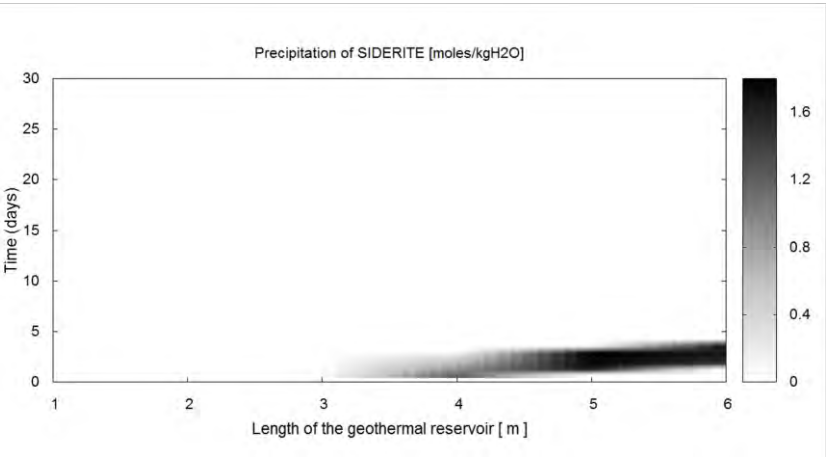
Precipitation of SIDERITE [moles/kgH2O]
Time (days)
Length of the geothermal reservoir [m]

Figure 9: Calculated spatio-temporal evolution of minerals that are strongly changed. Calcite and anorthite are mainly dissolved. Beidellite and siderite are mainly precipitated. The evolution of these minerals is presented with units of moles/kgH2O.

2.3.2 Sensitivity case studies

The sensitivity results are shown in Figures 10 and 11. For each sensitivity case, only the effects on porosity are shown and discussed. It is important to note again that in all sensitivity tests, the input data are the same as in the reference case, except for the tested sensitivity parameter. Furthermore, refer to Figure 9a for a comparable view with respect to the reference case, where the evolution of porosity for the reference case is shown.

Case 1: change of the Darcy velocity

Where the Darcy velocities are equal to 0.1 $m.h^{-1}$, 0.2 $m.h^{-1}$ and 2 $m.h^{-1}$, the porosity profiles are presented in Figures 4a, 4b and 4c, respectively. Where the Darcy velocity is 0.1 $m.h^{-1}$, meaning the injection rate is ten times lower than the reference case (1 m h^{-1}), the porosity at the end of the simulation ranged from 0.04 to 0.11. Compared to the reference case, the maximum porosity is higher, but the opened zone is only limited to 2 metres of depth, meaning 1 metre less than in the reference case. It is concluded that the low flow rate injection of chemicals is not a good scenario because it limits the penetration of the acid solution into deeper zones of the geothermal reservoir. Low flow rates of stimulation fluids in fractures can also result in the precipitation of secondary reaction products.

When the Darcy velocity is 0.2 m.h-1, the modelling analysis results indicate that the porosity varied from 0.045 to 0.075, and the open zone is limited to 3 metres. The porosity in the rest of the system, meaning from 3 metres to 6 metres away from the injection well, is not clearly open. The modelling results are quite similar to the ones in the reference case. When the Darcy velocity of the acid solution is 2 m.h-1, the porosity at the end of the simulation is in the range of 0.045 to 0.075, and the porosity is open up to 3 metres around the injection well. It is found that the modelling results are again quite similar to those of the reference case.

Case 2: increase of the injection duration by a factor 2

The evolution of porosity at the end of the simulation is presented in Figure 11a: the maximum porosity is 0.11, compared to 0.075 in the reference case. The simulated impact zone in this case is limited to 3 metres, which is similar to the reference case.

Case 3: increase of the acid concentration

For this case, the corresponding results with respect to the final porosity profile are shown in Figure 5b. The evolution of porosity is quite different from that of the reference case. The results indicate that when the pH of the tested acid solution is 0, the porosity in the impacted zone of the system opens significantly and can reach 0.35, compared to 0.075 in the reference case. Unfortunately, from 2 to 6 metres away from the injection well, the porosity decreases drastically. This can be explained by the fact that the higher concentration of the acid solution induced a stronger dissolution of minerals such as calcite and anorthite in the zone in direct contact with the injection well but also by the stronger precipitation of secondary minerals such as beidellite in the rest of the system. One may conclude that when applying a highly concentrated HCl solution, these non-desirable secondary reactions are strongly produced. This reduced the positive achievements of chemical stimulation.

Case 4: increase of the initial amount of calcite in the reservoir.

Figure 11c shows the final porosity profile when the initially presented calcite amount is 2%, compared to 0.46% in the reference case. Note that the other input parameters are the same as in the reference case. It can be seen in Figure 11c that the simulated porosity varies from 0.04 to 0.11 cm3 cm-3, which means that the maximum porosity is slightly higher than in the reference case in the zone in direct contact with the injection well; but, in the rest of the system, the porosity is unfortunately closed slightly more strongly than in the reference case. Once again, the impacted zone is always limited to 3 metres around the injection well. In this case, the higher initial amount of calcite induces a significantly higher amount of dissolution processes, which, in turn, induces the higher porosity.

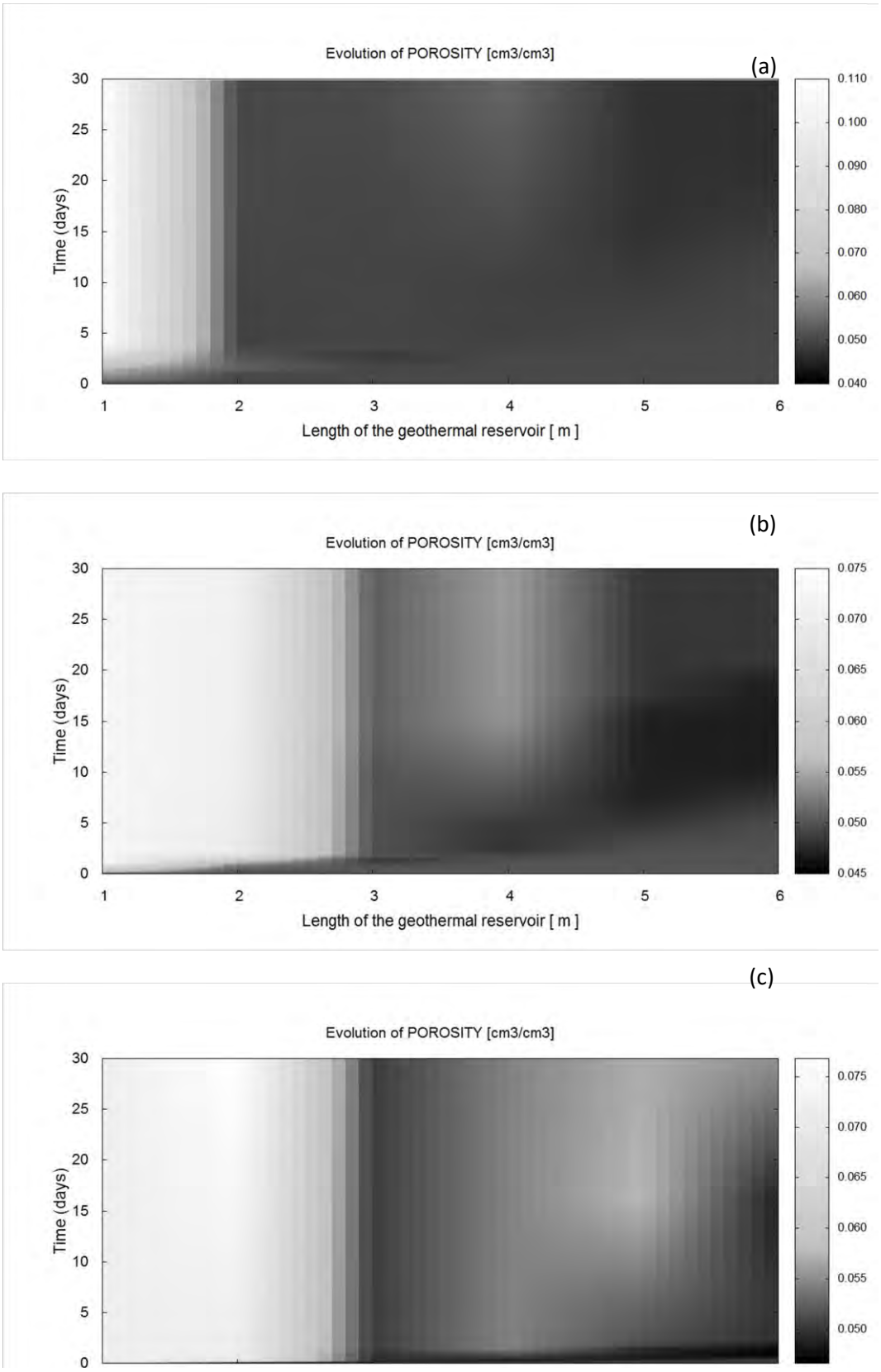

Figure 10: Calculated spatio-temporal evolution of porosity in the Soultz geothermal reservoir when the Darcy velocity is changed. (a) a Darcy velocity of 0.1 m/h; (b) a Darcy velocity of 0.2 m/h and (c) a Darcy velocity of 2 m/h.

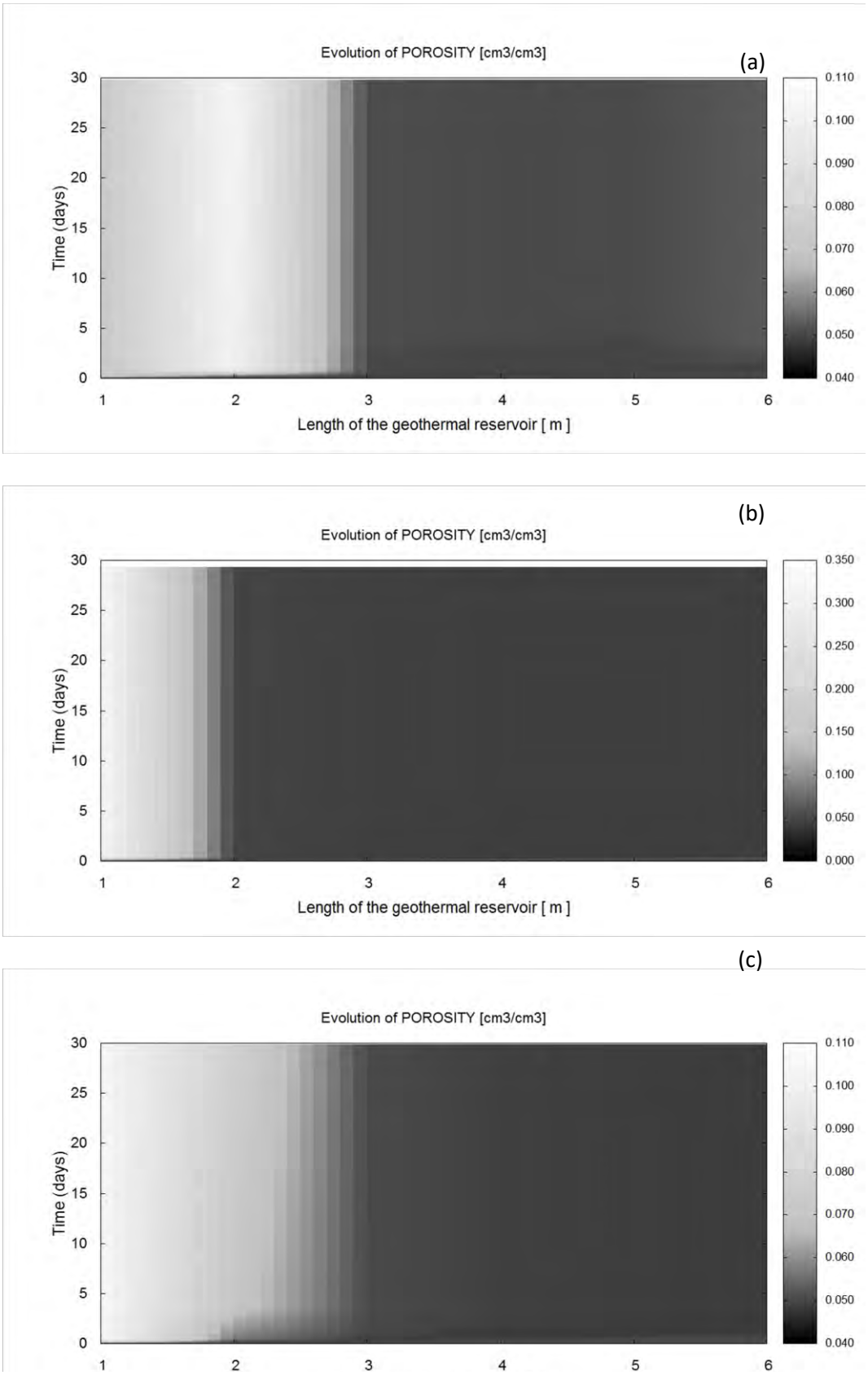

Figure 11: Calculated spatio-temporal evolution of porosity in the Soultz geothermal reservoir under different scenarios. (a) increase of the injection duration by a factor of 2; (b) increase of the acid concentration, pH =O and (c) increase of the calcite quantity that is initially present in the reservoir.

2.3.3 Double porosity model

Figure 12 shows the porosity profiles of the Soultz geothermal reservoir after 30 days of acid stimulation. Note again that in this model, we use different input data in terms of the mineralogical composition and the physical properties of the system. Similar to different cases of the single porosity model presented in detail in previous sections, the simulated porosity in the geothermal reservoir is divided into two zones. As expected, the zone in contact with the injection well is more significantly opened than in the previous case, where the model used assumes that the system is homogeneous. For this model, the maximum porosity reaches values of 0.16 and 0.14 when the ratio of surface contact and volume contact between the fracture and matrix zones are 1000 and 10000, respectively. It is not expected that in both cases of the double porosity model, the porosity of the rest of the system is very low. This also means that the stronger opening in the zone in direct contact also induces the stronger decrease of porosity in the rest of the system.

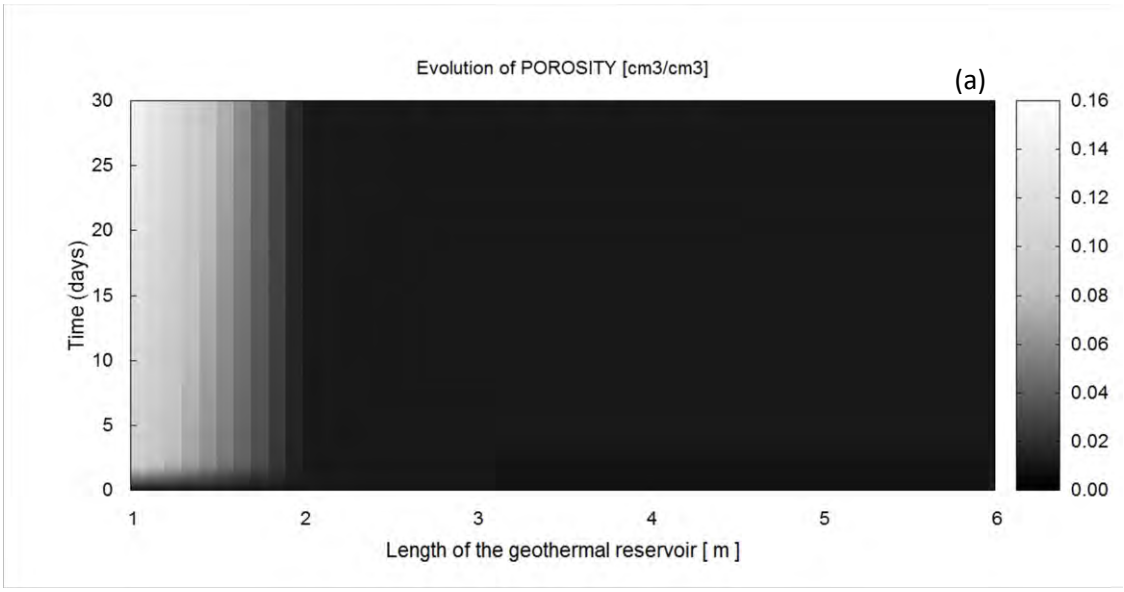

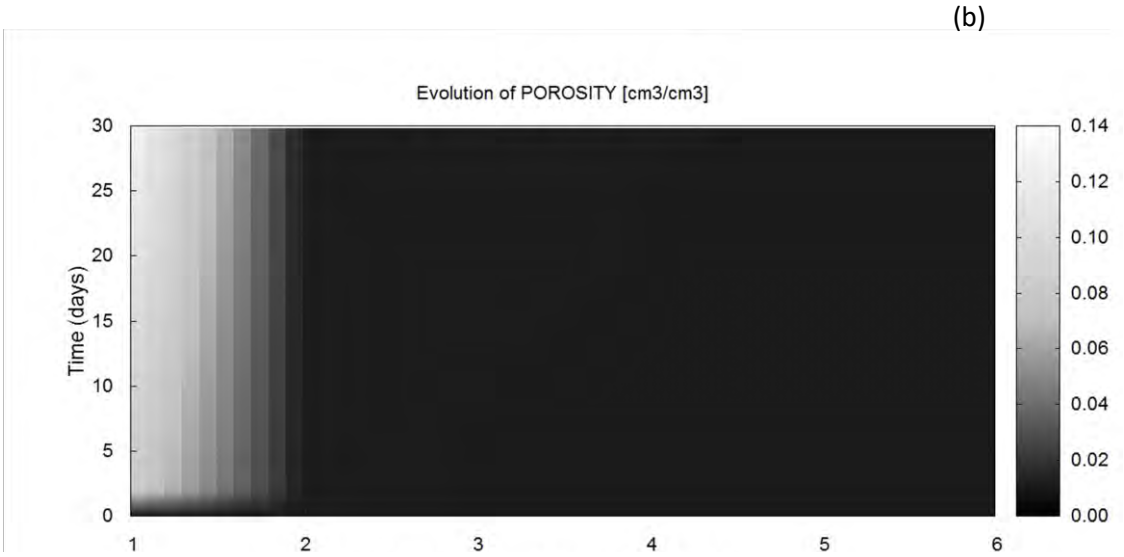

Figure 12: Calculated spatio-temporal evolution of porosity in the Soultz geothermal reservoir when using the double porosity model. The ratio of surface contact and volume contact between fractured and matrix zones are (a) 1000 and (b) 10000.

2.4 Discussion

2.4.1 Single porosity model

The modelling of the acid stimulation in different scenarios reveals that the evolution of porosity and permeability of the Soultz geothermal reservoir in direct contact with the injection well are significantly influenced by the Darcy velocities and the initial conditions of the acid solutions used. The modelling analysis results indicate that mineralogical transformations of minerals within the system controlled the evolution of the geothermal reservoir during the acid stimulation. These transformations are mainly related to the dissolution of minerals such as calcite and anorthite and to the precipitation of secondary formed minerals such as beidellite. The zone in direct contact with the injected acid solution is mostly open. The porosity increases from the initial value of 0.05 to a value of 0.35, similar to the modelling case where the volume of the injected acid solution increased two-fold. However, the impacted zone is always limited to a few metres around the injected acid stimulation.

It is recognized that the dissolution of primary minerals is governed by numerous factors that can have direct impacts on the dissolution of minerals. For example, in the case of calcite, its dissolution rate is controlled by many parameters, including the dissolution constant, the reactive surface area, the pH of the aqueous solution, and the temperature. In the current study, only a few scenarios are reported in detail. We can learn various lessons from these tests. The strong reaction rate of the interaction between the HCl solution and calcite induces an intense mineralogical transformation and therefore an important increase of porosity in the zone close to the acid injection well. However, this in turn limits the diffusion of the acid solution towards deeper zones of the system. The porosity decrease in the rest of the system is, therefore, a secondary effect that is not expected at all.

We can therefore acknowledge the key role of the Darcy velocity of the acid stimulation on the evolution of the geothermal reservoir at the end of the simulation. Unfortunately, the acid stimulation also induced temporal and local closing of the system because of the strong precipitation of secondary minerals. It is clear that a strong acid such as HCl, in combination with a low flow rate, produces not only many reaction products near the acid injected well in a short time but also causes these products to accumulate due to poor hydraulic conditions. In addition, precipitation of less soluble minerals will occur in the rest of the system. For future attempts at acid stimulation, on one hand, the accumulation of reaction products needs to be avoided, but on the other hand, a certain contact time for mineral dissolution is required for optimal efficiency.

2.4.2 Double porosity model

The use of the double porosity model shows a clear difference in the evolution of the porosity at the end of the simulation. The analysis of the porosity profile confirms the higher increase of porosity in the zone in direct contact with the injected acid solution.

In this modelling study, the initial volumes of calcite present in the geothermal reservoir are 0.3% and 3.9% for the matrix and fracture, respectively. The initial quantity in the fracture is in the range of those reported in the literature for the Soultz geothermal reservoir (e.g., Ledésert et al., 2009, 2010; Hébert et al., 2010). The literature review also shows that the mineralogical composition of the Soultz

geothermal reservoir is very heterogeneous and there is a large range of carbonate present in the reservoir. It is found that the carbonate's quantity in the fractures strongly depends on the interaction of the brine solution and the geothermal reservoir. Unfortunately, the precise determination of the mineralogical composition of the geothermal reservoir is a great challenge. Therefore, the amount of calcite used in the present study was selected to be in the range found from the literature review (e.g., Ledésert et al., 2009, 2010; Hébert et al., 2010).

Furthermore, the initial porosity of the system is potentially important for the modelling outputs. However, with the very limited availability of data, we have to assume that the porosity values in the matrix and fractures zones are 10% and 1%, respectively, in a simplified conceptual system. We acknowledge that these values are questionable compared to the variability of the Soultz geothermal reservoir. Nevertheless, the modelling results suggest that the accuracy in the determination of the input data for the Soultz geothermal reservoir and the real conditions of the system may control the modelling results of the evolution of the geothermal reservoir after acid stimulation. The experimental determination of the initial conditions related to the Soultz geothermal reservoir is still very limited, but this is expected to improve the quality of the modelling work, especially in the framework of the enhanced geothermal system.

2.4.3 The choice of acid solution

HCl acid is strong, effective, inexpensive, temperature stable, and its reaction rate increases with temperature. However, this acid may have several negative aspects in terms of the reactions. In the context of the Soultz geothermal system, it can be found from this modelling work that unwelcome secondary reactions are produced. This can happen when highly concentrated HCl is used or if low flow rate conditions are applied to the acid stimulation. The precipitation of secondary formed minerals can reduce the positive achievements of chemical stimulation.

In the last several years, public interest and discussion concerning the environmental impacts of chemical treatment in deep-seated formations has grown. This leads to an increasing amount of demand for mining and water authorities to use environmentally friendly and biodegradable chemicals. In addition, the demand for highly sophisticated chemical mixtures that are able to target different types of minerals is continuously attributed to the management of geothermal systems. Recently, environmentally friendly and biodegradable acids and chelating agents are increasingly used for acidizing operations, especially in the areas where wells are shallow or close to water protection areas (GEIE EMC, 2017). However, this is not the case for the Soultz geothermal system. The new formulations of chemical mixtures are very effective, combining acids and chelating agents, or even chemical systems at a moderate pH that do not contain acids. Their ability to dissolve various minerals such as sulfates, sulfides, clay minerals and carbonates make them unique and thus, they are appropriate for unconventional reservoir acidizing. Their successful application in the Upper Rhine Graben have already been shown (Lummer et al., 2015, Baujard et al., 2017).

The literature review shows that acid stimulation usually affects the near-field region around the well. In the Soultz geothermal reservoir, it is considered to reach a maximum diameter of 6 metres around the well. Since chemical stimulations often apply to a small volume compared to hydraulic stimulations, they would not affect reservoir volumes as much as hydraulic stimulation. The positive achievement for the near-field region around the well obtained from the acid stimulation is then considered as a "door-opener" that prepares slightly permeable fracture zones for further hydraulic

stimulation. The GPK-4 injection well has not been put into full operation yet due to its low injectivity. Therefore, the successful application of acid stimulation in this injection well could result in an increase of power plant economics and would further lower the potential for induced seismicity related to brine circulation.

2.5 Conclusions

The modelling of acid stimulation in the Soultz geothermal reservoir was conducted by using the KIRMAT code. The acid stimulation of the Soultz system was built with the assumption that the GKP-4 injection well and a simple acid such as HCl were chosen for the coming stimulation campaign. The calculation was simulated by two types of models: the single porosity and double porosity models.

In the single porosity model, the simulated results for the reference case explored an increase in porosity, resulting from a strong dissolution of the primary minerals such as calcite and anorthite in the zone around the acid-injected well. However, there is also a precipitation of secondary minerals such as beidellite, which leads to a porosity decrease in the rest of the system. It is concluded that the evolution of porosity and permeability in the Soultz system is mainly impacted by the dissolution of primary minerals, especially for a strong transformation of calcite and anorthite and for the formation of second minerals such as beidellite. The modelling results obtained from the sensitivity study cases show the significant impacts of the Darcy velocity, the initial concentration of the used acid, the duration of the injection and the initially presented calcite amount, and especially, the changes in porosity and the mineralogical transformation in the zone around the acid-injected well. The higher concentration of the HCl solution also increased the dissolution of the primary minerals and subsequently produced a stronger increase of the porosity in the zone around the injection well. It was further found that when applying a highly concentrated HCl solution, unwelcome secondary reactions are strongly produced. This unexpected precipitation reduces the positive achievements of chemical stimulation. Additionally, the quick reaction between the HCl solution and the primary minerals in the system limit the transport of the acid solution into further zones of the system, and this resulted in a very narrowly impacted zone around the acid-injected well.

The use of the double porosity model indicates a significant difference in the evolution of porosity in the system. The strong opening of the porosity is also mainly related to the dissolution of calcite and the formation of secondary minerals. The comparison of the modelling results by the single porosity and double porosity models confirm that the impacted zone is limited to a few metres around the acid-injected well.

Numerous factors were found to have impacts on the modelling outputs of the acid stimulation. The accuracy of the predicted results is likely related to possessing accurate knowledge about the conditions of the Soultz geothermal reservoir. Even though various experimental and modelling works have been carried out, the determination in situ of the reservoir is still very limited due to various challenges. In the future, more knowledge of the geothermal reservoir is needed to improve the accuracy of the modelling output.

B. Soultz-sous-Forêts: GPK-4 monitoring

3 GPK-4 hydraulic characteristics monitoring

This section corresponds, additionally, to confirmation of MS28 and takes the place of that document.

3.1 Update of hydraulic characteristics under operation

Since January 2017, the production flowrate has varied between 27-28 kg/s until April 2018, 31-32 kg/s between April 2018 and January 2019 and around 25 kg/s since then (Figure 1).

In parallel, continuous re-injection has been performed into the wells GPK-3 and GPK-4 since January 2017. Over the period covered by this report (January 2017 to February 2020), the injection into GPK-4 was stopped five times as shown on Figure 2:

- In May 2017: maintenance period,
- In September 2017: maintenance period,
- In April 2018: maintenance period,
- In January-February 2019: problem with the production pump,
- In September 2019: maintenance period

During the simultaneous injection, GPK-3 injection flowrate varied between 14 kg/s (mostly in 2019) and a maximum of 22-23 kg/s. Consequently, GPK-4 injection flowrate in normal operating conditions varied between 8 and 12 kg/s for a maximum observed wellhead pressure of 21.8 bar at 12 kg/s (Figure 23). Since April 2019, the flowrate has been set up at an average of 11 kg/s. Injection has still been performed through the surface pressure delivered by the production pump (~22 - 22.5 bar).

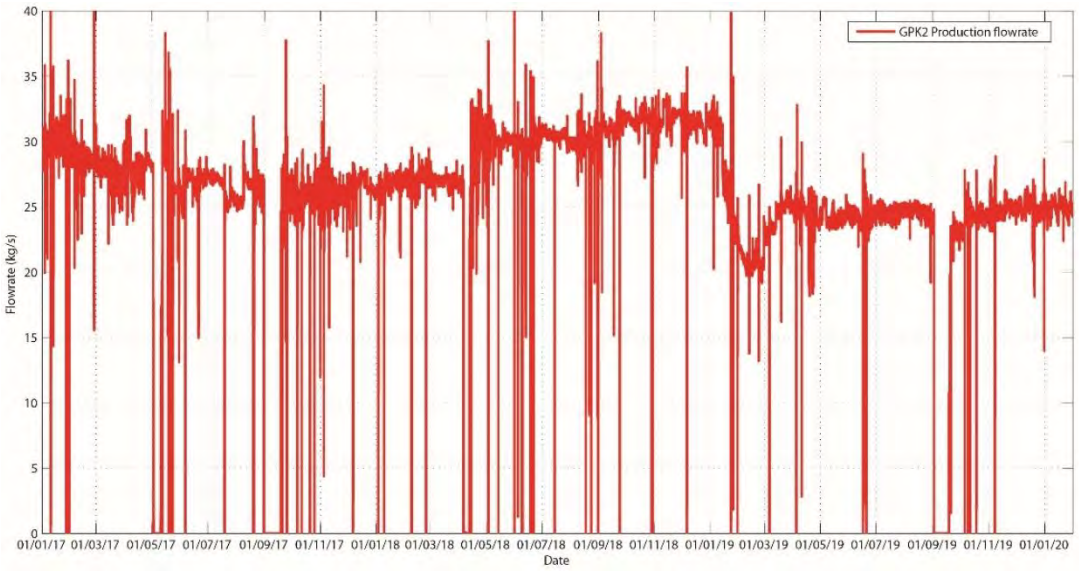

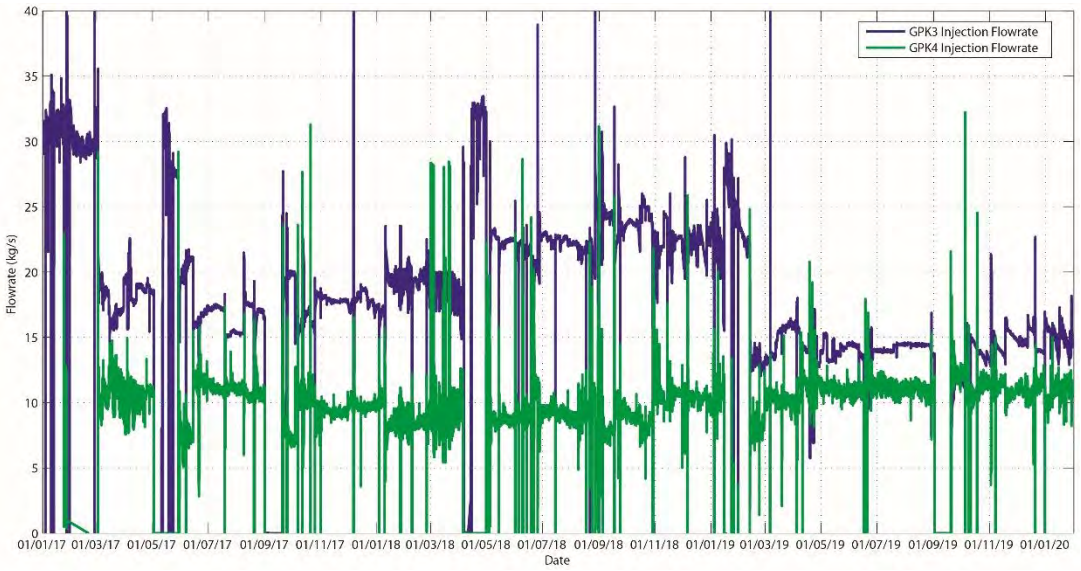

Figure 23: Production and injection flowrates at the Soultz-sous-Forêts power plant between January 2017 and February 2020 (Confidential data). Top: GPK-2 production flowrate (red curve); Bottom: GPK-3 (blue curve) and GPK-4 (green curve) injection flowrates.

3.2 Evolution of GPK-4 injectivity index

The monitoring of the evolution of GPK-4 injectivity index has been continued over the whole period covered by the DESTRESS project.

The following procedure was used to estimate the injectivity index: we plotted the data in a graph showing the differential pressure (measured GPK-4 wellhead pressure minus GPK-4 equilibrium pressure of 1 bar) as a function of the injection flowrate at a given time. 1984 couples of data (flowrate, differential pressure) over 35 months (March 2017 – February 2020) were used in the estimation. The results are shown in Figure 14.

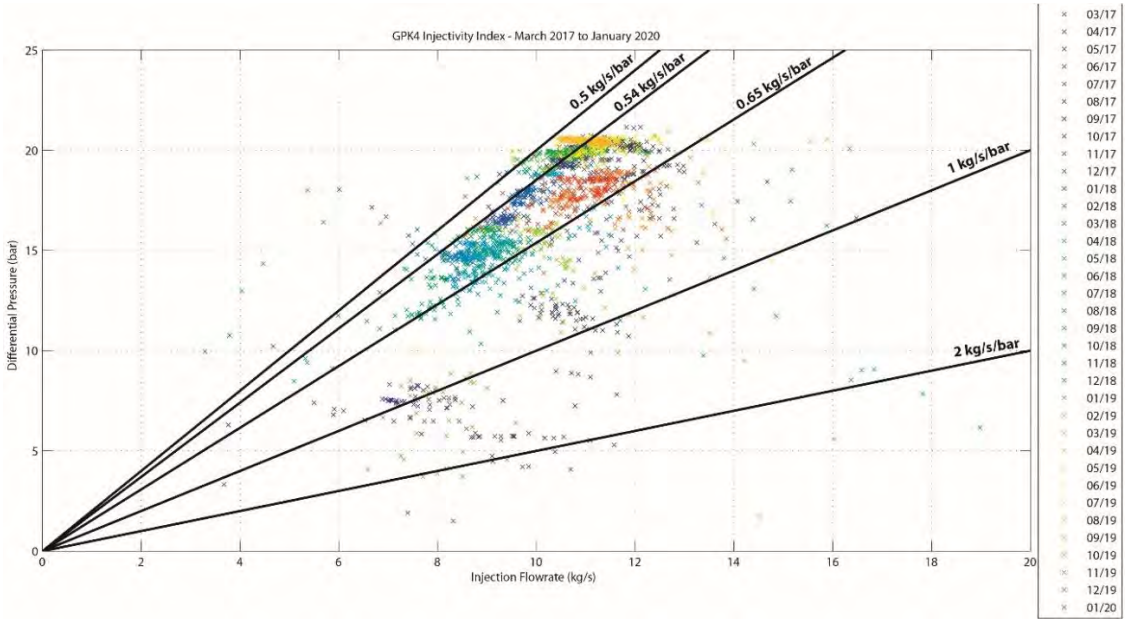

Figure 14: Estimates of GPK-4 injectivity index based on injection data from January 2017 to February 2020. The black lines show several values of injectivity from 0.5 kg/s/bar to 2 kg/s/bar. Color of the crosses corresponds to the date.

The data show a large spread over a wide interval of injectivity values between less than 0.5 kg/s/bar to more than 2 kg/s/bar. The effect of transient behavior after prolonged stop of injection can explain this large range of injectivity values. For instance, most of the sparse values around 1 kg/s/bar and those falling between 1 kg/s/bar and 2 kg/s/bar correspond to the periods immediately following GPK-4 injection shutdowns described in chapter A (1.1).

As shown on Figure 14, most of the injectivity values recorded under stable and permanent injection conditions seems to be comprised between **0.5 kg/s/bar and 0.65 kg/s/bar**. Furthermore, if we except a few values from December 2018 – January 2019 (dark green colors) and from July 2019 – September 2019 (light orange colors), GPK-4 injectivity index seems to be bounded by **a lower limit of 0.54 kg/s/bar and an upper limit of 0.65 kg/s/bar**. This looks valid for permanent flowrates between 8 kg/s to 12 kg/s, and pressure from ~13 to 21 bar. The latest values, i.e., from September 2019 to end of January 2020 (orange to red colors) fall in that range and looks closer to the upper limit. GPK-4 injectivity index observed after the chemical stimulation performed in December 2019 (red colors) will be discussed in detail in chapter B (5).

Figure presents the evolution of GPK-4 injectivity index from March 2017 to February 2020, covering 35 months of continuous monitoring. The figure confirms that most of injectivity values range between 0.54 and 0.65 kg/s/bar. However, in between these limits, we can observe quite a large spectrum of injectivity values and different behaviors. For example, in March, June and October 2017, after the transient period, the injectivity index falls quickly to 0.54 kg/s/bar. In February-March 2019, the injectivity falls also to the same value, but after a much longer time. On the contrary after the injection shutdowns in April 2018 and September 2019, the injectivity seems to stabilize at a higher value.

The last reliable estimate (September- February 2020), based on the latest observed values, reaches ~0.62 kg/s/bar. However, as observed between May and September 2018, such a value was already reached, before decreasing to around 0.54 kg/s/bar and even lower afterwards. The current value estimated after the chemical stimulation thus remains uncertain (see chapter B(5)). It also indicates that the evolution of GPK-4 injectivity index needs to be monitored for a longer time, possibly without prolongated injection shutdown, to assess a reliable value.

All the observed variations are nevertheless significantly small and thus, difficult to explain, as they may be related to several parameters, such as injection temperature, fluid density, status of the borehole. The question of the flow and pressure sensors sensitivity and calibration can even be addressed.

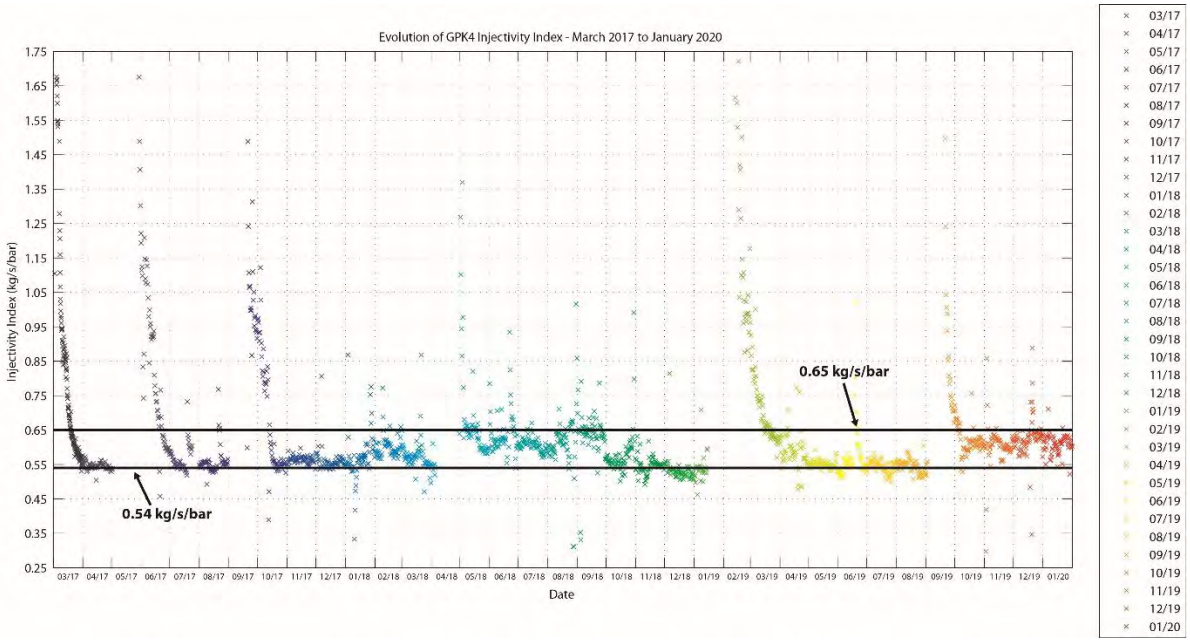

Figure 15: Evolution of GPK-4 injectivity index with time from March 2017 to February 2020. The black lines indicate the lower and upper limits of best-estimated injectivity values. Color of the crosses indicates the date.

4 Chemical Monitoring

4.1 Recent chemical monitoring under operation

Continuous chemical monitoring is applied to ensure a follow-up of the physical and chemical parameters of the geothermal brine produced and reinjected at the Soultz-sous-Forêts power plant. A complete baseline survey (chemical and physical) has been undertaken in September 2018 and January 2019.

Physical parameters of the geothermal brine produced at GPK-2 well are given in Figure . Electrical conductivity and pH have been measured at an average temperature of about 60°C. Both parameters are monitored using a multimeter tool and dedicated sensors. Electrical conductivity is constant over time, about 116 mS/cm in average. pH is quite constant as well. A few variations could be observed due to sampling temperature differences. Measurements at 65°C exactly give a pH value of 5.3.

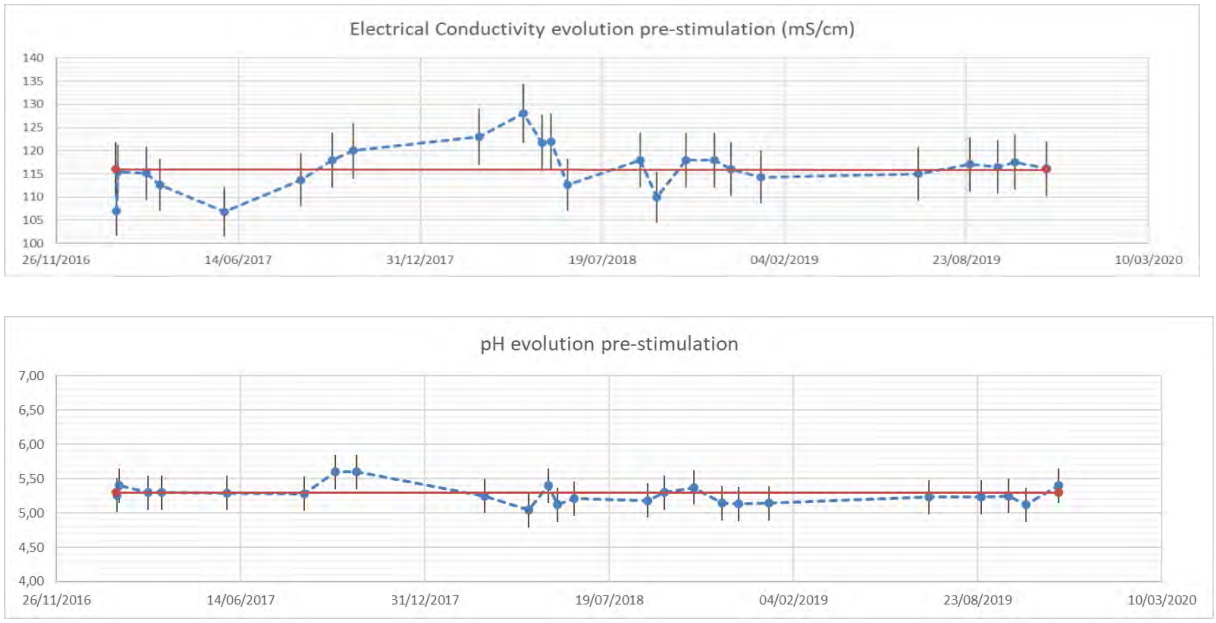

Figure 16: Electrical conductivity (up) and pH (down) monitoring of geothermal brine at production wellhead from 2016 to 2019. Red lines give pH and conductivity average values. Error bars represent 10% uncertainties for field measurements.

Early 2020, physico-chemical monitoring highlighted pH and electrical conductivity values in agreement with pre-stimulation monitoring values (Mouchot et al., 2020).

Geothermal brines from production wellhead and before reinjection wellhead are both monitored. Two types of sampling have been performed:

- One based on under pressure fluid sample, which is then depressurized in order to separate gas from liquid phases enabling to assess the gas liquid ratio. The gas phase is trapped in a vessel and sent to a lab for NCG analysis by Gas Chromatograph Mass-Spectrometry (GC-MS). The liquid phase is sent to another lab to perform a chemical analysis by Inductively Coupled Plasma Mass-Spectrometry (ICP-MS).

  The Gas-Liquid Ratio (GLR) was measured in April 2019 close to GPK-2 and GPK-3 wellheads. The geothermal fluid has been sampled using a small heat exchanger in a by-pass system to cool down the geothermal fluid at a constant flow rate. Flow rate, temperature and pressure

are monitored continuously. For the gas sampling, the fluid goes through a vessel and separates into two phases: liquid and gas. The gas phase is then cooled down to condensate any H_2O vapor. A vial is connected to this device for measuring flow and trapping non-condensable gases (NCG) to be analyzed. NCG are then analyzed in an external lab with a GC-MS. At both production and injection sides, GLR is about 1.02 m^3/m^3 corrected to standardized conditions. The gas content is presented in Figure 6: it shows a high content of CO_2, around 90% of the total dissolved gases, into GPK-2 brine (P=24 bars, T=150°C) and GPK-3 brine (P=24 bars, T=65°C).

- Another one based on a gas sample taken from the degasser at GPK-3 wellhead. This sample is also sent to a lab for NCG analysis by GC-MS.

  At the GPK-3 wellhead, emitted gases have been sampled from a degasser (gas phase only) given the third point of analyze (Figure). The fluid pressure and temperature conditions at this point are about 2 bars and 65°C respectively, and results of analyses highlight a higher content of Methane and Helium. Nitrogen and Carbon dioxide reach about 44% and 47% of the total dissolved gases respectively.

Figure 17: Gas sampling at GPK-3 wellhead degasser. April 2019

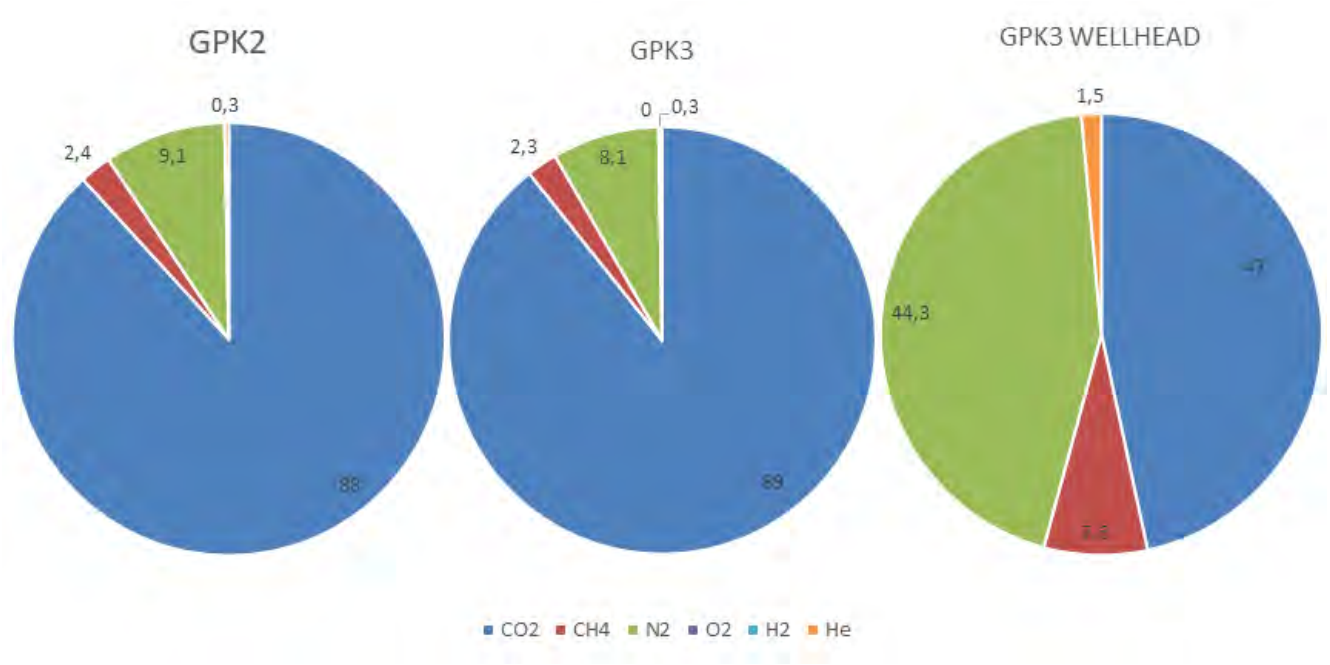

Figure 18: Comparison of Gas analyses at the Soultz wells. April 2019

Figure and Figure present the chemistry evolution over time of the brine produced at GPK-2 and the brine reinjected into GPK-3/-4 respectively (compilation of ICP-MS data from lab 1, Mouchot et al., 2018, Mouchot et al., 2019, Jähnichen et al., 2019). From a general point of view, chemistry is constant over time and from production to injection (no effect of the process). Some trends can be observed: Sb and Pb content have been slightly increasing for both GPK-2 and GPK-3 brine analyses over time.

Elementary geochemical analyses have been performed over the years and during exploitation and thus by different labs. Table presents the results of ICP-MS analyses of GPK-2 brine (sampled under same conditions). Analyses from lab 1 are published in Scheiber et al., 2013, and are taken as reference for comparison with the others. Since 2013, lab 1 has performed many fluid sampling and analyses within the frame of a German public funded project for scaling inhibition purposes. Reference data from 2013 are compared to the average of datasets acquired and analyzed between 2013 and 2018 by this same lab. It highlights the stability of brine chemistry for a Total Dissolved Solid (TDS) content of about 94-99 g/L (Mouchot et al., 2019). The analyses of lab 2 are quite in agreement with the reference data, showing a TDS content of about 95 g/L and less than 20% variation for each species in general (DESTRESS M18 report). However, in the lab 3 analyses, many differences can be observed, regarding lab 1 reference dataset. To sum up, the salinity of the fluid is about 77 g/L, considering the amount of each element. The measurement uncertainties from lab 3 analyses are far too high to give reliable results for accurate chemical monitoring. Dataset from lab 4 shows reliable results, except for some elements: for example, a significant decrease of Ba and SO_4 can be noticed. This could be explained either by the precipitation of barium sulfate between the time of sampling and the time of analyses, or by real changes in the brine chemistry from reservoir. To remove any doubt and to confirm the best-practices, chemical monitoring should be performed by specialized labs, able to manage such highly saline fluid, at least once a year.

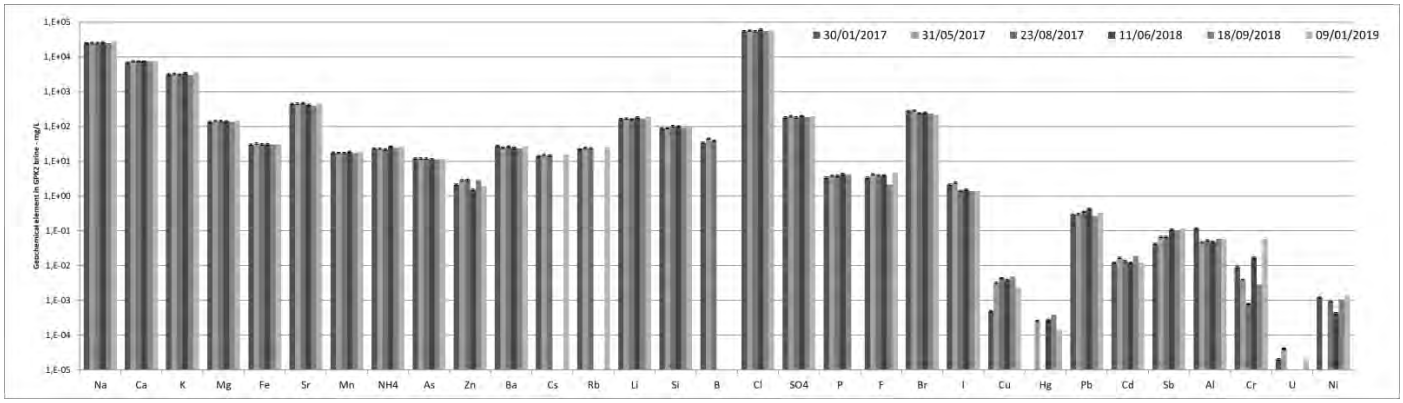

Figure 19: Evolution of chemical elements in GPK-2 brine during exploitation

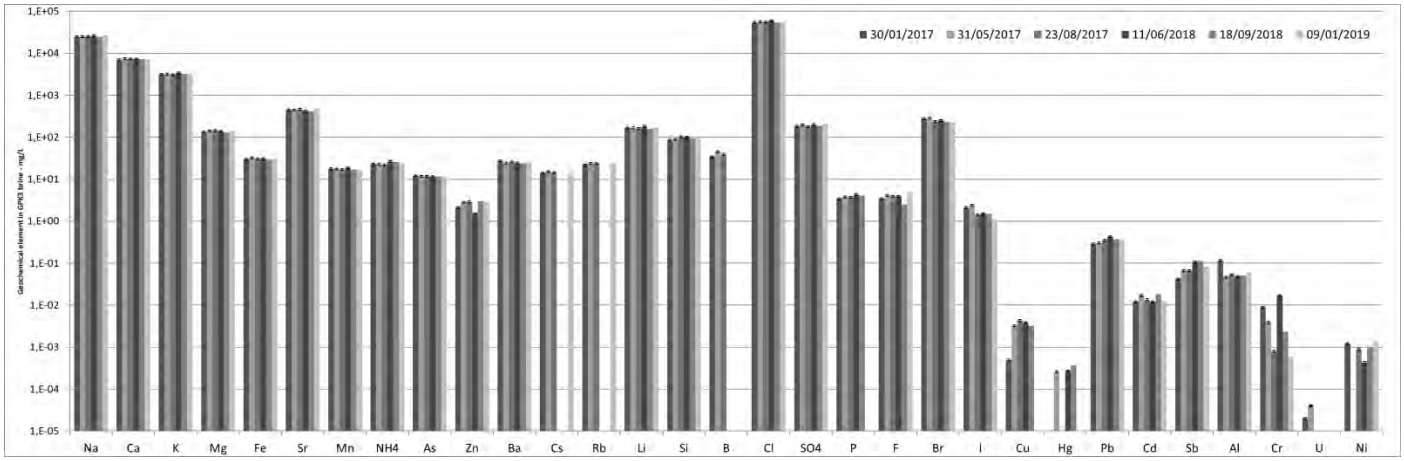

Figure 20: Evolution of chemical elements in GPK-3 brine during exploitation

In January 2020, a new sampling campaign has been performed, notably to assess if any change could have occurred after GPK-4 chemical stimulation.

Table 6: ICP-MS analyses of GPK-2 brine: comparison of lab results

(mg/L)	(2013) lab 1	(2017) lab 2	DEV.	(2018) lab 3	DEV.	(2018) lab 4	DEV.	(average 2013-2018) lab 1	DEV.
Na	25200	26200	4%	21400	-15%	27275	8%	25400	1%
Ca	7440	7200	-3%	6380	-14%	7185	-3%	7477	0%
K	3360	3700	10%	3830	14%	3122	-7%	3227	-4%
Mg	142	120	-15%	46	-68%	130	-8%	139	-2%
Fe	30	27	-10%	4	-87%	27	-10%	31	3%
Sr	418	480	15%	615	47%	382	-9%	432	3%
Mn	18	17	-6%	3	-83%	16	-11%	18	0%
As	11	10	-9%	8	-27%	9	-18%	11	0%
Zn	3	3,5	17%	0	-93%	2	-27%	3	0%
Ba	26	21	-19%	24	-8%	6	-77%	26	0%
Li	169	120	-29%	354	109%	152	-10%	172	2%
Cl	57300	57000	-1%	41100	-28%	56456	-1%	57444	0%
SO4	228	79	-65%	210	-8%	107	-53%	201	-12%
Br	237	200	-16%	230	-3%		-100%	252	6%
Pb	0,066	0,8	1112%	0,02	-70%	0,2	203%	0,16	142%

The next gas monitoring survey will be performed mid-2020, but not in the framework of Destress.

C. Soultz-sous-Forêts: GPK-4 soft chemical stimulation

1 Soft Chemical Stimulation concept

1.1 GPK-4 integrity and flow logs

In order to better define the stimulation concept, the well GPK-4 was logged in January 2019. The aim was to gather information on the well integrity and on permeable zones in the well, in order to better define the injection methodology and target zones for stimulation.

The logging consisted in a multifinger caliper, gamma ray, CCL, ABI, CBL/VDL and flow log. The flow and temperature logs allowed to identify leakage points in the cemented part of the cased hole and permeable ones in the open hole. The ultrasonic (ABI), caliper and CBL/VDL logs confirmed the damages identified in the flow log and help determining the criticality of the potential acid injection in those zones. Figure shows the well completion with the identified leakage zones and the associated log images:

- The first leakage zone at 4 376 mMD is assumed to take about 50% of the injection flowrate. But the damage is too severe and thus, the risk for the well integrity is too high to envisage an acid injection in that zone.
- The second leakage zone at around 4 700 mMD is assumed to take about 40% of the injection flowrate. The integrity of the casing and the cement quality is good enough to envisage an acid injection in that zone.
- The Open Hole is assumed to take the last 10% of the flowrate. There is a priori no blocking point for acid injection in that zone.

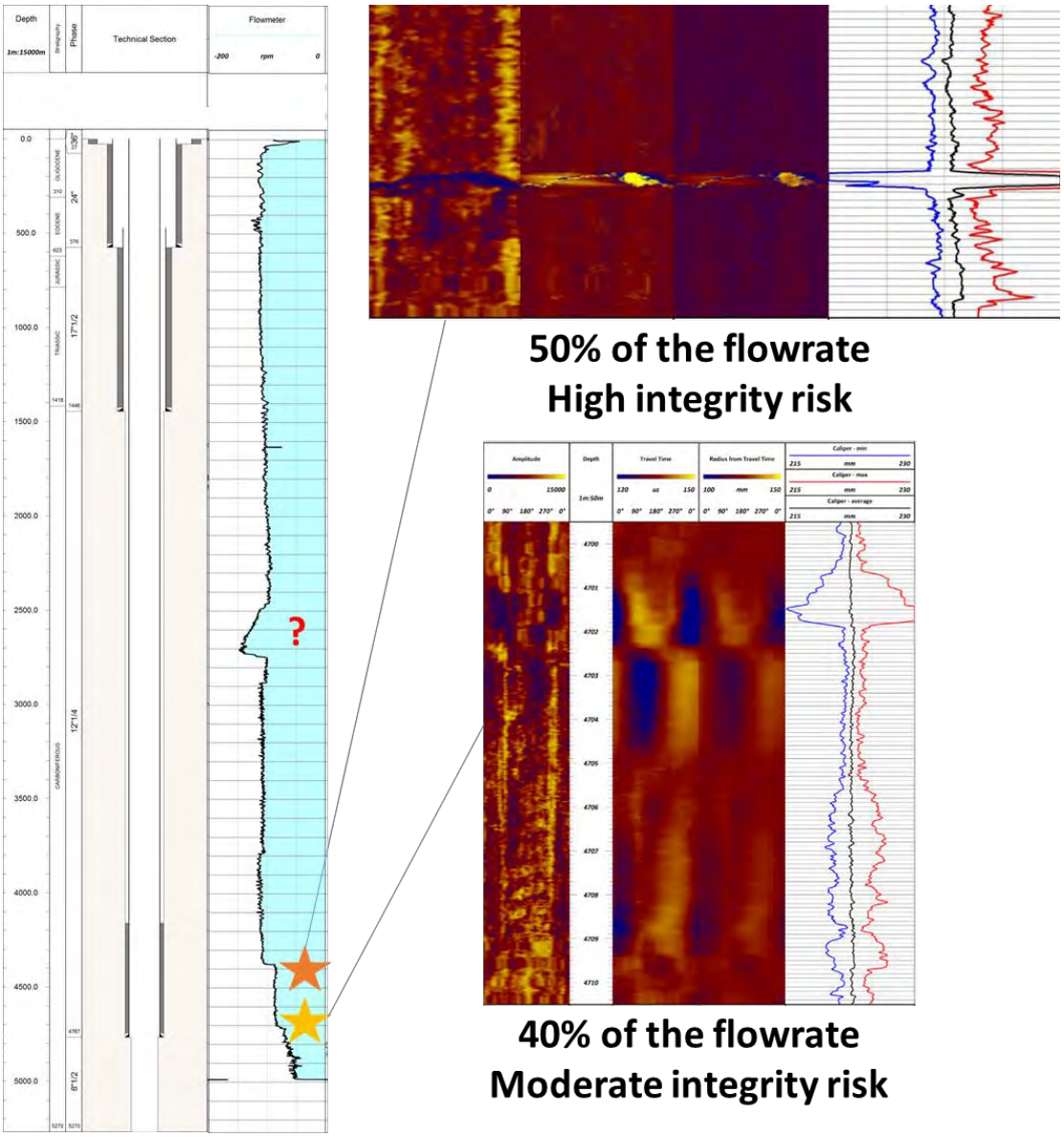

Figure 21 : GPK-4 casing integrity logs and interpretations.

1.2 Target zones selection

Based on the logging data presented in the last section, three different zones have been selected considering the observed injection flowrate, the geology and the corresponding borehole images that allowed identifying the related fracture zones, fillings and minerals. Two of them are in the Open Hole section and the last one is the deepest leakage zone in the cemented part of the casing at 4 700 mMD. The top leakage zone at 4 376 mMD has been considered to be too risky for a potential acid injection, so it has been excluded from the potential target zones.

Table presents the selected zones and their characteristics such as thickness, flow contribution, fillings, etc.

Table 7: Stimulation zones identification and characterization.

Depth Casing/OH	Estimated Fracture zone size in m	Alteration thickness in m	Flow contribution in %	Mineral 1 to dissolve: Carbonate (calcite mainly)	Mineral 2 to dissolve: Clays	Mineral 3 to dissolve (possible): Quartz
Zone 1: 4707 m MD casing	About 400 m of lateral extension Large fracture zone	20 m	40%	Low carbonate content (3.5%)	Illite and Illite / Smectite interstratified	Secondary quartz
Zone 2: 4823 m MD OH	Minimum 150-200m of lateral extension Medium size	6 m	5%	Low carbonate content (4.6%)	Illite and Illite / Smectite interstratified	Secondary quartz
Zone 3: 4924 m MD OH	Minimum 100-150m of lateral extension Medium size	2 m	5%	High carbonate content (17.8%)	Illite and Illite / Smectite interstratified	Secondary quartz

1.3 Stimulation methodology

In order to avoid any acid injection in the wrong zone of the casing, it has been decided to realize the stimulation using a Coiled Tubing. This technology uses a steel tubing with a 2" diameter and a total length of 6 km, coiled on a drum and controlled by a winch, which can be deployed at the desired depth and moved up and down during the injections.

This methodology allows to inject deeper than the risky leakage zone (4 376 mMD) in order not to inject in that zone. The injection at depth also allows to prevent the acid to be in prolonged contact with the casing from the wellhead down to the casing shoe and with the scalings already present inside the casing.

Use of coiled tubing is a good alternative for deep injection because it is easy to rig up, fast and less expensive than a workover rig. Another envisaged solution was the “under packer injection” but the integrity of the casing has been considered too low for safe packer jobs. Figure shows the setup of the coiled tubing.

From a methodological point of view, another challenge of the operation consisted in the injection scheme: as the top leakage zone takes about half of the injection flow, it is necessary to have at least the same flowrate injected through the annulus of the coiled tubing from the wellhead, as the flowrate injected through the coiled tubing itself. Doing so, the acid injected through the coiled tubing at 4 700 mMD is constrained by the annulus flow to stay in the deeper section of the well (no upward flow) and to be injected in the open hole or in the deeper leakage zone at 4 707 mMD.

It has been decided to perform the annulus injection using geothermal water. In fact, the stimulation scheme didn’t plan any stop of the production of the powerplant. In nominal plant operation, GPK-4 injection flowrate is around 10 L/s with 20 bar of surface injection pressure. During the stimulation, the easiest way to inject through the annulus is to set the geothermal injection flowrate to 5 L/s and perform a 5 L/s acid injection through the Coiled Tubing at the same time. In that way, the injection pressure of 20 bar delivered by GPK-2 production pump is conserved and the acid can’t flow upward while released in the well.

Figure 22: Setup of the coiled tubing in the wellhead of GPK-4, from the coiled tubing unit on the left to the coiled tubing frame on the right.

Based on the target zone selection and on the corresponding geological data presented in the Table , the most effective acid has been selected. Lab tests were realized by the acid providing service company in the past on Soultz cores, which showed that their acids are very effective at dissolving Calcite and Quartz. Figure 23 shows the results of a dissolution test. Based on those studies, the first product can dissolve 54 kg of Calcite ($CaCO_3$) with 1 m^3 of acid and 5 kg of $Al_4(Si_4O_{10})(OH)_8$ (Kaolinite) and 13 kg of SiO_2 (Quartz) with 1 m^3 of the 2nd acid. The injection scheme was designed to prevent precipitation reactions between the geothermal fluid and the acid in the near wellbore region.

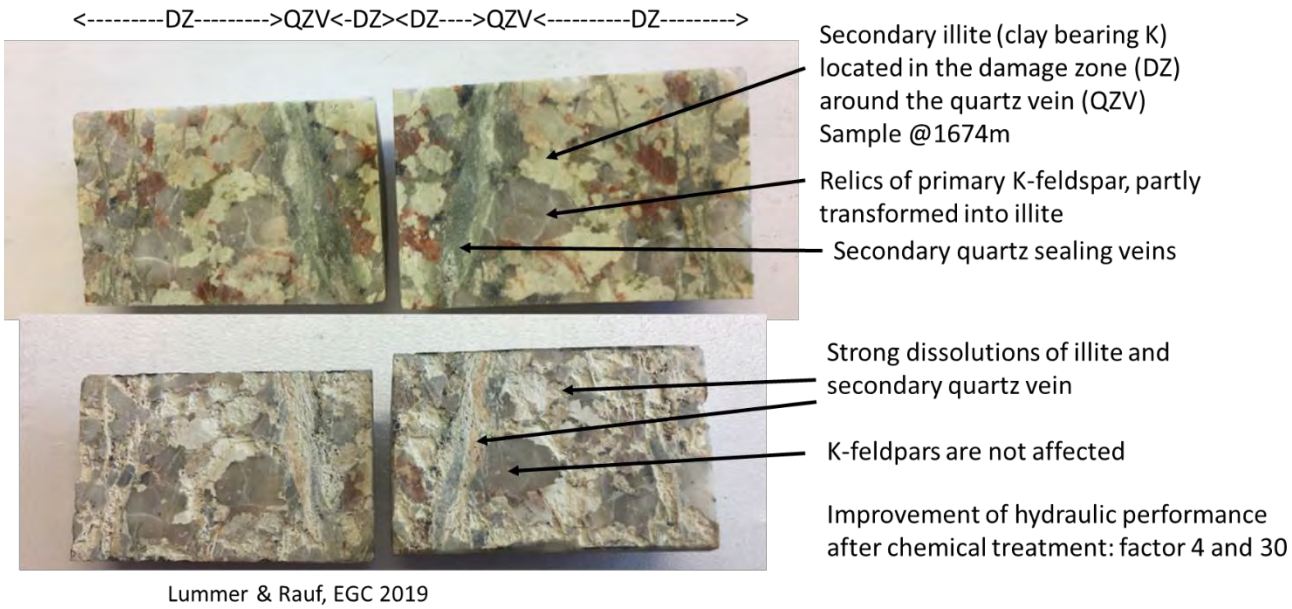

Figure 23: Results of lab tests on Soultz cores showing the effect of the acids planned to be used in GPK-4.

2 Risk Analysis

In order to avoid any trouble/damage/injury during the operation, a risk analysis has been done for HSE and risks related to the interaction between the coiled tubing and the powerplant operations. The risk analysis process has been developed in the framework of the Destress project's WP3.1 (Peterschmitt et al., 2018). It consists in a succession of risk identification, risk analysis, risk evaluation and mitigation. Figure presents the general concept of the applied risk assessment

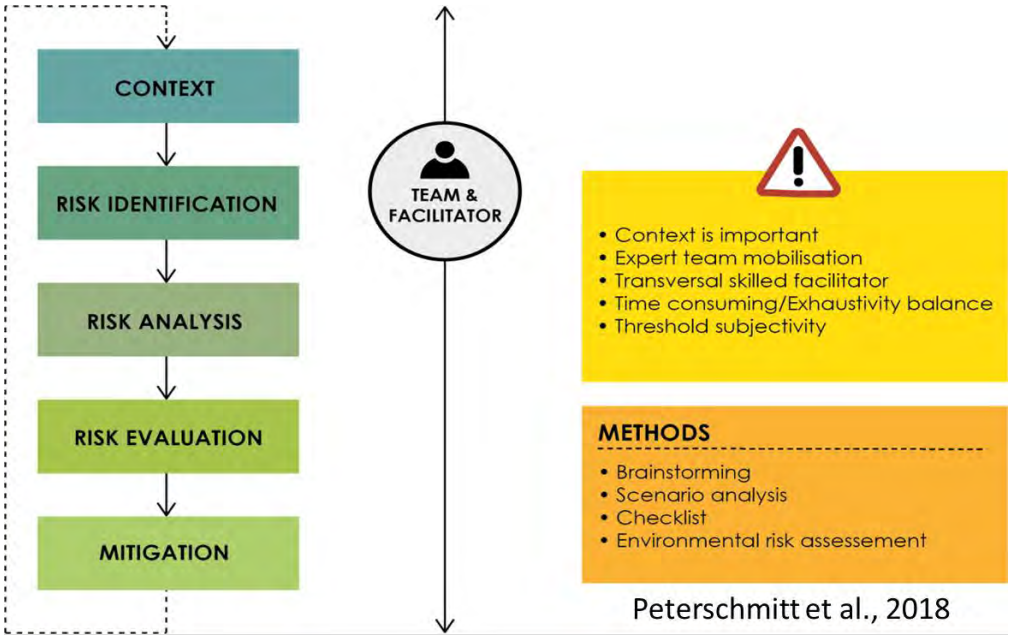

Figure 24: General risk assessment concept.

The same protocol has been applied on the chemical stimulation performed on Illkirch geothermal borehole for the Destress project ‘s Milestone 7. Figure presents the associated deliverable.


DESTRESS
Demonstration of soft stimulation treatments of geothermal reservoirs

Soft stimulation risk management guidelines and workflows

Milestone 7: MS7

The Illkirch geothermal drilling site, France ©ES

Authors

Genter Albert (ES-Géothermie), Hehn Régis (ES-Géothermie)

Publication Date

28.06.2019

This project has received funding from the European Union's Horizon 2020 research and innovation programme under grant agreement No 691728

Figure 25: Milestone 7 on risk assessment of the chemical stimulation of Illkirch geothermal well.

2.1 Expert meeting and site visit

In order to proceed to risk identification and to find directly the mitigation measures, a technical site visit has been organized with representatives of the Coiled Tubing and Chemical service company. This site visit gave the opportunity to discuss the following points:

- Location plan of the equipment onsite (Figure)
- Companies' electricity needs and supply points
- Water needs, supply capacity and points
- Grounding of equipment
- Safety assembly points
- Availability of crane and forklift
- Water segregation and safety equipment
- Etc.

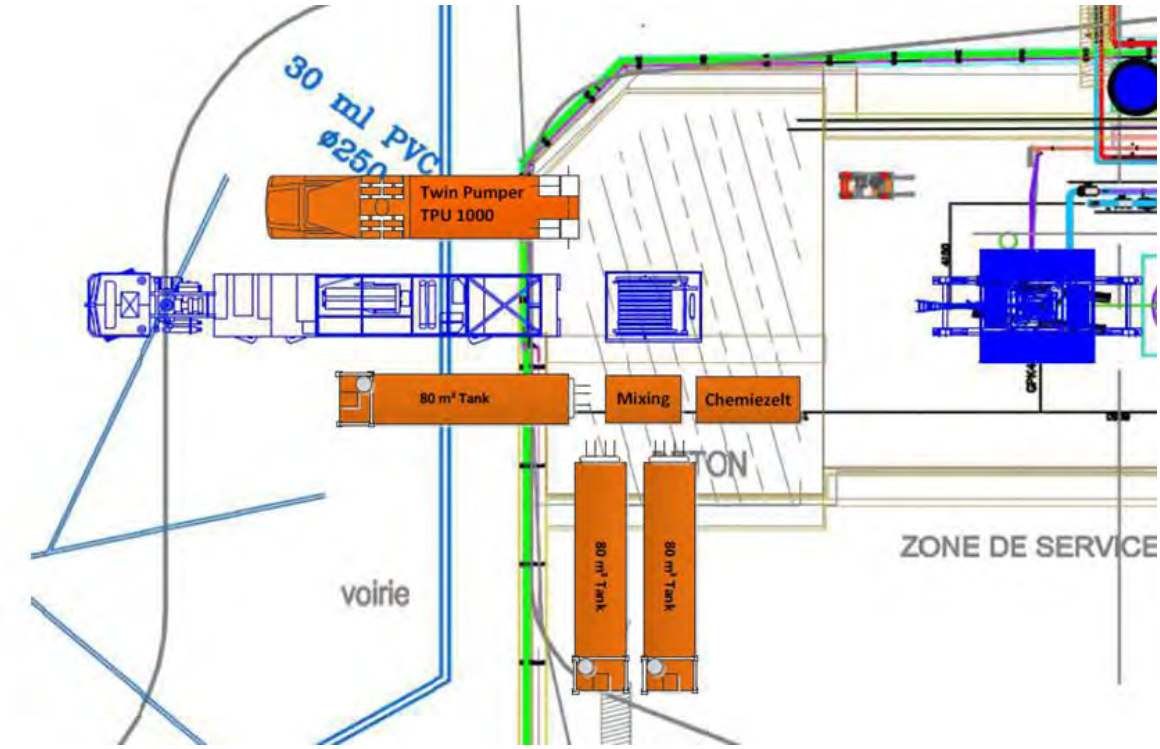

Figure 26: Location plan for the operation. Acid injection equipment in orange, coiled tubing equipment in blue.

2.2 HSE risks

During the technical site visit, 28 HSE risks have been identified and assessed. Those risks have been analyzed and evaluated based on the safety standards already in use onsite and on experts' experience. The expert group was composed of Geologists, Geochemists, Seismologists, Hydrogeologists and technical personnel in charge of Soultz powerplant operation.

From the risk analysis and evaluation, 4 major risks have been identified:

- Nuisances due to noise and vibration of pumps
- Corrosion of casing due to the acid injection
- Induced seismicity
- Personnel exposed to corrosive products on surface

Mitigation measures have been deployed in order to minimize all 28 risks and especially the 4 major ones. Another risk evaluation has been realized after the identification of the mitigation measures in order to check the final state of the HSE risk assessment for the project, that is, to be sure that the applied mitigation measures are suitable to lower the levels of identified risks. Table presents all the results of the HSE risk analysis, with the list of the risks, their analysis, evaluation, mitigation measures and final mark compared to the threshold of risk acceptability.

Figure shows the risk matrix before and after the mitigation measures identification. Finally, all risks have been considered as controlled.

Table 8: General summary of the HSE risk assessment.

								Avant mitigation			Après mitigation				
Déscription	Référence	Phase	Risque	Cause	Context de sécurité	Mesures de mitigation	Conséquence	Fréquence	Gravité	Niveau final	Fréquence	Gravité	Niveau final	Seuil	Référence
Troubles musculos-squelétiques liés au travail de bureau	R1	Design	Dommage physique	Mauvaise ergonomie du poste de travail	Suivi par la medecine du travail		Trouble musculos quelettique	2	2	4	2	2	4	7	R1
Brulure chimique due à un accident de laboratoire	R2	Design	Brulure chimique	Accident de laboratoire	Measures de sécurité et formation de la companie de services		Blessure grave	2	3	6	2	3	6	7	R2
Blessure du à un accident de laboratoire	R3	Design	Explosion et dégagement de chaleur	Accident de laboratoire	Measures de sécurité et formation de la companie de services		Blessure grave	2	3	6	2	3	6	7	R3
Accident de camion avec dommages aux infrastructures	R4	Transport	Dégâts aux infrastructures	Accident de la route	Control des permis de conduire par l'employeur et respect du code de la route et du site	Circulation de jour uniquement	Destruction des infrastructure de 1ère nécessité	1	3	3	1	3	3	7	R4
Accident de camion avec dommages corporels	R5	Transport	Dommage physique et traumatisme	Accident de la route	Control des permis de conduire par l'employeur et respect du code de la route et du site	Circulation de jour uniquement	Victimes, blessures, stress post-traumatique	1	4	4	1	4	4	7	R5
Accident de camion avec pollution des sols	R6	Transport	Dommage environmental	Accident de la route	Control des permis de conduire par l'employeur et respect du code de la route et du site	Transport des produits sous forme non active. Circulation de jour uniquement	Pollution des sol, dommage à la faune et la flore	1	2	2	1	2	2	7	R6
Accident de camion avec pollution des eaux de surface	R7	Transport	Dommage environmental	Accident de la route	Control des permis de conduire par l'employeur et respect du code de la route et du site	Transport des produits sous forme non active. Circulation de jour uniquement	Pollution des eaux de surface, dommage étendu de la faune et de la flore	1	4	4	1	3	3	7	R7
Accident de grue avec libération de produits chimiques sur la plateforme et dans l'environnement alentours	R8	Transport	Dommage environmental	Accident de levage	Control des permis du grutier par l'employeur et respect des procédures de sécurité du site	Produits disposés sur une zone drainée de la plateforme. Levage de jour uniquement	Pollution de l'environnement alentours	2	2	4	2	2	4	7	R8
Accident de grue avec libération de produits chimiques provoquant des brulures chimiques	R9	Transport	Brulure chimique	Accident de levage	Control des permis du grutier par l'employeur et respect des procédures de sécurité du site	Levage de jour uniquement. Zones de levage signalisée	Blessure grave	1	3	3	1	3	3	7	R9
Accident de grue provoquant des dommages corporels	R10	Transport	Dommage physique	Accident de levage	Control des permis du grutier par l'employeur et respect des procédures de sécurité du site	Levage de jour uniquement. Zones de levage signalisée	Victimes, blessures	1	4	4	1	4	4	7	R10
Fuite sur la zone de stockage à cause de l'endommagement d'un colis provoquant une pollution de l'environnement alentours	R11	Stockage	Dommage environmental	Conditionnement de stockage endommagé	Respect des procédures de sécurité liées au site et de la règlementation sur le stockage	Produits disposés sur une zone drainée de la plateforme	Pollution de l'environnement alentours	2	2	4	2	2	4	7	R11
Fuite sur la zone de stockage à cause de l'endommagement d'un colis provoquant des dommages corporels	R12	Stockage	Brulure chimique	Conditionnement de stockage endommagé	Respect des procédures de sécurité liées au site et de la règlementation sur le stockage	Produits entreposés dans un container	Blessure grave	1	3	3	1	3	3	7	R12
Brulure chimique due à la manipulation de l'acide	R13	Préparation	Brulure chimique	Accident manuel	Formation des opérateurs	Equipements et produits de soin immédiats adaptés aux produits présents sur site	Blessure grave	2	3	6	2	3	6	7	R13
Blessure lors de l'utilisation du coilet tubing et des packers	R14	Préparation	Dommage physique	Accident opérationnel	Formation des opérateurs, repect des procédures de sécurité du site	Pas de packer	Victimes, blessures	1	4	4	1	4	4	7	R14
Bruit et vibration des pompes et autres machines provoquant une nuisance	R15	Préparation	Nuisance par bruit et vibrations	Travaux opérationnels	Loin des habitations	Pas d'injection entre 22h et 8h. Equipements isolés phoniquement	Gêne, dérangement insupportable	3	3	9	2	2	4	7	R15
Blessure à cause de forte pression	R16	Injection d'acide	Dommage physique	Accident opérationnel	Respect des procédures de sécurité du site, Formation des opérateurs et certification des équipements	Délimitation des zones de travail	Victimes, blessures	1	4	4	1	4	4	7	R16
Brulure chimique à cause d'un accident de produit chimique sous pression	R17	Injection d'acide	Brulure chimique	Accident opérationnel	Respect des procédures de sécurité du site, Formation des opérateurs et certification des équipements	Délimitation des zones de travail	Blessure grave	1	3	3	1	3	3	7	R17
pollution de l'environnement à cause d'un accident sous pression	R18	Injection d'acide	Dommage environmental	Accident opérationnel	Respect des procédures de sécurité du site, Formation des opérateurs et certification des équipements	Produits et équipements placés sur une zone drainée la plateforme	Pollution de l'environnement alentours	1	2	2	1	2	2	7	R18
Corrosion des tubages à cause d'une mauvaise procédure d'injection, de mauvais inhibiteurs ou équipements, avec impact sur les eaux de surface	R19	Injection d'acide	Dommage environmental	Accident d'intégrité de puits	Respect des procédures d'injection	Coiled tubing pour protéger les tubages. Injection via l'annulaire en continu pour	Pollution des acquifères	3	4	12	2	3	6	7	R19
Grave accident à cause d'une remontée de gaz ou de blow out avec dommages corporels.	R20	Injection d'acide	Dommage physique	Réponse géologique inattendue	Présence d'un BOP sur le coiled tubing	Injection en continu empêchant la remontée de gaz. Présence d'un BOP	Victimes, blessures	1	4	4	1	3	3	7	R20
Grave accident à cause d'une remontée de gaz ou de blow out avec pollution de l'acquifère	R21	Injection d'acide	Dommage environmental	Accident d'intégrité de puits	Compéltion de puits adaptée et pas d'aquifère en surface	Injection en continu empêchant la remontée de gaz. Présence d'un BOP	Pollution des acquifères	1	4	4	1	3	3	7	R21
Sismicité induite à cause des pressions d'injection causant des dommages aux infrastructures.	R22	Injection d'acide	Dégâts aux infrastructures	Sismicité induite	Respect de la règlementation	Faible pression d'injection, limitée à 20 bar. Procédure de suivi en place pour la centrale	Destruction des infrastructure de 1ère nécessité	2	3	6	2	2	4	7	R22
Sismicité induite à cause des pressions d'injection causant des dommages corporels	R23	Injection d'acide	Dommage physique	Sismicité induite	Respect de la règlementation	Faible pression d'injection, limitée à 20 bar. Procédure de suivi en place pour la centrale	Victimes, blessures	2	4	8	2	3	6	7	R23
Dégasage des produits de réaction de l'acide avec pollution de l'atmosphère	R24	Injection d'acide	Dommage environmental	Produits de réaction/corrosion inattendus	Design des produits adapté	Injection en continu empêchant la remontée de gaz	Pollution de l'environnement	3	2	6	1	2	2	7	R24
Dégasage des produits de réaction de l'acide avec dommages corporels	R25	Post injection	Dommage physique	Produits de réaction/corrosion inattendus	Design des produits adapté. Détecteurs de gas en surface	Injection en continu empêchant la remontée de gaz	Victimes, blessures, desease	3	4	12	1	4	4	7	R25
Production d'acide n'ayant pas réagit et pouvant fuiter du bassin avec pollution de l'environnement.	R26	Post injection	Dommage environmental	Fuite sur un bassin	Design et construction des bassins adaptés	Pas de production de prévue	Pollution de l'environnement alentours	2	2	4	1	2	2	7	R26
Brulures à cause des hautes températures	R27	Post injection	Dommage physique	Tuyaux et fluide chauds	Respect des procédures de travail sur site	Injection limitée à 70 °C	Blessures	2	3	6	2	2	4	7	R27
Pollution de l'atmosphère à cause des opérations	R28	Tout	Dommage environmental	Travaux opérationnels	Respect de la règlementation sur les carburants		Pollution de l'air	4	1	4	4	1	4	7	R28

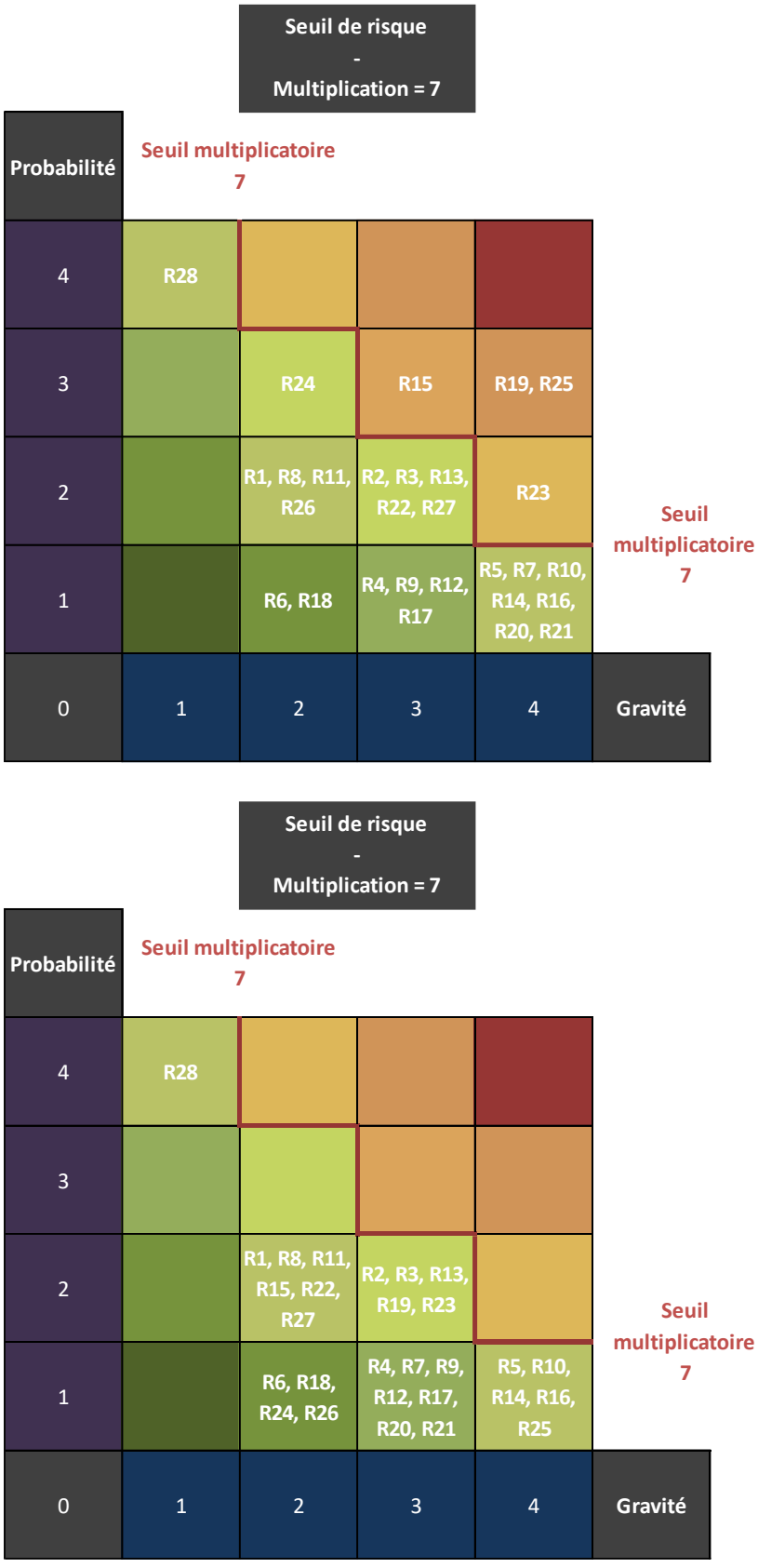

Figure 27: Risk matrix before and after mitigation for HSE risks.

2.3 Coiled tubing / Power plant interaction risks

During the technical site visit, 27 interaction risks have been identified and assessed. Those risks have been analyzed and evaluated based on the safety standards already in use onsite and on experts' experience. The expert group was composed of Geologists, Geochemists, Seismologists, Hydrogeologists and technical personnel in charge of Soultz powerplant operation.

From the risk analysis and evaluation, 10 major risks have been identified:

- 5 major risks due to the power plant
    - Power black out
    - Fire
    - Production pump stop
    - Air compressor stop
    - Lack of space on the platform
- 2 major risks due to coiled tubing
    - Coiled tubing stuck
    - Too high pressure in the coiled tubing
- 3 major independent risks
    - Storm
    - Very low temperature and snow
    - Lack of light

Mitigation measures have been deployed in order to minimize all 27 risks and especially the 10 major ones. Here is an example of the deployed mitigation measures:

- Have a backup pump on a backup power unit for annulus injection
- Have an expert in powerplant operation during all operation
- Put the mixing equipment in a water segregated area in order to avoid leakage in the environment.
- Adjust powerplant and Coiled tubing injection flowrate to protect the upper leak in the casing
- No acid mixing during night
- Etc.

Another risk evaluation has been realized after the identification of the mitigation measures in order to check the final state of the interaction risk assessment for the project. Table presents all the results of the HSE risk analysis, with the list of the risks, their analysis, evaluation, mitigation measures and final mark compared to the threshold of risk acceptability.

Figure shows the risk matrix before and after the mitigation measures identification. Finally, all risks have been considered as controlled.

Table 9: General summary of the Coiled Tubing / Power plant interaction risk assessment.

						Avant mitigation			Après mitigation				
Installation	Référence	Scénario	Conséquence sur la centrale	Conséquence sur le coiled tubing	Mesures de sécurité à mettre en œuvre	Fréquence	Gravité	Niveau final	Fréquence	Gravité	Niveau final	Seuil	Référence
Centrale	C1	Coupure de courant	Arrêt de la centrale pendant 1h maximum Pas d'électricité pendant 1h maximum Groupe électrogène pour les vannes et organes de sécurité	Pas de problème de sécurité à cause du manque d'électricité Si la centrale s'arrêt il faudra arrêter l'opération	Arrêter l'injection d'acide et chasser à l'eau douce Mettre en place une pompe de secours et la brancher sur le groupe électrogène Ne sera pas suffisant pour éviter que l'acide ne remonte pendant la chasse	2	4	8	1	4	4	7	R1
	C2	Fuite en surface	Eau géothermale. Haute pression et température.	Risque d'avoir de la saumure à 70°C sur les équipements et les personnes	Présence d'ESG en permanence pendant les opérations pour gérer une éventuelle fuite Possibilité de contenir une petite fuite pendant une semaine avec des équipements prévus à cet effet Possibilité de rincer les installations à l'eau douce en cas de présence de saumure sur les équipements	2	3	6	1	3	3	7	R2
	C3	Départ de feu	Arrêt de toutes opérations. Risque de fuite. Risque d'explosion (zone ATEX)	Inhibiteurs de corrosion inflamable Machines fonctionnant au GNR	Zone ATEX interdite d'accès lors de l'opération En cas de feu, une procédure d'évacuation d'urgence sera lancée. La procédure d'urgence de la centrale s'applique avec les point de rassemblement et chemins d'évacuation Impossible en cas d'incendie de gérer l'acide	2	4	8	1	4	4	7	R3
	C4	Arrêt de pompe de production	Aucun débit dans GPK-4 Besoin d'un certain temps pour redémarrer la centrale	Si l'injection d'acide n'est pas arrêté il y a une risque que l'acide remonte dans les tubages	Pompe de secours (sur groupe électrogène) mais avec un débit faible de 20 m3/h Fangmann possède également une pompe en secours	3	4	12	3	2	6	7	R4
	C5	Arrêt du compresseur	Arrêt de la centrale	Voir scénario "Arrêt de pompe de production"	Présence de personnel ESG en permanance pour redémarrer les installations Compresseur en secours	2	4	8	1	4	4	7	R5
	C6	Débit de GPK-4 trop élevé	Aucune conséquence	Pas dangereux mais peut diluer l'acide	Réduction du débit d'injection d'acide et pompe d'injection en secours dans l'annulaire.	2	1	2	2	1	2	7	R6
	C7	Débit de GPK-4 trop faible	Risque l'acide remonte dans le casing	Aucune conséquence	Débit d'acide dans le coiled tubing facile à ajuster pour éviter cette situation	2	3	6	2	2	4	7	R7
	C8	Pression de GPK-4 trop élevé	Aucune conséquence	Aucune conséquence		0	0	0	0	0	0	7	R8
	C9	Pression de GPK-4 trop faible	Aucune conséquence	Aucune conséquence		0	0	0	0	0	0	7	R9
	C10	Température de GPK-4 trop élevée	Arrêt de la centrale	Pas de limite de température pour le coiled tubing Peut faire réagir l'acide plus vite.	Adapter la concentration d'inhibiteur pour une température de 150°C au lieu de 100°C.	2	3	6	2	2	4	7	R10
	C11	Température de GPK-4 trop faible	Aucune conséquence	Aucune conséquence		0	0	0	0	0	0	7	R11
	C12	Pas assez de place sur la plateforme	Besoin d'accès secours en cas d'urgence	Besoin d'accès secours en cas d'urgence	Prévoir l'implatation pour garder un chemin de circulation autour de la centrale Définir et signaler les zones de travail de chaque entreprise	2	4	8	2	3	6	7	R12
Coiled Tubing	CT1	Coiled tubing coincé	Risque de ne pas pouvoir fermer le puits	Risque de laisser le coiled tubing dans le puits	Si la BHA est coincée avec circulation, il est possible d'envoyer une boulle pour déconnecter la BHA et remonter le reste du coiled tubing Si la BHA est coincée sans circulation, il est possible de tirer jusqu'à rupture du coiled tubing (point de rupture inconnu) Si le coiled tubing est coupé (rupture ou BOP) il est toujours possible de tuer le puits et fermer la vanne maitresse.	2	4	8	1	4	4	7	R13
	CT2	Fuite du coiled tubing en surface	Risque pour l'homme et l'environnement	Fuite d'acide	Faire passer le point de fuite dans le puits, chasser l'acide à l'eau douce et remonter le coiled tubing pour réparation Les équipements seront sur une zone de la plateforme entièrement drainée Bac de rétention sous le coiled tubing en cas de fuite	2	3	6	1	3	3	7	R14
	CT3	Fuite du coiled tubing dans le puits	Avoir de l'acide dans les casing et risque de corrosion	Aucune conséquence	Fuite indétectable tant que le coiled tubing est dans le puits mais l'injection via l'annulaire sera poursuivie en continu pour diluer et pousser.	1	4	4	1	2	2	7	R15
	CT4	Arrêt des pompes d'injection	Risque d'arrêt de la centrale si la pression descend trop	Risque d'avoir de l'acide statique dans le coiled tubing et de la corrosion	Fangmann possède une pompe de secours	2	2	4	1	2	2	7	R16
	CT5	Fuite d'acide en surface	Risque pour l'Homme et l'environnement	Aucune conséquence	Fangmann mélange l'acide dans un espace fermé dédié et possède les équipements de sécurité nécessaire (EPI, médiacaments, neutralisateurs, etc) La zone de mélange de l'acide est drainée vers des bassins et ne ruissellera pas dans la nature	2	3	6	2	2	4	7	R17
	CT6	Débit d'acide trop élevé	Risque pour les tubages si le débit dépasser 1/2 du débit total injecté (GPK-4 + coiled tubing)	Aucune conséquence	Débit d'acide dans le coiled tubing facile à ajuster pour éviter cette situation	2	3	6	2	2	4	7	R18
	CT7	Débit d'acide trop faible	Pas de risque mais dilution de l'acide	Aucune conséquence	Débit d'acide dans le coiled tubing facile à ajuster pour éviter cette situation	2	2	4	2	2	4	7	R19
	CT8	Pression du coiled tubing trop élevée	Aucune conséquence	Risque d'éclatement du coiled tubing	Soupapes de sécurité sur le coiled tubing pour éviter la montée en pression	2	4	8	1	4	4	7	R20
	CT9	Pression du coiled tubing trop faible	Aucune conséquence	Aucune conséquence		0	0	0	0	0	0	7	R21
Indépendant	I1	Température extérieure trop élevée	Aucune conséquence	Aucune conséquence		0	0	0	0	0	0	7	R22
	I2	Température extérieure trop faible	Risque pour l'Homme et les équipements s'il y a trop de verglas	Risque de gel dans les équipements en cas d'eau stagnante	Présence de sel sur place pour éviter le gel et déneiger Les équipments seront purgés en fin d'opération	2	3	6	2	2	4	7	R23
	I3	Pluie trop forte	Aucune conséquence	Risque en cas d'orage et nécessité d'arrêter l'opération	Repousser les opérations (personne ne doit travailler sous la tour en cas d'orage)	2	4	8	1	4	4	7	R24
	I4	Trop de neige	Aucune conséquence	Problème d'accès en cas de neige	Saler la route et prévoir des moyens de déneigement	3	3	9	2	2	4	7	R25
	I5	Trop de vent	Aucune conséquence	Risque en cas de vent très fort	Limite de sécurité très haute. Très peu de probabilité d'occurrence. Repousser les opérations en cas de dépassement du seuil	1	4	4	1	4	4	7	R26
	I6	Pas assez de luminosité	Aucune conséquence	Risque avec le maniement de l'acide	Pas de maniement d'acide pendant la nuit. Site éclairé la nuit, possible de passer en mode manuel pour allumer les projecteurs en plein jour si besoin.	3	3	9	2	3	6	7	R27

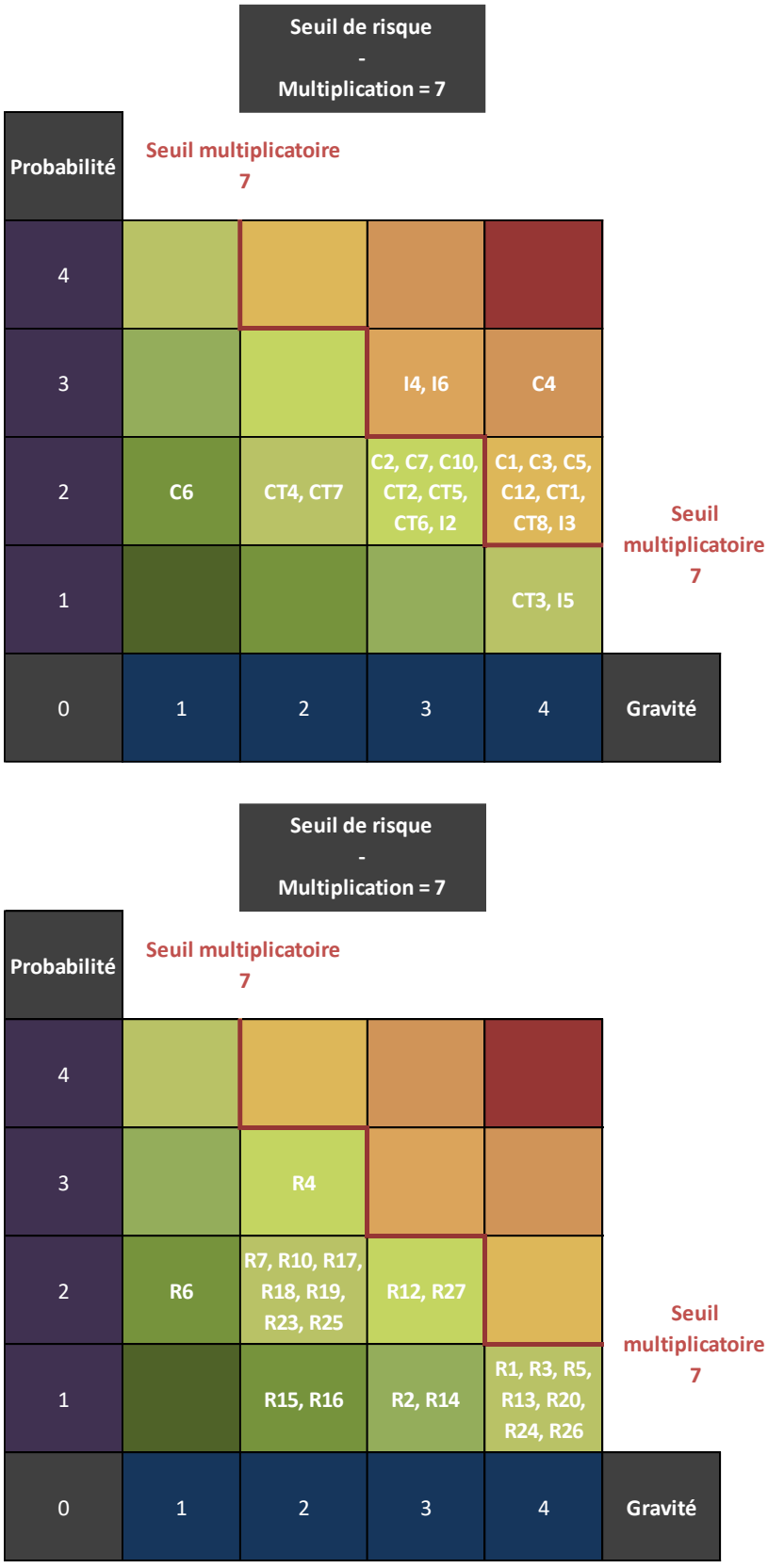

Figure 28: Risk matrix before and after mitigation for Coiled Tubing / Power plant interaction risks.

2.4 Reporting

A general report on the risk assessment has been written in French by ESG and transmitted to the site owner and to the French mining authorities (DREAL) before the operations. The delivery of this report was considered by the DREAL and the GEIE EMC as a prerequisite for the operation. Figure shows the 1st page of this report.

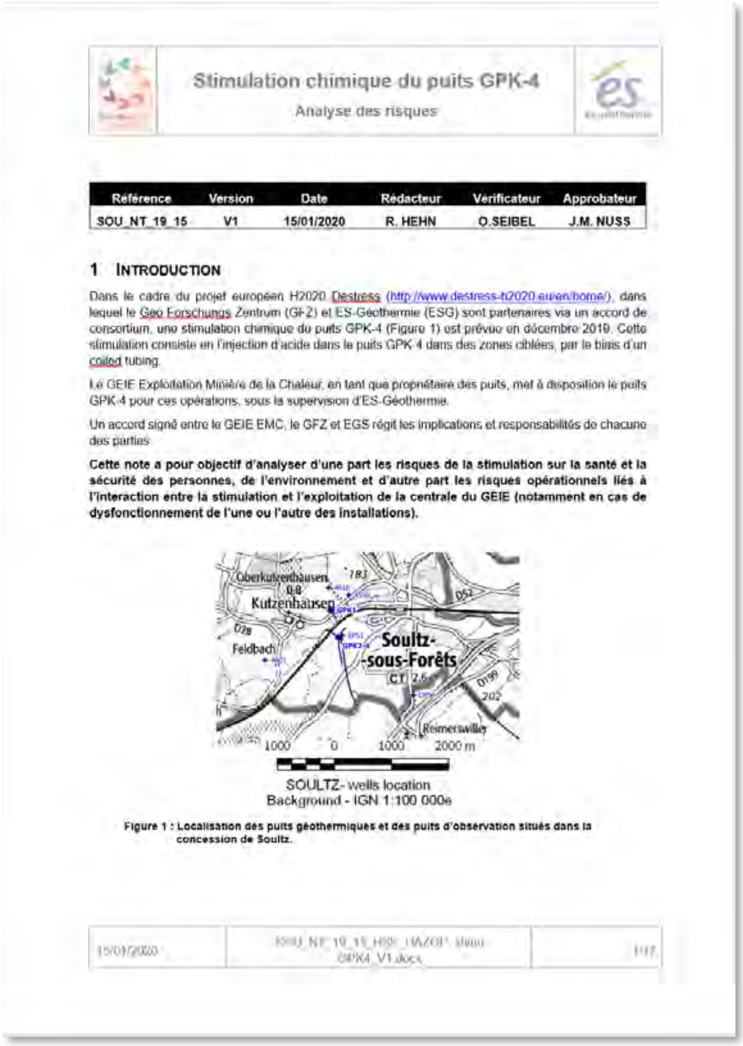

Stimulation chimique du puits GPK-4

Analyse des risques

Référence	Version	Date	Rédacteur	Vérificateur	Approbateur
SOU_NT_19_15	V1	15/01/2020	R. HEHN	O.SEIBEL	J.M. NUSS

1 Introduction

Dans le cadre du projet européen H2020 Destress (http://www.destress-h2020.eu/en/home/), dans lequel le Geo Forschungs Zentrum (GFZ) et ES-Géothermie (ESG) sont partenaires via un accord de consortium, une stimulation chimique du puits GPK-4 (Figure 1) est prévue en décembre 2019. Cette stimulation consiste en l'injection d'acide dans le puits GPK-4 dans des zones ciblées, par le biais d'un coiled tubing.

Le GEIE Exploitation Minière de la Chaleur, en tant que propriétaire des puits, met à disposition le puits GPK-4 pour ces opérations, sous la supervision d'ES-Géothermie.

Un accord signé entre le GEIE EMC, le GFZ et EGS régit les implications et responsabilités de chacune des parties.

Cette note a pour objectif d'analyser d'une part les risques de la stimulation sur la santé et la sécurité des personnes, de l'environnement et d'autre part les risques opérationnels liés à l'interaction entre la stimulation et l'exploitation de la centrale du GEIE (notamment en cas de dysfonctionnement de l'une ou l'autre des installations).

SOULTZ- wells location
Background - IGN 1:100 000e

Figure 1 : Localisation des puits géothermiques et des puits d'observation situés dans la concession de Soultz.

15/01/2020

Figure 29: 1st page of ESG's report on risk assessment for the soft chemical stimulation of GPK-4.

3 Field Work

The operations lasted from the 16th to the 23rd of December 2019. Figure shows the timeline of the operations.

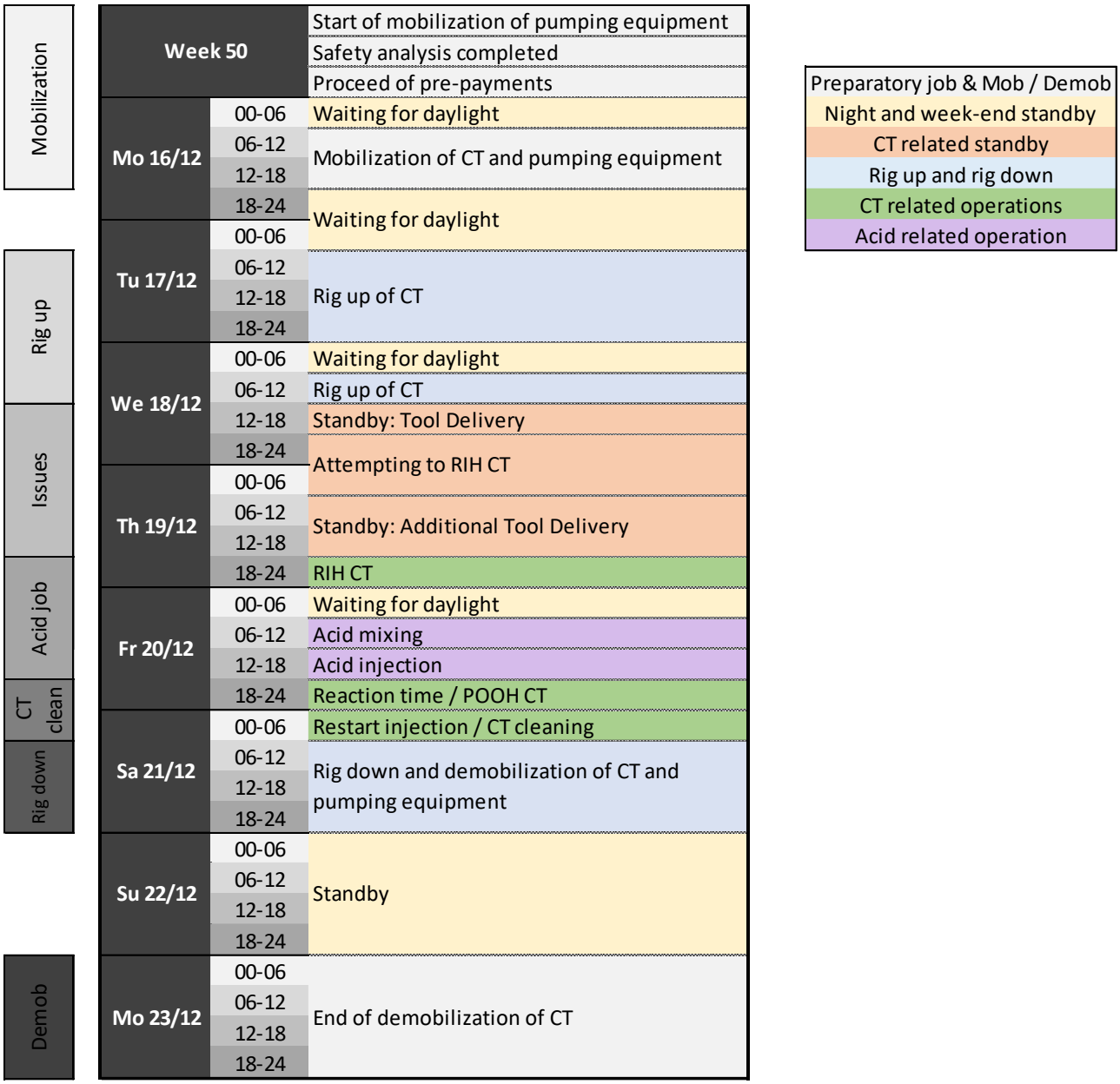

Figure 30: Timeline of the operations of the soft chemical stimulation of GPK-4.

3.1 Mobilization

Mobilization started the week before the job with the onsite arrival of a part of the chemicals in solid form. Those products have been stored in a safe place inside the power plant facilities before the

appropriate container arrived onsite on week 51. The rest of the mobilization took place on the 16th of December 2019. Figure shows the trucks parked on the parking place of the Soultz site.

Figure 31: Picture of Soultz parking place with arrival of trucks during mobilization phase of the stimulation.

3.2 Rig up

On Tuesday, the 17th of December, the rig up of the equipment started after a morning safety meeting and the signature of the prevention plan by all involved parties (Figure). The trucks have been unloaded during the day. A small incident occurred during the unloading: the BOP felt from the truck on the ground, because of communication issues between the unloading team and the crane driver. Some electrical issues have also been solved in the coiled tubing control unit.

The rig up could not be finished on Tuesday (Figure). It was achieved on Wednesday morning with pull out tests and pressure tests. Figure shows the final site installation after rig up.

GEIE
Route de Soultz
67250 Kutzenhausen

PLAN DE PREVENTION 2019 DE LA CENTRALE GEOTHERMIQUE DE SOULTZ-SOUS-FORÊTS
(pour une opération > 400 H, un contrat annuel et les travaux dangereux)
(en application du décret 92-158 du 20 février 1992)

DATE : 17/12/2019

Intervention ponctuelle ☒ Intervention annuelle ☐ Maintenance ☐ Travaux neufs ☐

N°DE COMMANDE :	Agreement on the implementation of the DESTRESS programme on the geothermal central of Soultz-sous-Fôrets
DESCRIPTION DE L'OPERATION :	Stimulation du puits GPK-4

MAITRE D'OUVRAGE : GEIE		
REPRESENTEE PAR :	FONCTION :	TEL :
TRAU Philippe	Chef de projets	03.88.20.67.13 / 06.78.72.18.09

ENTREPRISE UTILISATRICE : ESG		
REPRESENTEE PAR :	FONCTION :	TEL :
HEHN Régis	Ingénieur réservoir	0673755161

ENTREPRISES EXTERIEURES (EE) ET SOUS-TRAITANTS				
Raison sociale :	WSG	[illegible]	MEDIACO	[illegible]
Responsable :	[illegible]	[illegible]	GROSSHANS	
Effectif pour l'opération :	5	8	1	
Durée des travaux :	3 j	3 j	2 j	
Date début et fin	17-19/12/19	17-19/12/19	17-19/12/19	
Heures	72 H	72 H	72 H	
NOMBRE D'HEURES AU TOTAL POUR L'OPERATION :			72 H	

INSPECTION COMMUNE AVANT LE DÉBUT DES TRAVAUX		DATE : 17/12/2019
REPRESENTANT GEIE (Nom, Signature)	REPRENTANT ESG (Société, Nom, Signature)	REPRENTANT EE (Société, Nom, Signature)
TRAU	HEHN	

URGENCE INCENDIE OU ACCIDENT : TEL 112

Point de rassemblement selon le sens du vent (voir manche à air) « entrée Est » ou « entrée Ouest ».
Tout accident doit être déclaré le jour même au service sécurité et au responsable ESG « donneur d'ordre ».

L'ACCES AU SITE SE FAIT PAR LA PORTE PRINCIPALE DE LA CENTRALE COTE RD264.
LE SITE DISPOSE D'UN SYSTÈME DE DÉTECTION D'INTRUSION.

- L'accès au site s'effectue par la porte principale, tout intervenant dans les bâtiments de la centrale s'enregistre dans le registre de la salle de contrôle.
- L'accès aux installations non concernées par les opérateurs est interdit.
- La circulation en véhicule dans l'enceinte de l'usine doit se limiter à entrer ou à sortir du matériel, et doit respecter le sens de circulation indiqué sur site.

INSTALLATION SITE	Vestiaires fournis par	GEIE ☒	EE ☐
	Réfectoire fournis par	GEIE ☒	EE ☐
	Emplacement des bungalows :		
INFORMATIONS SÉCURITÉ :	Principes généraux + Règles d'or	OUI ☒	NON ☐
	Consignes générales d'incendie	OUI ☒	NON ☐
	Présentation des risques spécifiques	OUI ☒	NON ☐

INTERDICTION DE FUMER SAUF DANS LES LIEUX OÙ L'AUTORISATION EST AFFICHÉE
Décret du 1er février 2007
INTERDICTION DE BOIRE DE L'ALCOOL SUR LE SITE

SI, AU COURS DE L'OPERATION, LES RISQUES PROFESSIONNELS VIENNENT À ÊTRE MODIFIÉS, OU SI DE NOUVEAUX RISQUES APPARAISSENT, L'ENTREPRISE QUI EST À L'ORIGINE DE LA NOUVELLE SITUATION EN INFORME L'AUTRE. ELLES DÉCIDENT D'UN COMMUN ACCORD DES MESURES À PRENDRE ET, SI BESOIN, DE FAIRE UNE RÉUNION DE COORDINATION POUR INFORMER LES PERSONNES CONCERNÉES

Figure 32: Prevention plan signed after the safety meeting of Tuesday, the 17th of December 2019.

Figure 33: Picture of Soultz site after rig up of the stimulation equipment.

3.3 Issues

Two issues occurred during the rig up and the attempts to run in hole. The first issue was related to the stuffing box of the BOP assembly. The Coiled Tubing Company realized during the tests included in the rig up procedure that a part of the stuffing box was missing. This part was critical for the safety of the job and the Coiled Tubing Company was obliged to delay the operations in order to wait for the delivery of a spare part from their base in the Netherlands and then fix the stuffing box. The part took approximately 8h to be brought onsite.

The second issue occurred during the first step of run in hole with the Coiled Tubing, while trying to go through the wellhead. Indeed, GPK-4 is designed with a 9''5/8 casing from 4 756 mMD to the wellhead, inside the 13"3/8 expansion casing. In order to accommodate the temperature dilation of the 9''5/8 which is only cemented after 4 200 mMD, a 8 m cellar has been built and the 9''5/8 casing can freely go up and down from -8 m to the surface depending on its temperature (Figure). But once the coiled tubing went through the top valve of the wellhead it was probably too bended and got stuck above the 9''5/8 casing at around -2 or -3 m.

The coiled tubing company tried different technics in order to go through the top of the 9"5/8 casing. Manual bending of the CT and water injection during RIH were unsuccessful. It was decided to order additional straight bars and a knuckle joint to allow for RIH. After delivery, RIH was possible during the first try.

After this issue had been solved, running in hole went without any problem down to the casing shoe and for the rest of the operations.

The main consequence of those added equipment on the stimulation design was that running in the open hole was considered too dangerous with the knuckle joint (high risk to get stuck). In consequence, it has been decided to target only the casing leakage zone at 4 700 mMD and not to fill the open hole with acid before start of acid injection.

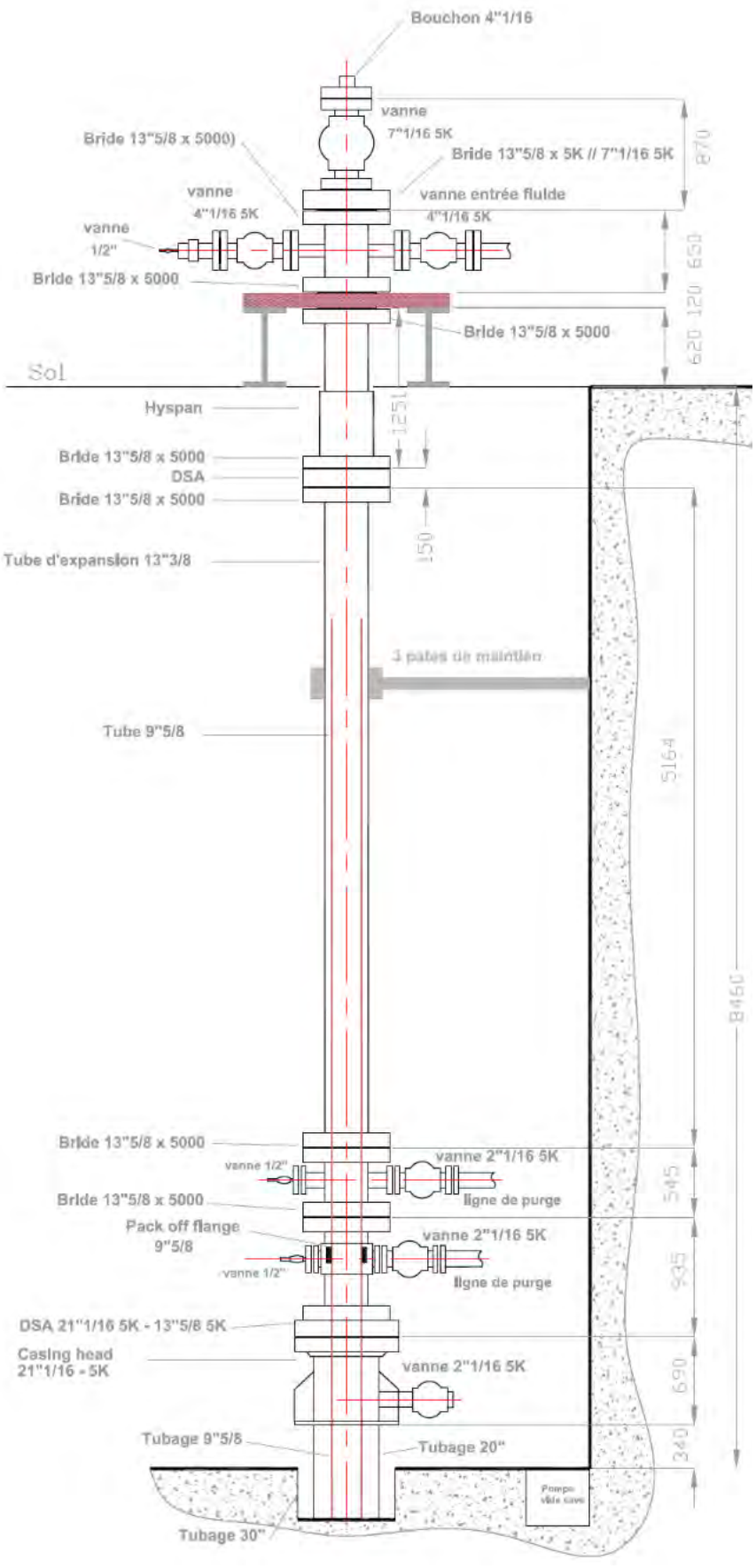

Figure 34: GPK-4 wellhead design with a 9''5/8 floating casing.

3.4 Acid job

The acid job started on Friday, the 20th of December 2019. Once the coiled tubing had been set up at the exact injection depth (4 720 mMD, just below the leakage zone), the acid service companie made a safety meeting and started the acid mixing on surface.

Once the acid had been mixed, the acid injection could start. Table 10 presents the different volumes and flowrate of acid and water injected through the coiled tubing and through the annulus respectively. The acid job consisted in 6 phases surrounded by injection of geothermal fluid only at 10 L/s (nominal power plant operation conditions).

The Pre-flush was meant to cool down the coiled tubing and to test the parallel injection through the coiled tubing and annulus. The behavior of the surface facilities was reliable enough to ensure a good repartition of the injection flowrates in order to constrain the fresh water (and acid during the next steps) to go in the lower leakage zone and in the open hole.

The Main flush consisted in the injection of 50 m^3 of the first acid (SSB-007) followed by the injection of the same volume of the second product (SFB-007). Those chemicals aimed to dissolve preferentially carbonates and silicate minerals (clays, quartz) which generally sealed the natural fractures crossing the geothermal well.

The post-flush consisted in emptying the coiled tubing with fresh water in order to be sure that all acid had been displaced out of the coiled tubing. It has been directly followed by a Squeeze step aimed at pushing the acid into the formation for its expected reaction inside the targeted fracture zones.

A waiting time of 5 hours (“acid reaction time”) was then needed, during which the full reaction of acid is expected within a distance of 1 to 10 m from the borehole (based on the simulations made by the pumping company). During this step, injection into the well was fully shut down.

The whole acid job took more than 12 hours. Finally, the nominal power plant operation restarted with the 10 L/s injection flowrate of geothermal water.

Table 10: Summary of volumes, flowrates and type of product injected during the acid job.

Phase	Duration	Coiled tubing		Annulus	
Pre acid job	-	0 L/s	-	10 L/s	Geothermal water
Pre flush	00:35	5 L/s - 11 m3	Fresh water	5.5 L/s	Geothermal water
Main flush 1	02:43	5 L/s - 49 m3	SSB-007	5.5 L/s	Geothermal water
Main flush 2	02:40	5 L/s - 48 m3	SFB-007	5.5 L/s	Geothermal water
Post flush	00:40	5 L/s - 11 m3	Fresh water	5.5 L/s	Geothermal water
Squeeze	00:35	0 L/s	-	10 L/s - 15 m3	Geothermal water
Waiting time	05:00	0 L/s	-	0 L/s	-
Post acid job	-	0 L/s	-	10 L/s	Geothermal water

3.5 Coiled Tubing Cleaning

After the acid had been injected, the coiled tubing was not needed anymore. It has been pulled out and brought to surface for cleaning. The remaining acid in the tanks has been diluted and pumped into 4 IBCs (1 m^3 tanks). A solution of soda ash has been circulated in the coiled tubing for its complete passivation. This solution has then been displaced with Nitrogen out the coiled tubing and discharged into 5 other IBCs. Those IBCs have been stored onsite and waste disposal solutions were being considered. Figure shows the IBCs and the preliminary analysis made before treatment selection.

IBC volume : 1000 L
Date 21/12/2019
T° de mesure 9°C

Total vol. 9000L
Date de mesure: 14/01/2020

IBC ref	Vol.	pH	Observations
1 Soude	100%	10,43	Claire, verdatre
2 Soude	100%	10,42	Claire verdatre
3 Soude	100%	10,83	Claire rougatre
4 Soude	100%	10,7	Claire verdatre
5 Soude	100%	10,9	Claire vedatre
6 Eau de rinçage	100%	3,3	Claire bleue
7 Eau de rinçage	100%	5,89	Claire, bleue
8 Eau de rinçage	100%	8,3	Couche d'huile
9 Eau de rinçage	100%	10	

Figure 35: Acid tank and coiled bubing cleaning wastes with preliminary analysis.

3.6 Rig down and Demobilization

Rig down operations started on Saturday, the 21st of December 2019, just after the coiled tubing cleaning. It has been done within one day, but all the equipment could not leave the site before Sunday. As trucks are banned from the road in France on Sunday, the trucks parked outside the site and leaved early morning on Monday, the 23rd of December 2019.

A contamination issue raised on Saturday, the 21st as measurements revealed a low natural radioactivity on greasy materials deposited on the coiled tubing. The coiled tubing may have scratched some old scaling, deposited inside GPK-4 9''5/8 casing during years of operation. Elevated radioactivity (<2x natural background) was measured on the CT, the bottom hole assembly as well as several components of the well control equipment and the injector head.

ESG performed radioactivity measurements on the equipment and assessed that there the contamination was low and below the threshold for transportation, according to the European regulation for transportation of dangerous goods. The coiled tubing company made some internal deliberation and finally accepted to transport the equipment to a dedicated treatment facility. Some days were necessary to clean all the equipment. The risk associated with the possible NORM contamination of the CT equipment was not foreseen in the risk analysis.

4 Results on GPK-4 Injectivity

After the soft chemical stimulation operation, GPK-4 injection parameters have been monitored and analyzed for one complete month, in order to see the impact of the stimulation on the well injectivity.

Figure shows the details of GPK-4 injection parameters during the week of the stimulation operation. One can see that the stimulation operation needed some temporary modifications of the injection flowrate and pressure. After the acid reaction time, GPK-4 injection restarted, based on its nominal parameters, but the reservoir around GPK-4 took some time to stabilize and a transient state of several days could be observed. Even if the parameters are still transient, the flowrate and the pressure are not very different from the initial ones.

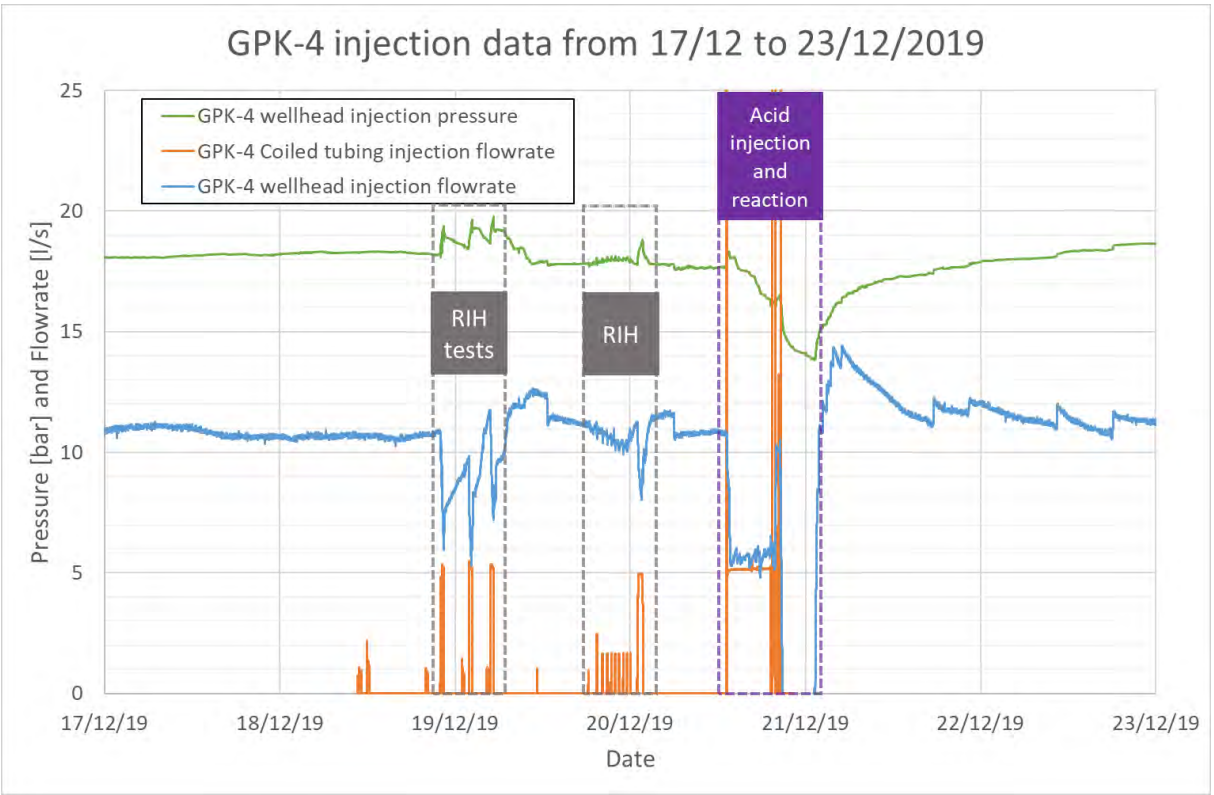

Figure 36: GPK-4 injection parameters from 17/12 to 23/12/2019.

In order to better estimate the evolution of the injectivity, it is necessary to look at a longer scale. Figure plots the calculated injectivity of GPK-4 from March 2017 to the end of January 2020. Many different phases are represented, and a dark line highlights the observed steady state periods. The transient state periods correspond to restarting phases after power plant shutdowns or maintenance phases. The last step of injectivity data (red colors) represents the injection parameters after the soft chemical stimulation.

On can see that the injectivity after the stimulation is about 0.62/0.63 kg/s/bar, whereas it was about 0.60 kg/s/bar before. The data seem to show that there is a small increase in the injectivity. However, Figure shows that in 2018 the injectivity of GPK-4 reached even higher values. In fact, the small

difference observed before and after the soft chemical stimulation of December 2019 is in the order of magnitude of sensors precision. Finally, the injectivity might vary more because of sensors uncertainties and calibration than because of injectivity increase. Other parameters such as injection temperature, fluid density, casing status may also have an impact on the estimated injectivity index.

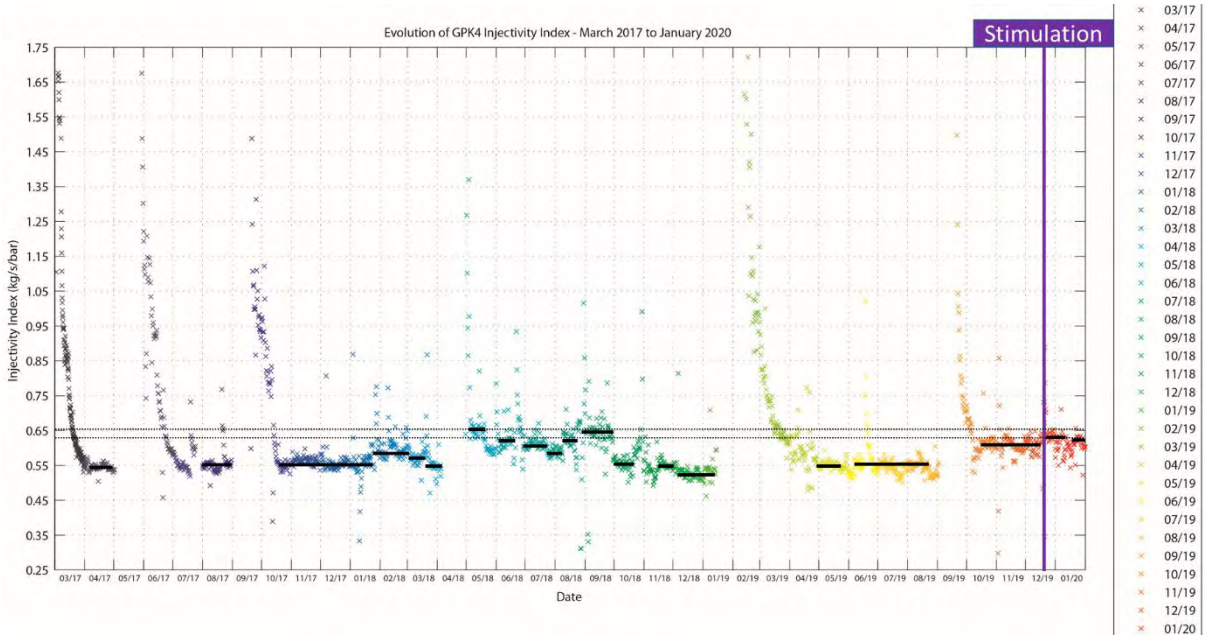

Figure 37: GPK-4 injection parameters from 03/2017 to 02/2020.

From a pure transient point of view, it is possible to plot the injectivity over time after each power plant shutdowns. It is then possible to compare the past transient state period of GPK-4 injectivity after a restart of injection, to the one after the soft chemical stimulation (Figure). From this figure one can see that the last restart after the acid reaction time is in the range of the previously observed one.

Those data show that so far, the soft chemical stimulation of December 2019 had no obvious impact on GPK-4 injectivity, neither on transient nor permanent state.

.

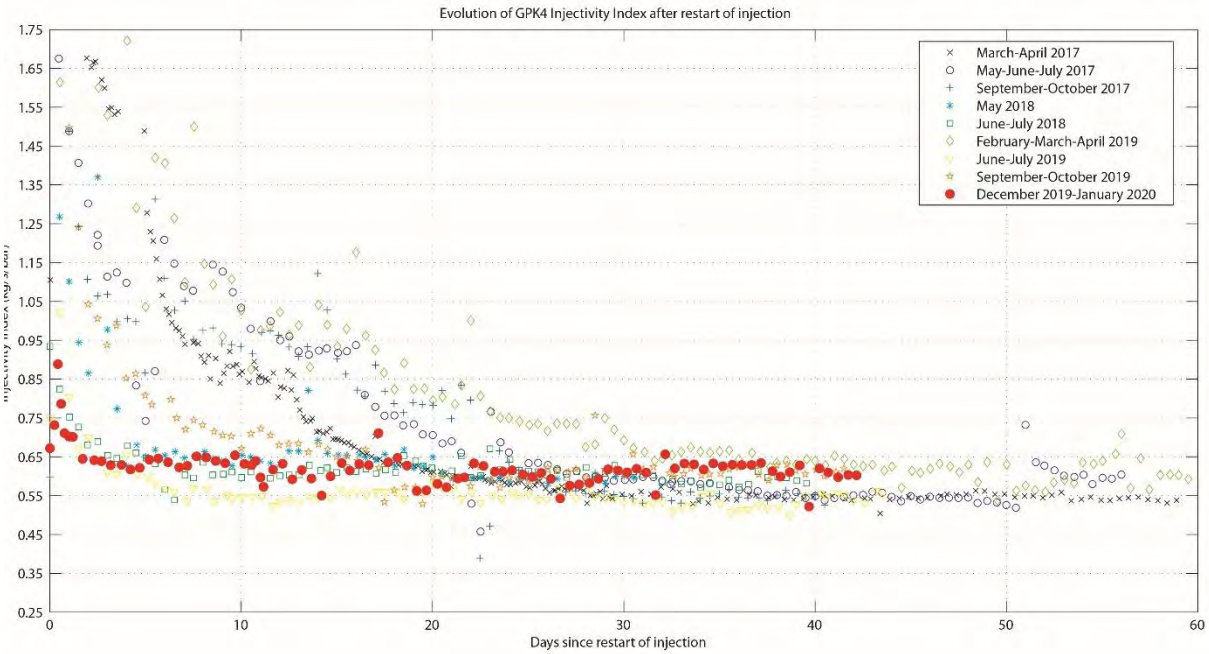

Figure 38: GPK-4 injection parameters in transient state after power plant restarts.

5 Impact on Chemistry and Seismicity

Induced seismicity is continuously monitored with the network presented in Figure . This network records the seismicity in real time during power plant operation. The same network was in place and recording before, during and after the soft chemical stimulation.

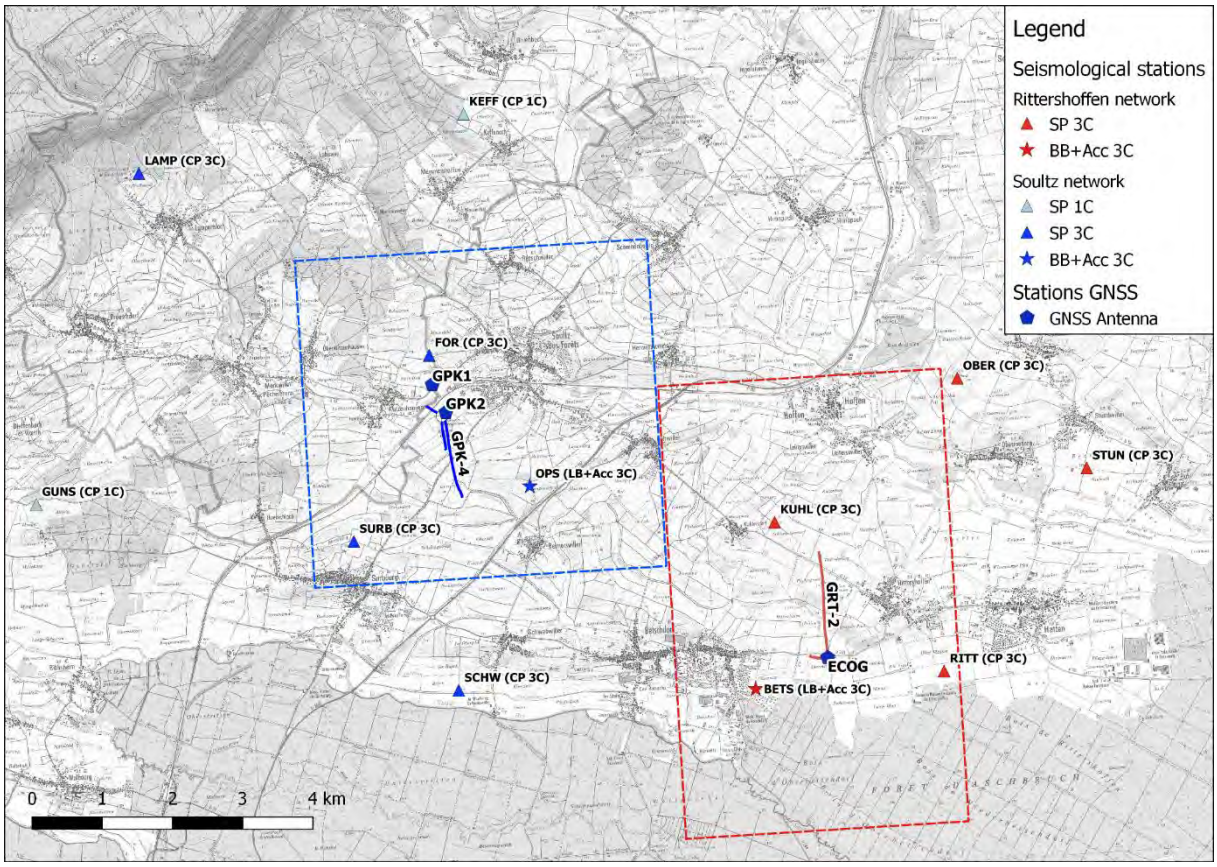

Figure 39: Seismic monitoring network around the Soultz site (Maurer et al., 2020).

Figure shows the micro-seismic event rate, the corresponding Peak Ground Velocity and Magnitude of events from the 01/12/2019 to the 13/01/2020.

Two seismic events were detected one day after the stimulation (22/12/2019, see Figure). But from Figure one can see that some events also occurred during standard operation of the power plant. So, the two events of the 22/12/2019 can't be definitively attributed to an effect of the stimulation. The same argument can be used for both PGV and Magnitudes of the corresponding events.

From the observation of seismic rate, PGV and Magnitude, there is no evidence that the two events which were detected the 22/12/2019 are directly related to the soft chemical stimulation. If fact, those events are not different in number and energy compared to the observed induced micro-seismic activity baseline of Soultz site. They might have been triggered by the stop and the restart of the injection, which was part of the stimulation procedure, or even just related to the injection itself.

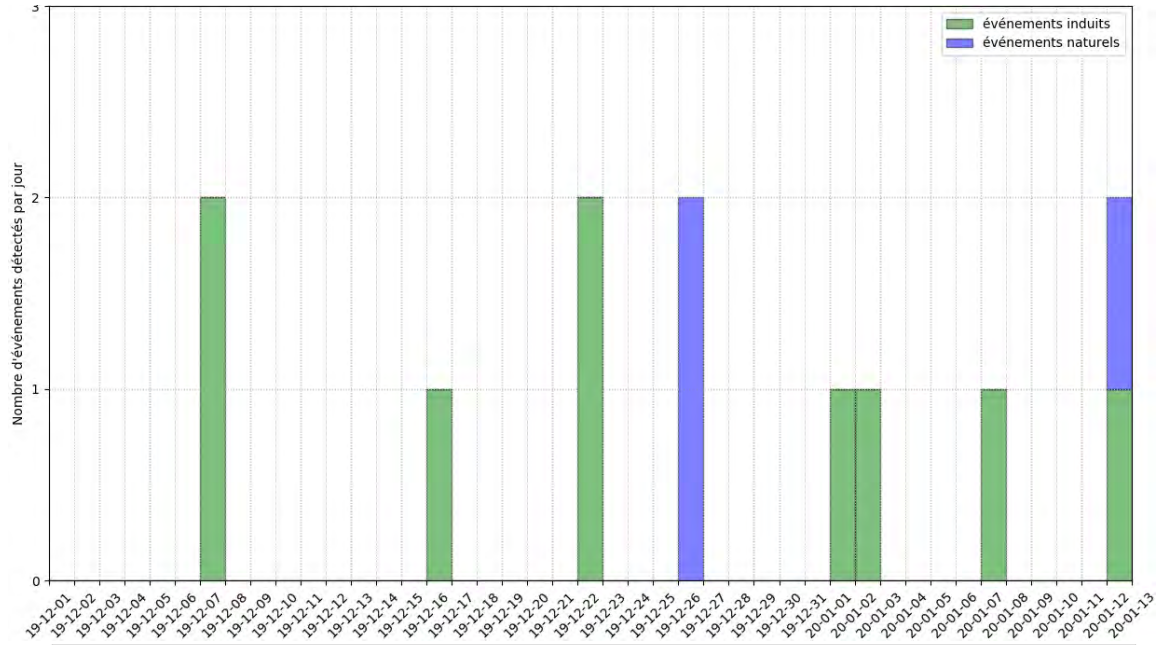
événements induits
événements naturels
Nombre d'événements détectés par jour

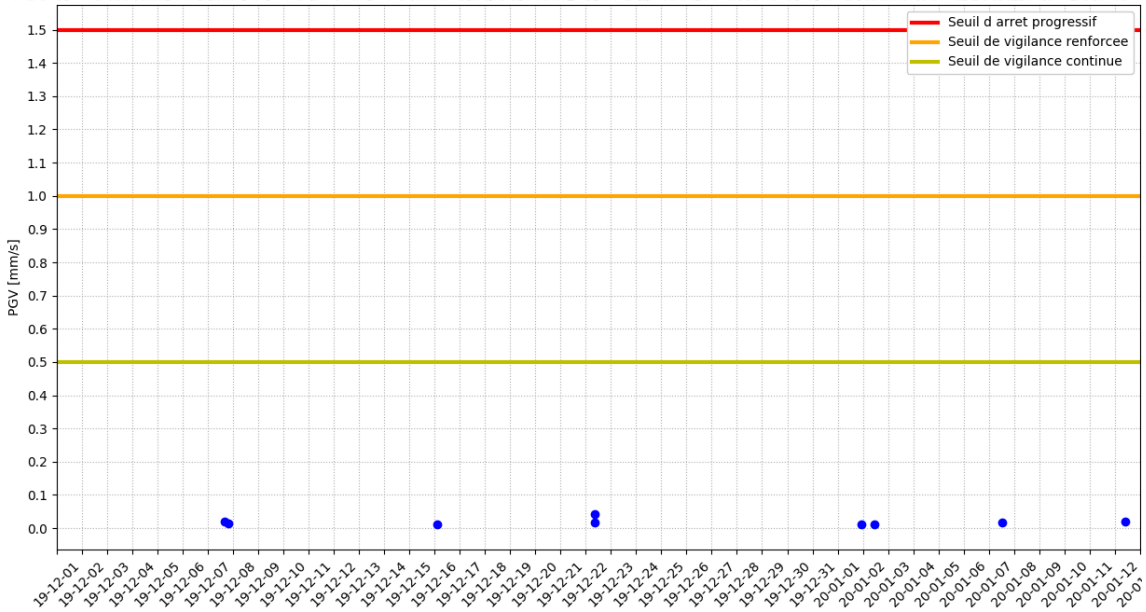
Seuil d arret progressif
Seuil de vigilance renforcee
Seuil de vigilance continue
PGV [mm/s]

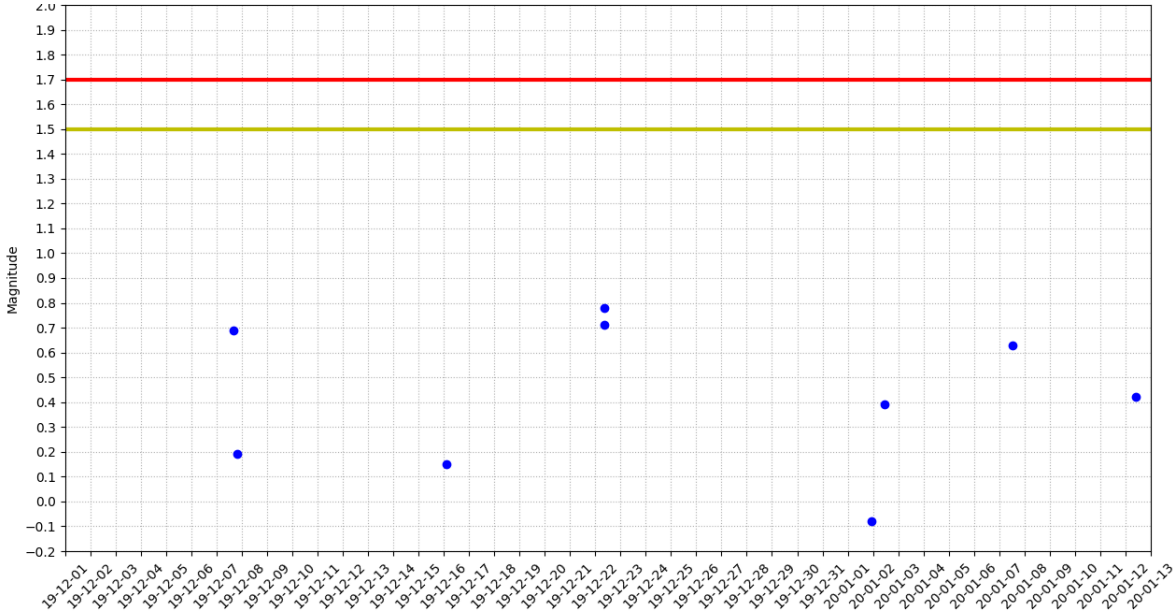
Magnitude

Figure 40: Seismic rate (Top), PGV (Middle) and Magnitude (Bottom) of Soultz events from the 01/12/2019 to the 13/01/2020.

Early January, the physico-chemical monitoring highlighted pH and electrical conductivity values in agreement with pre-stimulation monitoring values (Mouchot et al., 2020). In addition, a new sampling campaign has been performed. A complete chemical analysis has been done, notably to assess if any change could have occurred after GPK-4 chemical stimulation. So far, there is no evidence that GPK-4 chemical stimulation changed the chemical state of GPK-2 production water.

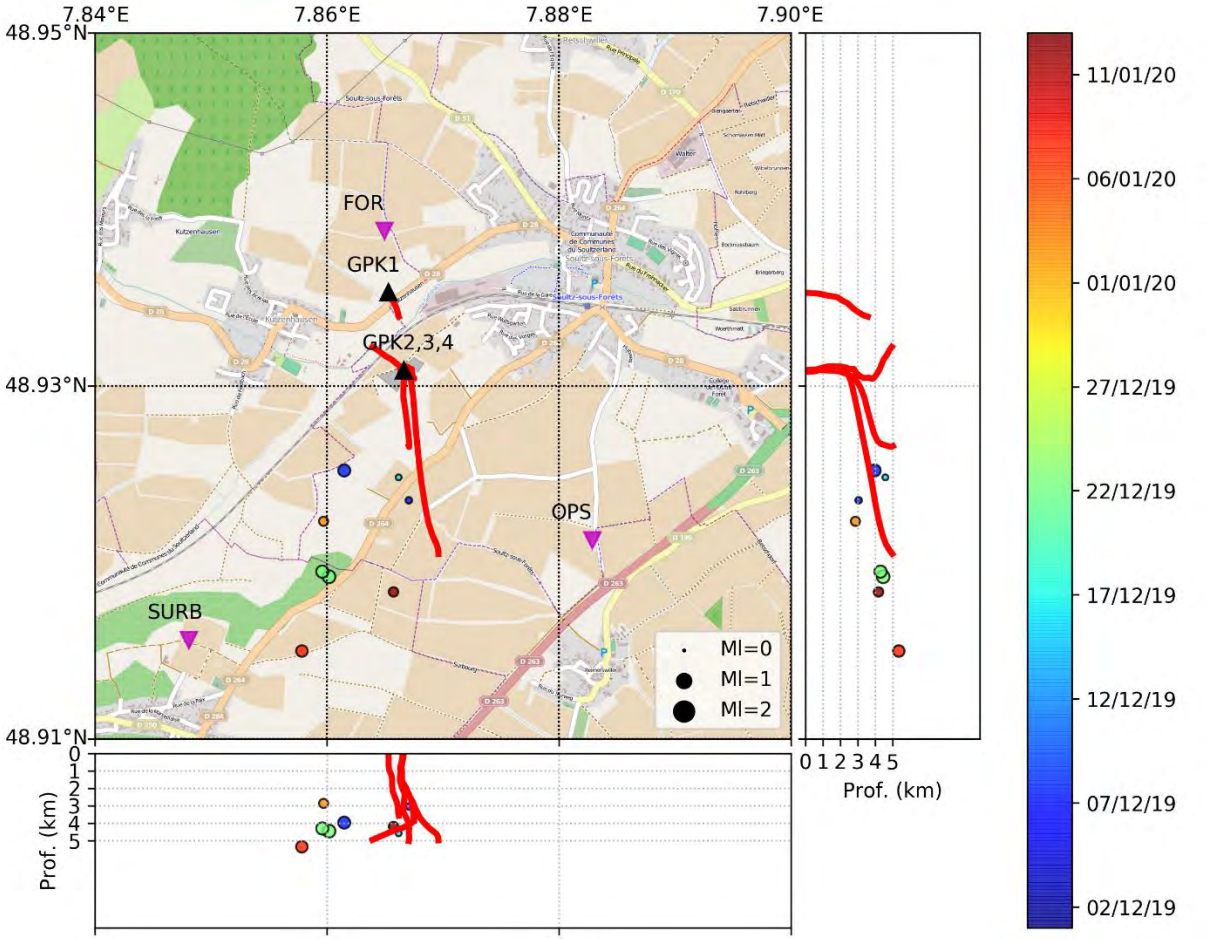

Figure 41: Location of seismic events detected on Soultz site from the 01/12/2019 to the 14/01/2020. The two events that occurred one day after the chemical stimulation are in green.

6 Conclusions and follow-up

6.1 Summary of operations

A soft chemical stimulation of the Soultz-sous-Forêts geothermal well GPK-4 was done on December 2019 within the framework of Horizon 2020 Destress project.

A lot of efforts have been deployed in order to plan and organize this stimulation. A well integrity and productivity study was done in GPK-4, through a logging survey and the consecutive interpretation of the data. The results of this study allowed identifying the potential targets for the chemical stimulation and defining the potential risks associated with the known injection technics.

Based on the productivity study, on geological and mineralogical data, four potential targets have been identified in the deep granite section of the well. They correspond to permeable fracture zones filled in with Illite, Smectite and Calcite, which constitute the best candidates for secondary mineral dissolution.

Based on the integrity study, the shallower target zone has been removed from the stimulation program for safety issues.

The identification of service companies for the stimulation, and the definition of the contractual framework between GFZ (responsible for this task and Destress partner), ESG (operator of the Soultz-sous-Forêts site and Destress partner), and GEIE EMC (owner of the Soultz-sous-Forêts site but not Destress partner) has been concluded in December 2019.

The soft chemical stimulation of GPK-4 has been performed on week 51, with the acid injection on the 20/12/2019. Preliminary results have been presented during the Destress final conference in Delft (20/01/2020). Final results are presented in this report.

During the operation, no HSE issues occurred (no injury, no environmental damage), and no impact on well integrity has been detected. The whole operation has been realized without any shutdown of the power production of Soultz ORC powerplant.

A thorough risk analysis was performed prior to the operation. Possible risks were identified and mitigated if necessary. A risk of radioactive contamination of the CT equipment was not foreseen. Appropriate standard procedures of ESG and the coiled tubing company ensured that the situation could be handled without additional HSE issues after slightly elevated NORM values were detected. The contaminated equipment could be transported to and cleaned at a dedicated treatment facility according to European and national standards. The risk of elevated NORM concentrations, however, must be included in future risk analysis.GPK-4 hydraulic characteristics

During the monitoring period (early 2017 to February 2020), the injectivity index varied between 0.54 kg/s/bar and 0.65 kg/s/bar. The maximum valued has been reached between May and September 2018, before decreasing to around 0.54 kg/s/bar and even lower afterwards.

Just before the chemical stimulation of December 2019, the injectivity of GPK-4 was stabilized around 0.60 kg/s/bar. The current value estimated after the chemical stimulation remains uncertain, but the post stimulation estimate (late December 2019 to early February 2020) reaches approximately 0.62

kg/s/bar. However, as observed, such a value was already reached in the past, and this very small increase may not be related to the acid reaction itself.

All the observed variations are small and thus, difficult to explain, as they may be related to several parameters, such as injection temperature, fluid density, status of the borehole. The question of the flow and pressure sensors sensitivity and calibration can even be addressed.

6.2 Seismicity monitoring

The seismic monitoring performed the months before and after the stimulation didn't highlight any change in behavior during and after the stimulation. Two events were detected on 22/12/2019, but from seismic rate, PGV and Magnitude observations, there is no evidence that those events are directly related to the soft chemical stimulation. If fact, those events are not different in number and energy compared to the observed induced micro-seismic activity baseline of Soultz site. They might have been triggered by the stop and the restart of the injection, which was part of the stimulation procedure, or even just related to the injection itself.

6.3 Chemical monitoring

The physical and chemical parameters of the brine produced from GPK-2 well are well-known and constant overtime. Gas content have been also analyzed and fluid characterization was done as a baseline prior to the GPK-4 chemical stimulation.

First value of monitoring post stimulation shows that physical parameters are quite constant, and that the chemical stimulation didn't impact the chemical composition of the production brine from GPK-2.

6.4 Preliminary interpretation of GPK-4 chemical stimulation effects

So far, no significant impact of the chemical stimulation of GPK-4 has been observed. Many reasons could explain the poor efficiency of acid job. Indeed, 2 hydraulic and 3 chemical stimulations have been done in GPK-4, after the drilling operations. Those past operations have probably already improved the near wellbore permeability of the well. Consequently, the recent chemical stimulation could only have a limited effect on the already near well stimulated zones.

Moreover, the near wellbore targeted by the chemical stimulation is maybe not the limiting parameter of GPK-4 injectivity. The low reservoir permeability could explain the poor efficiency of the chemical treatment, as the radius of acid reaction is too small to enhance far field reservoir permeability.

Additional logging (PLT, casing integrity log) could help determining which potential flow zones would have been impacted by the stimulation.

Further information
www.destress-h2020.eu

7 References

ANDRE, L., RABEMANANA, V., VUATAZ, F.D., 2006. INFLUENCE OF WATER-ROCK INTERACTIONS ON FRACTURE PERMEABILITY OF THE DEEP RESERVOIR AT SOULTZ-SOUS-FORÊTS, FRANCE. GEOTHERMICS 35(5-6), 507-531

BÄCHLER, D., KOHL, T., 2005. COUPLED THERMAL-HYDRAULIC-CHEMICAL MODELLING OF ENHANCED GEOTHERMAL SYSTEMS. GEOPHYSICAL JOURNAL INTERNATIONAL 161(2), 533-548

BALDEYROU, A., VIDAL, O., FRITZ, B., 2003. EXPERIMENTAL STUDY OF PHASE TRANSFORMATION IN A THERMAL GRADIENT; APPLICATION TO THE SOULTZ-SOUS-FORÊTS GRANITE (FRANCE). COMPTES RENDUS - GEOSCIENCE 335(4), 371-380

BALDEYROU-BAILLY, A., SURMA, F., FRITZ, B., 2004. GEOPHYSICAL AND MINERALOGICAL IMPACTS OF FLUID INJECTION IN A GEOTHERMAL SYSTEM: THE HOT FRACTURED ROCK SITE AT SOULTZ-SOUS-FORÊTS, FRANCE. IN: GEOLOGICAL SOCIETY SPECIAL PUBLICATION, VOL. 236. PP. 355-367.

BARTIER, D., LEDÉSERT, B., CLAUER, N., MEUNIER, A., LIEWIG, N., MORVAN, G., ADDAD, A., 2008. HYDROTHERMAL ALTERATION OF THE SOULTZ-SOUS-FORÊTS GRANITE (HOT FRACTURED ROCK GEOTHERMAL EXCHANGER) INTO A TOSUDITE AND ILLITE ASSEMBLAGE. EUROPEAN JOURNAL OF MINERALOGY 20(1), 131-142

BLANC, P., LASSIN, A., PIANTONE, P., AZAROUAL, M., JACQUEMET, N., FABBRI, A., GAUCHER, E.C., 2012. THERMODDEM: A GEOCHEMICAL DATABASE FOCUSED ON LOW TEMPERATURE WATER/ROCK INTERACTIONS AND WASTE MATERIALS. APPLIED GEOCHEMISTRY 27(10), 2107-2116

BRANDT, F., BOSBACH, D., KRAWCZYK-BÄRSCH, E., ARNOLD, T., BERNHARD, G., 2003. CHLORITE DISSOLUTION IN THE ACID PH-RANGE: A COMBINED MICROSCOPIC AND MACROSCOPIC APPROACH. GEOCHIMICA ET COSMOCHIMICA ACTA, 67(8), 1451-1461.

DEZAYES, C., GENTER, A., HOOIJKAAS, G. R., 2005. DEEP-SEATED GEOLOGY AND FRACTURE SYSTEM OF THE EGS SOULTZ RESERVOIR (FRANCE) BASED ON RECENT 5KM DEPTH BOREHOLES. IN PROCEEDINGS WORLD GEOTHERMAL CONGRESS.

DUBOIS, M., LEDÉSERT, B., POTDEVIN, J.L., VANÇON, S., 2000. DETERMINATION OF THE FORMATION CONDITIONS OF CARBONATES IN AN ALTERATION ZONE OF THE SOULTZ-SOUS-FORETS GRANITE (RHINE GRABEN): THE FLUID INCLUSION RECORD. COMPTES RENDUS DE L'ACADEMIE DE SCIENCES - SERIE IIA: SCIENCES DE LA TERRE ET DES PLANETES 331(4), 303-309

DUBOIS, M., OUGOUGDAL, M.A., MEERE, P., ROYER, J.J., BOIRON, M.C., CATHELINEAU, M., 1996. TEMPERATURE OF PALEO- TO MODERN SELF-SEALING WITHIN A CONTINENTAL RIFT BASIN : THE FLUID INCLUSION DATA (SOULTZ-SOUS-FORÊTS, RHINE GRABEN, FRANCE). EUROPEAN JOURNAL OF MINERALOGY 8(5), 1065-1080

FRITZ, B., JACQUOT, E., JACQUEMONT, B., BALDEYROU-BAILLY, A., ROSENER, M., VIDAL, O., 2010. GEOCHEMICAL MODELLING OF FLUID-ROCK INTERACTIONS IN THE CONTEXT OF THE SOULTZ-SOUS-FORÊTS GEOTHERMAL SYSTEM. COMPTES RENDUS - GEOSCIENCE 342(7-8), 653-667

GAUCHER, E. C., BLANC, P., 2006. CEMENT/CLAY INTERACTIONS–A REVIEW: EXPERIMENTS, NATURAL ANALOGUES, AND MODELING. WASTE MANAGEMENT, 26(7), 776-788.

GEIE EMC 2017, DESTRESS – FEASIBILITY STUDY: CHEMICAL STIMULATION OF AN INJECTION WELL AT SOULTZ-SOUS-FORÊTS - FRANCE. KUTZENHAUSEN, GEIE EMC CONFIDENTIAL REPORT PP. 75.

GENTER, A., TRAINEAU, H., 1992. BOREHOLE EPS-1, ALSACE, FRANCE: PRELIMINARY GEOLOGICAL RESULTS FROM GRANITE CORE ANALYSES FOR HOT DRY ROCK RESEARCH. SCIENTIFIC DRILLING, 3(5), 205-214.

GÉRARD, F., CLEMENT, A., FRITZ, B., 1998. NUMERICAL VALIDATION OF A EULERIAN HYDROCHEMICAL CODE USING A 1D MULTISOLUTE MASS TRANSPORT SYSTEM INVOLVING HETEROGENEOUS KINETICALLY CONTROLLED REACTIONS. JOURNAL OF CONTAMINANT HYDROLOGY, 30(3), 201-216.

HÉBERT, R., LEDÉSERT, B., GENTER, A., BARTIER, D., DEZAYES, C., 2011. MINERAL PRECIPITATION IN GEOTHERMAL RESERVOIR: THE STUDY CASE OF CALCITE IN THE SOULTZ-SOUS-FORÊTS ENHANCED GEOTHERMAL SYSTEM. IN: 36RD WORKSHOP ON GEOTHERMAL RESERVOIR ENGINEERING, PP. SGP-TR-191

HEBERT, R.L., LEDESERT, B., 2012. CALCIMETRY AT SOULTZ-SOUS-FORÊTS ENHANCED GEOTHERMAL SYSTEM: RELATIONSHIPS WITH FRACTURE ZONES, FLOW PATHWAYS AND RESERVOIR CHEMICAL STIMULATION RESULTS. IN: GEOTHERMAL ENERGY, TECHNOLOGY AND GEOLOGY. PP. 93-113.

HÉBERT, R.L., LEDÉSERT, B., BARTIER, D., DEZAYES, C., GENTER, A., GRALL, C., 2010. THE ENHANCED GEOTHERMAL SYSTEM OF SOULTZ-SOUS-FORÊTS: A STUDY OF THE RELATIONSHIPS BETWEEN FRACTURE ZONES AND CALCITE CONTENT. JOURNAL OF VOLCANOLOGY AND GEOTHERMAL RESEARCH 196(1-2), 126-133

JÄHNICHEN S., DEGERING D., SEIBT A., SCHEIBER J., MOUCHOT J., BUSE C., HEBERLING F., 2019. INHIBITION OF SCALES IN GEOTHERMAL PLANTS IN UPPER RHINE GRABEN: MONITORING OF FLUIDS AND SCALES. EUROPEAN GEOTHERMAL CONFERENCE 2019, DEN HAAG, NETHERLAND, 11-14 JUNE 2019.

JACQUOT, E., 2000. MODELISATION THERMODYNAMIQUE ET CINETIQUE DES REACTIONS GEOCHIMIQUES ENTRE FLUIDES DE BASSIN ET SOCLE CRISTALLIN: APPLICATION AU SITE EXPERIMENTAL DU PROGRAMME EUROPEEN DE RECHERCHE EN GEOTHERMIE PROFONDE (SOULTZ-SOUS- FORETS, BAS-RHIN, FRANCE). LOUIS PASTEUR UNIVERSITY

KÖHLER, S.J., DUFAUD, F., OELKERS, E.H., 2003. AN EXPERIMENTAL STUDY OF ILLITE DISSOLUTION KINETICS AS A FUNCTION OF PH FROM 1.4 TO 12.4 AND TEMPERATURE FROM 5 TO 50°C. GEOCHIMICA ET COSMOCHIMICA ACTA 67, 3583-3594.

KOMNINOU, A., YARDLEY, B.W.D., 1997. FLUID-ROCK INTERACTIONS IN THE RHINE GRABEN: A THERMODYNAMIC MODEL OF THE HYDROTHERMAL ALTERATION OBSERVED IN DEEP DRILLING. GEOCHIMICA ET COSMOCHIMICA ACTA 61(3), 515-531

LEDESERT, B., BERGER, G., MEUNIER, A., GENTER, A., BOUCHET, A., 1999. DIAGENETIC-TYPE REACTIONS RELATED TO HYDROTHERMAL ALTERATION IN THE SOULTZ-SOUS-FORETS GRANITE, FRANCE. EUROPEAN JOURNAL OF MINERALOGY 11(4), 731-741

LEDÉSERT, B., DUBOIS, J., GENTER, A., MEUNIER, A., 1993A. FRACTAL ANALYSIS OF FRACTURES APPLIED TO SOULTZ-SOUS-FORETS HOT DRY ROCK GEOTHERMAL PROGRAM. JOURNAL OF VOLCANOLOGY AND GEOTHERMAL RESEARCH 57(1-2), 1-17

LEDÉSERT, B., DUBOIS, J., VELDE, B., MEUNIER, A., GENTER, A., BADRI, A., 1993B. GEOMETRICAL AND FRACTAL ANALYSIS OF A THREE-DIMENSIONAL HYDROTHERMAL VEIN NETWORK IN A FRACTURED GRANITE. JOURNAL OF VOLCANOLOGY AND GEOTHERMAL RESEARCH 56(3), 267-280

LEDÉSERT, B., HEBERT, R., GENTER, A., BARTIER, D., CLAUER, N., GRALL, C., 2010. FRACTURES, HYDROTHERMAL ALTERATIONS AND PERMEABILITY IN THE SOULTZ ENHANCED GEOTHERMAL SYSTEM. COMPTES RENDUS - GEOSCIENCE 342(7-8), 607-615

LEDESERT, B., HEBERT, R.L., GRALL, C., GENTER, A., DEZAYES, C., BARTIER, D., GERARD, A., 2009. CALCIMETRY AS A USEFUL TOOL FOR A BETTER KNOWLEDGE OF FLOW PATHWAYS IN THE SOULTZ-SOUS-FORÊTS ENHANCED GEOTHERMAL SYSTEM. JOURNAL OF VOLCANOLOGY AND GEOTHERMAL RESEARCH 181(1-2), 106-114

LOWSON, R. T., COMARMOND, M. C. J., RAJARATNAM, G., BROWN, P. L., 2005. THE KINETICS OF THE DISSOLUTION OF CHLORITE AS A FUNCTION OF PH AND AT 25 C. GEOCHIMICA ET COSMOCHIMICA ACTA, 69(7), 1687-1699.

LUMMER N.R., RAUF O., (2019). PREMIUM TREATMENT SYSTEM FOR GRANITE AND SANDSTONE FORMATIONS - FLUID DEVELOPMENT AND FIELD TRIAL IN A GEOTHERMAL WELL, EUROPEAN GEOTHERMAL CONGRESS, EGC 2019, 11-14 JUNE 2019, THE HAGUE, THE NETHERLANDS.

MARTY, N.C.M., TOURNASSAT, C., BURNOL, A., GIFFAUT, E., GAUCHER, E.C., 2009. INFLUENCE OF REACTION KINETICS AND MESH REFINEMENT ON THE NUMERICAL MODELLING OF CONCRETE/CLAY INTERACTIONS. JOURNAL OF HYDROLOGY 364(1–2), 58-72 DOI:10.1016/J.JHYDROL.2008.10.013

MAURER V., GAUCHER E., GRUNBERG M., KOEPKE R., PESTOURIE R., CUENOT N., (2020). SEISMICITY INDUCED DURING THE DEVELOPMENT OF THE RITTERSHOFFEN GEOTHERMAL FIELD, FRANCE. GEOTHERMAL ENERGY 8, 5 (2020). HTTPS://DOI.ORG/10.1186/S40517-020-0155-2

MOUCHOT J., HEHN R., CUENOT N., BAUJARD C., GENTER A., 2020. LONG-TERM GEOCHEMICAL DURING EXPLOITATION PRIOR TO GPK4 CHEMICAL STIMULATION. POSTER, FINAL CONFERENCE, DELFT 20-21 JANUARY 2020.

MOUCHOT J., SCHEIBER J., FLORENCIO J., SEIBT A., JÄHNICHEN S., 2019. SCALE AND CORROSION CONTROL PROGRAM, EXAMPLE OF TWO GEOTHERMAL PLANTS IN OPERATION IN THE UPPER RHINE GRABEN, EUROPEAN GEOTHERMAL CONFERENCE 2019, DEN HAAG, NETHERLAND, 11-14 JUNE 2019.

MOUCHOT, J., CUENOT, N., BAUJARD, C., PELLISSIER DE FELLIGONDE, G., GENTER, A., LUCAS, Y., SCHÄFER, G., 2017. DETAILED REPORT ON RESERVOIR PERFORMANCE IN TERMS OF SUSTAINABILITY. DESTRESS DELIVERABLE 4.3_M18. UNIVERSITY OF STRASBOURG AND ES-GÉOTHERMIE, FRANCE.

NAMI, P., SCHELLSCHMIDT, R., SCHINDLER, M., TISCHNER, R., 2008. CHEMICAL STIMULATION OPERATIONS FOR RESERVOIR DEVELOPMENT OF THE DEEP CRYSTALLINE HDR/EGS SYSTEM AT SOULTZ-SOUS-FORÊTS (FRANCE). IN: PROCEEDINGS OF THE 32ND WORKSHOP ON GEOTHERMAL RESERVOIR ENGINEERING, STANFORD UNIVERSITY, STANFORD, CA, USA, 5 PP.

NGO, V. V., LUCAS, Y., CLEMENT, A., FRITZ, B., 2016. MODELING THE IMPACT OF TEMPERATURE ON THE SATURATION STATE AND BEHAVIOR OF MINERALS IN THE SOULTZ-SOUS-FORÊTS GEOTHERMAL SYSTEM. GEOTHERMICS, 64, 196-208.

NGO, V.V., DELALANDE, M., CLÉMENT, A., MICHAU, N., FRITZ, B., 2014. COUPLED TRANSPORT-REACTION MODELING OF THE LONG-TERM INTERACTION BETWEEN IRON, BENTONITE AND CALLOVO-OXFORDIAN CLAYSTONE IN RADIOACTIVE WASTE CONFINEMENT SYSTEMS. APPLIED CLAY SCIENCE 101(0), 430-443

PALANDRI, J. L., KHARAKA, Y. K., 2004. A COMPILATION OF RATE PARAMETERS OF WATER-MINERAL INTERACTION KINETICS FOR APPLICATION TO GEOCHEMICAL MODELING (NO. OPEN-FILE-2004-1068).

PETERSCHMITT A., HEHN R., BOSIA C., CUENOT N., PRATIWI A.S., GENTER A., (2018). RISK ASSESSMENT FOR CHEMICAL STIMULATION OF EGS RESERVOIRS: APPLICATION TO EGS GEOTHERMAL PROJECTS IN THE UPPER RHINE GRABEN, GEOTHERMAL RESOURCE COUNCIL, GRC2018, OCTOBER 14-17, RENO, NEVADA, USA, 2203-2218.

PORTIER, S., VUATAZ, F.D., NAMI, P., SANJUAN, B., GÉRARD, A., 2009. CHEMICAL STIMULATION TECHNIQUES FOR GEOTHERMAL WELLS: EXPERIMENTS ON THE THREE-WELL EGS SYSTEM AT SOULTZ-SOUS-FORÊTS, FRANCE. GEOTHERMICS 38(4), 349-359

RABEMANANA, V., DURST, P., BÄCHLER, D., VUATAZ, F.D., KOHL, T., 2003. GEOCHEMICAL MODELLING OF THE SOULTZ-SOUS-FORÊTS HOT FRACTURED ROCK SYSTEMCOMPARISON OF TWO RESERVOIRS AT 3.8 AND 5 KM DEPTH. GEOTHERMICS 32(4), 645-653

SANJUAN, B., MILLOT, R., DEZAYES, C., BRACH, M., 2010. MAIN CHARACTERISTICS OF THE DEEP GEOTHERMAL BRINE (5KM) AT SOULTZ-SOUS-FORÊTS (FRANCE) DETERMINED USING GEOCHEMICAL AND TRACER TEST DATA. COMPTES RENDUS GEOSCIENCE 342(7), 546-559

SANJUAN, B., PINAULT, J.L., ROSE, P., GÉRARD, A., BRACH, M., BRAIBANT, G., CROUZET, C., FOUCHER, J.C., GAUTIER, A., TOUZELET, S., 2006. TRACER TESTING OF THE GEOTHERMAL HEAT EXCHANGER AT SOULTZ-SOUS-FORÊTS (FRANCE) BETWEEN 2000 AND 2005. GEOTHERMICS 35(5-6), 622-653

SAUSSE, J., 2002. HYDROMECHANICAL PROPERTIES AND ALTERATION OF NATURAL FRACTURE SURFACES IN THE SOULTZ GRANITE (BAS-RHIN, FRANCE). TECTONOPHYSICS 348(1-3), 169-185

SAUSSE, J., FOURAR, M., GENTER, A., 2006. PERMEABILITY AND ALTERATION WITHIN THE SOULTZ GRANITE INFERRED FROM GEOPHYSICAL AND FLOW LOG ANALYSIS. GEOTHERMICS 35(5-6), 544-560

SAVAGE, D., NOY, D., MIHARA, M., 2002. MODELLING THE INTERACTION OF BENTONITE WITH HYPERALKALINE FLUIDS. APPLIED GEOCHEMISTRY 17(3), 207-223

SAVAGE, D., WALKER, C., ARTHUR, R., ROCHELLE, C., ODA, C., TAKASE, H., 2007. ALTERATION OF BENTONITE BY HYPERALKALINE FLUIDS: A REVIEW OF THE ROLE OF SECONDARY MINERALS. PHYSICS AND CHEMISTRY OF THE EARTH 32(1-7), 287-297

SCHEIBER, J., SEIBT A., BINNER J., GENTER A., MOECKES W., 2013. APPLICATION OF A SCALING INHIBITOR SYSTEM AT THE GEOTHERMAL POWER PALNT ON SOULTZ-SOUS-FORÊTS: LABORATORY AND ON-SITE STUDIES.

SCHEIBER, J., SEIBT, A., BIRNER, J., GENTER, A., MOECKES, W., 2013. APPLICATION OF A SCALING INHIBITOR SYSTEM AT THE GEOTHERMAL POWER PLANT IN SOULTZ-SOUS-FORÊTS: LABORATORY AND ON-SITE STUDIES. IN: PROCEEDINGS OF EUROPEAN GEOTHERMAL CONGRESS, PISA, ITALY

TANG, Y., MARTIN, S. T., 2011. SIDERITE DISSOLUTION IN THE PRESENCE OF CHROMATE. GEOCHIMICA ET COSMOCHIMICA ACTA, 75(17), 4951-4962.

ZHU, C., LU, P., 2009. ALKALI FELDSPAR DISSOLUTION AND SECONDARY MINERAL PRECIPITATION IN BATCH SYSTEMS: 3. SATURATION STATES OF PRODUCT MINERALS AND REACTION PATHS. GEOCHIMICA ET COSMOCHIMICA ACTA 73(11), 3171-3200.

Imprint

Project Lead
GFZ German Research Centre for Geosciences
Telegrafenberg
14473 Potsdam (Germany)
www.gfz-potsdam.de/en/home/

Project Coordinator
Prof. Ernst Huenges
huenges@gfz-potsdam.de
+49 (0)331/288-1440

Project Manager
Dr. Justyna Ellis
ellis@gfz-potsdam.de
+49 (0)331/288-1526

Project Website
www.destress-H2020.eu

Report Authorship
Hehn R., Cuenot N., Mouchot J., Maurer V., Genter A., Seibel O., Peterschmitt A., Imbs B., Reinsch Th., Huenges E. (2020). Reservoir performance in terms of sustainability. Application to the geothermal well GPK-4, Soultz-sous-Forêts, Destress report, Deliverable D4.3 (M42), February 2020.

Liability claim

DESTRESS is co-funded by

National Research Foundation of Korea (NRF)
Korea Institute for Advancement of Technology (KIAT)
Swiss State Secretariat for Education, Research and Innovation (SERI)